Rational design and synthesis of mesoporous silica nanostructure-based drug delivery systems

by

Lauren Chlebanowski

B.A., Augustana College, 2015

AN ABSTRACT OF A DISSERTATION

submitted in partial fulfillment of the requirements for the degree

DOCTOR OF PHILOSOPHY

Department of Chemistry
College of Arts and Sciences

KANSAS STATE UNIVERSITY
Manhattan, Kansas

2019

Abstract

Among the most threatening diseases in the world, cancer and multi-drug resistant bacteria infections are two of the most serious. Mesoporous silica nanoparticles or nanostructures (MSNs) provide nanovesicles for transporting anti-cancer or anti-microbial drugs. The MSNs can easily be functionalized with gatekeepers to ensure that these drugs are released when and where they are needed. It is known that membrane disruption is more difficult for bacteria to gain resistance. For this reason, a small surfactant library was designed with potential of having significant activity toward both gram-positive and gram-negative bacteria. Once the surfactants were synthesized, they were characterized using NMR, IR, and mass spectroscopy. Their activity was then tested against *Micrococcus luteus* and Methicillin Resistant-*Staphylococcus aureus*. The surfactants with best activity were then successfully incorporated into MSN structures. Benzalkonium chloride (BAC), a commercially available antiseptic, had the lowest minimum inhibitory concentration (MIC) of the surfactants tested, thus making it the best candidate for use in the proof of study for the designed delivery system. The MSN-based system for treatment of bacterial infections consisted of BAC loaded, amine functionalized MSNs anchored to a vancomycin gatekeeper via a protease cleavable peptide linker. The peptide was designed to have two cleavage positions by proteases for optimal cleaving. Vancomycin was chosen for its bulky size and activity toward bacteria. The system designed for treatment of cancer was focused on the non-specific nature of the therapeutic peptide SA-D-K_6L_9-AS. The peptide needed to be "gift-wrapped" and sent to the exact location of the tumor to minimize systemic toxicity. The proposed system for this was to use MSNs built directly around a self-assembling version of D-K_6L_9, then embedding iron oxide nanoparticles on the surface of the MSN, and finally enveloping the MSN in a lipid membrane. The drug would be released when the iron oxide particles were heated via radio-wave mediated

hyperthermia. As proof of concept, MSNs built around a rhodamine-B labeled, self-assembling version of D-K_6L_9 were used and tested against GL26 (glioma), B16F10 (melanoma), and NSC (neural stem cells) cell lines, both with and without the gatekeeping system. The outcome was as anticipated, the gatekeeper kept the peptide inside and the cell viabilities remained high. The next steps of these projects will be to continue *in-vitro* testing before moving on to mouse model studies. The MSNs in both projects were characterized using DLS, Zeta potential, TGA, and TEM. Overall, the proposed MSN-based drug delivery systems appear to exhibit promising potential for new approaches towards treatment of both antibiotic resistance and cancer.

Rational design and synthesis of mesoporous silica nanostructure-based drug delivery systems

by

Lauren Chlebanowski

B.A., Augustana College, 2015

A DISSERTATION

submitted in partial fulfillment of the requirements for the degree

DOCTOR OF PHILOSOPHY

Department of Chemistry
College of Arts and Sciences

KANSAS STATE UNIVERSITY
Manhattan, Kansas

2019

Approved by:

Major Professor
Dr. Stefan H. Bossmann

Copyright

Abstract

Among the most threatening diseases in the world, cancer and multi-drug resistant bacteria infections are two of the most serious. Mesoporous silica nanoparticles or nanostructures (MSNs) provide nanovesicles for transporting anti-cancer or anti-microbial drugs. The MSNs can easily be functionalized with gatekeepers to ensure that these drugs are released when and where they are needed. It is known that membrane disruption is more difficult for bacteria to gain resistance. For this reason, a small surfactant library was designed with potential of having significant activity toward both gram-positive and gram-negative bacteria. Once the surfactants were synthesized, they were characterized using NMR, IR, and mass spectroscopy. Their activity was then tested against *Micrococcus luteus* and Methicillin Resistant-*Staphylococcus aureus*. The surfactants with best activity were then successfully incorporated into MSN structures. Benzalkonium chloride (BAC), a commercially available antiseptic, had the lowest minimum inhibitory concentration (MIC) of the surfactants tested, thus making it the best candidate for use in the proof of study for the designed delivery system. The MSN-based system for treatment of bacterial infections consisted of BAC loaded, amine functionalized MSNs anchored to a vancomycin gatekeeper via a protease cleavable peptide linker. The peptide was designed to have two cleavage positions by proteases for optimal cleaving. Vancomycin was chosen for its bulky size and activity toward bacteria. The system designed for treatment of cancer was focused on the non-specific nature of the therapeutic peptide SA-D-K_6L_9-AS. The peptide needed to be "gift-wrapped" and sent to the exact location of the tumor to minimize systemic toxicity. The proposed system for this was to use MSNs built directly around a self-assembling version of D-K_6L_9, then embedding iron oxide nanoparticles on the surface of the MSN, and finally enveloping the MSN in a lipid membrane. The drug would be released when the iron oxide particles were heated via radio-wave mediated

hyperthermia. As proof of concept, MSNs built around a rhodamine-B labeled, self-assembling version of D-K_6L_9 were used and tested against GL26 (glioma), B16F10 (melanoma), and NSC (neural stem cells) cell lines, both with and without the gatekeeping system. The outcome was as anticipated, the gatekeeper kept the peptide inside and the cell viabilities remained high. The next steps of these projects will be to continue *in-vitro* testing before moving on to mouse model studies. The MSNs in both projects were characterized using DLS, Zeta potential, TGA, and TEM. Overall, the proposed MSN-based drug delivery systems appear to exhibit promising potential for new approaches towards treatment of both antibiotic resistance and cancer.

Table of Contents

List of Figures

List of Tables

Acknowledgements

First, I would like to thank my Advisor, Dr. Stefan H. Bossmann. Your support and guidance have been held near and dear since the first day of my REU summer when you described the work that was being done as “designing car bombs to kill cancer cells.” You never fail to make our work feel exciting (because it is!) and most importantly, make us as individuals feel valid and included. I owe much of my confidence to you. You allowed me to blossom into my best self and I could not be more grateful. From the bottom of my heart, Thank you!

I would also like to thank Katrin Bossmann. You have been like an amazing mom/big sister away from home. You are always willing to fight for us when we feel small and hold us close when life throws our plans out the window. You and Stefan have become a strong source of comfort for Lilly and me. Thank you over and over, and over again.

I would also like to thank my current and previous committee members: Dr. Daryl Troyer, Dr. Paul Smith, Dr. Ping Li, and Dr. Jianzhong Yu for their continued accountability and suggestions throughout the duration of my graduate career. Thank you Dr. Rollie Clem for being the chairperson of my defense.

Thank you to our collaborators at the University of Alabama, Birmingham for the MIC calculations. To Dr. Tej Shrestha and Marla Pyle for the help and teaching in the *in-vitro* cell studies. To Dr. Prem Thapa at the University of Kansas for his assistance with TEM imaging.

None of my work would be possible if it were not for the Chemistry department at Kansas State University, the wonderful Chemistry Faculty, and the University itself. I am beyond grateful for the opportunity to conduct research and work for this institution. A special thank you to the Organic Chemistry Faculty for their feedback and suggestions on our presentations during the weekly Organic seminars.

With the most sincerity, I would like to acknowledge the past and current members of the Bossmann group. You have been like family to me and I always look forward to seeing you. I have loved getting to know more about you, your families, and your cultures. I wish you all the absolute best in life and hope we will remain in contact! A huge thank you must be giving to Obdulia. From our first day of orientation to early morning study sessions and late-night exams, you have been one of the most wonderful friends I could have asked for. A massive thank you to my undergrads, Joe Hammer and Sonia Barrett, as well. I appreciate all you have done and wish you the best! Thank you to Sebastian for being an excellent mentor and an even better friend. You were the first person to make Kansas feel like home.

Finally, I would like to take a moment to thank those who have helped me outside of the lab. Thank you to my friends who have supported me and listened to my "science talk" even when I know you did not understand. Thank you for pushing me and cheering me on throughout my academic career. I would not have stayed sane, gone to nationals, or met the love of my life during my graduate studies if it were not for the Women's Rugby Club at Kansas State University. You all are my closest friends and my escape, I will miss you!

An overwhelming amount of gratitude must be given to my loving fiancé, Lilly. I will be forever grateful for the countless hours you have listened to me practice presentations, proof read emails, talk about my hurdles at work, waited on me outside of the building, and calmed my nerves. Without you and your support this journey would have felt impossible. Thank you for being my rock and consistently giving motivation and courage to continue.

Last, but certainly not least, thank you to my family. You have given me a lifetime of encouragement and unconditional love. Thank you for never doubting my potential and sticking with me through the many crazy years of school!

Dedication

I would like to dedicate this work to my Grandmother, Shirley Miceli. She has been my biggest supporter not only during my time as a graduate student, but throughout my entire life. She told me she would *always* invest in my future and I quite literally could not have gotten to this point without her. Thank you, Grandma. I love you a bushel and a peck, to the moon and back.

Chapter 1 - Introduction

Nanotechnology

Nanotechnology is increasing in popularity for treatment of a wide range of diseases. This may be due to the versatility of nanoparticles (NPs). NPs already are in wide use in the industry extending from cosmetics to electrical transformer and so much more.[1] Over the last several years, NP or nanotechnology-based treatments have been approved for clinical use in the medical field for cancer treatment, imaging, vaccinations, and more. Some better-known examples include Abraxane and Doxil.[2] As of 2016, 51 "nanomedicines" had been approved by the Food and Drug Administration and nearly 80 more where in clinical trials.[3] Agricultural uses currently in use or being investigated range from fertilizers to plant breeding.[4] As interest increases the field of nanotechnology, more issues begin to emerge. One common issue in NP synthesis is the ability to produce NPs in bulk in a cost effective and time efficient manner.

Mesoporous silica nanoparticles

Mesoporous silica nanoparticles (MSNs) are one type of NP that is relatively easy to synthesize and cost effective. As their name suggests they are comprised of a silica-oxygen scaffold that contains pores. The pores can be filled with cargo that either occupies the empty space or that interacts with the silica scaffold. Their synthesis generally consists of mixing a surfactant in water and allowing micelles to form in the presence of a catalyst. Then a templating agent, usually tetraethyl orthosilicate, is added and allowed to reactant for several hours producing a white precipitate that is easily isolated by filtration or centrifugation.[5] The synthesis occurs though a simple sol-gel reaction, where the silicate is first hydrolyzed and then allowed to condense with another silicate or silanol molecule forming a network of silica-oxygen bonds around the templating agent.[6] The size of the nanoparticles and their pore size can be manipulated by varying

the concentration of the starting reagents, by changing the length of the reaction, or by changing the temperature/pressure of the reaction. The resulting MSNs must be acid washed or calcinated to remove the surfactant prior to drug loading. These NPs are readily functionalized and biocompatible, making them an excellent option for drug delivery.[7] Unfortunately, MSNs do have their drawbacks. One of these drawbacks is loading efficiency. A "high" MSN loading efficiency can be as low as 10%.[8] This can be increased with a novel type of synthesis, which will be discussed chapter 3. The use of cetrimonium bromide (CTAB) as a templating agent also can pose a problem because it is toxic and difficult to completely remove from the MSN. Another issue is the non-specific release and release rate of MSNs. Luckily, this can be finetuned using gatekeepers.

Antibiotic Resistance

Antibiotics are one of the most widely used medications globally. From 2010-2011 there were over 154 million antibiotics prescribed in the United States alone. Nearly half of the outpatient prescriptions were written for common illnesses that do not require antibiotic treatment. Of the total prescribed, it is estimated nearly 1 in 3 prescriptions were considered unnecessary.[9] This is also not accounting for the antibiotics provided to livestock in an attempt to ensure food safety and quality. In 2014 there were nineteen European countries where antibiotics were available over the counter.[10] The misuse and overuse of antibiotics is rapidly creating a global threat. Bacteria are often thought to be simple, single celled organisms, but their means of evading antibiotics can be quite intricate. Due to their single cell nature, they can quickly adapt and become resistant. The typical path of resistance is as follows: antibiotics are administered, a small population of bacteria are resistant and survive the treatment, then these bacteria repopulate and form a resistant colony or strain.[11] With proper use, this process can take a long time due to the host's ability to fight the few remaining cells, but with the widespread use of antibiotics this

process is occurring much more quickly and “superbugs” are becoming commonplace names. The CDC estimates that over two million illnesses are causes by antibiotic resistance. Of these, approximately twenty-three thousand resulted in death.[11] More shockingly, over half of the deaths are attributed to one infection: *Clostridium difficile.* Resistance is not a new concept, in fact resistance was reported three years prior to the introduction of the first approved antibiotic, penicillin, in 1943.[11] One of the biggest issues being faced are multi-drug resistance.

Bacterial means of resistance can be extremely diverse. Bacteria can develop efflux pumps to manually push the drug out of the cell. They are also capable of modifying their cell wall to be less permeable causing less drug to enter the cell.[12] If the drug manages to enter the cell, some bacteria have been known to alter the target site rendering the antibiotic useless. Another form of resistance occurs when the cell develops an inactivating enzyme or manage to use other enzyme altogether.[12] Taking a closer look, it becomes clear that traditional antibiotics have a mechanism of action that target a biological function within the cell thus leading to cell death. Bacteria, however, have often found ways to resist this time of treatment suggesting a new mechanism of action may be needed.

Surfactants

Those familiar with surfactants likely associate them with industrial or home-cleaning usage. They have been known for their foaming and emulsification abilities, but have be used as wetting agents, anti-corrosion agents, and much more since their discovery.[13] Benzalkonium chloride (BAC) is a unique example of a commonly used surfactant in hospitals and antiseptic wipes. With antibiotic resistance on the rise, research is beginning to focus on development of new treatment for these resistant infections. The antimicrobial activity of surfactants has become a leading question for new research. The mechanism of action of surfactants is still under

investigation, but is widely accepted as an association of the surfactant molecules with the cell membrane of the bacteria which leads to penetration and cytoplasmic leakage. This method of action would be more difficult to gain resistance towards in comparison to traditional antibacterial reagents.[22] Recently, surfactants have also been studied for their application in nanotechnology as capping agents and templates for mesoporous structures.[23]

Structurally, surfactants are relatively simple. They consist of a hydrophilic head group and a hydrophobic tail group. This makes them amphiphilic molecules. Their hydrophobic tail often consists of a hydrocarbon tail, while the hydrophilic head group can varies drastically depending on the desired function of the surfactant. Head groups can also carry charges which are balanced by a counter ion, breaking surfactants into five main groups: biosurfactants, cationic, anionic, zwitterionic, and non-ionic. Each group generally has its own set of primary uses, as well as advantages and disadvantages. Often surfactants are not easily biodegradable and are toxic to aquatic life.[13] This is one of the main hurdles in the field of surfactants. Surfactants can also be "Gemini" meaning that they have two hydrophilic heads and/or hydrophobic tails. Gemini surfactants have been more powerful than their single headed counterpart. Some studies that have investigated surfactants with multiple heads have found an increase in antimicrobial activity as well. Cationic surfactants have shown to have particularly high antimicrobial activity. They have been heavily investigated over the last several decades. Cationic surfactants can range from single headed to multi-headed molecules with varying chain lengths and types. The spacers between the heads has also been manipulated. Changes in the head, tail, and spacer have been proven to change their activity. The most common head group is quaternary ammonium. These amines are considered "war-heads" and often have great biological activity.[13] Further manipulation and better characterization could give way to a new treatment of bacterial infections.

Cancer

It is well known that cancer is among the leading causes of death globally, however, the word cancer itself is misleading. It paints a picture of singularity, while the reality is that cancer is a large group of diseases that all share the common trait of uncontrolled cell division. The number of expected new cases of cancer in the United States alone is 1,762,450 for the year of 2019.[14] The expected deaths from cancer in the U.S. for the same period is over six hundred thousand. Although the overall death rate in the U.S. has fallen over the last serval years, more than half of the global new cases of cancer have occurred in developing portions of the world where novel treatments are not as readily available. There are also several cancer risk factors that are on the rise in developed nations, such as obesity, which threaten to increase the number of new and potentially fatal cases of the cancer.[14]

Cancer treatment

Cancer is an extremely complex set of diseases, making treatment difficult. The same treatment may have significantly different outcomes on two different types of cancer. Generally, the most common forms of treatment include chemotherapy, radiation therapy, and surgery, but recently immunotherapy and targeted therapies have been becoming more prevalent. There are also treatments such as hormone therapy and stem-cell therapy that are used to help mitigate the symptoms and progression on cancer, but do not cure cancer.[15]

Surgery

Surgery is a type of treatment that is utilized when a solid, tumorous mass occurs in the body. The goal is to remove the entire tumor, but sometimes this is not possible. If the tumor has become too vascular or the surgery threatens to damage an organ, the tumor may only be reduced in size and then treated with another type of therapy.[16] There are various methods for removing

cancerous tissue including, but not limited to, traditional surgical removal using scalpels, laser removal of tissue, cryosurgery, and hyperthermia. All these surgery techniques are performed with the use of anesthesia, whether it be local, regional, general.[16] Minimally invasive surgery is preferred to open surgery because of the lowered risk of infection and the shorter recovery time, but the surgeon will perform open surgery if there are complications or laparoscopic techniques are not possible.[16] Painful recovery, risk of infection, risks associated with general anesthesia, and high cost of surgery are common flaws associated with the treatment.

Radiation therapy

Radiation therapy is another treatment technique commonly used for solid tumorous masses, but it can also be used for treatment of cancer-caused conditions. Radiotherapy utilizes high doses of radiation in an attempt to shirk tumors and cell cancerous cells. It is often used in combination with another type of cancer treatment.[17] There are two types of radiation therapy, external beam radiation and internal radiation. The type that is used for treatment is dependent on many factors including type of cancer, size, and location of tumor. When used properly radiation therapy's success can range from curing cancer, slowing its growth, or preventing return of cancerous cells.[17] A major drawback for the technique is that radiation itself is known to cause cancer in some cases. The technique also generally comes with a laundry list of side effects ranging from hair loss to fertility issues depending on the location radiation is applied to.[18]

Chemotherapy

Chemotherapy is a treatment that utilizes a cancer-killing drug that can be administered to the patient either orally on intravenously. Often, these drugs are non-specific and kill healthy cells in the process leading to undesirable side effects. Chemotherapy can be used as a sole source of treatment or before, during, or after one of the other therapy options depending on the type and

stage of cancer.[19] This is process can be extremely taxing on the body and may not be possible for all patients depending on their health. For several years now, there has be much research done in an attempt to make drugs that are either more specific or that have reduced side effects.

Immunotherapy

Immunotherapy is one of the newest forms of treatment for cancer. It is a technique that may not be available to all patients at this time. In immunotherapy, naturally occurring immune cells within the body to treat cancer. This process can be done in a few different ways. Checkpoint inhibitors are drugs given to a patient that increase the likelihood of the immune system recognizing cancerous cells.[20] Adaptive cell transfer is a method that takes T-cells from the tumor and determines which are most likely to attack the cancerous cells. These cancer-sensitive T-cells are then cultured *ex-vivo* over the course of a few weeks to amplify the number of cells and then they are re-administered to the patient.[20] Another type of immunotherapy utilizes monoclonal antibodies, or antibodies that have been synthesized to bind specially to certain receptor in the body. Monoclonal antibodies used for immunotherapy are engineered to bind to receptors of cancer cells and attach immune cells to the area.[20] There are several other forms of immunotherapy being investigated, but currently there are only five classes of immunotherapy that have been approved for clinical use in the U.S.[21] Immunotherapy appears to be promising field of treatment for cancer, but is not without side effects of its own. These side effects may include pain and swelling to heart palpitations and risk of infection.[20] Immunotherapy results also can vary greatly from patient to patient.[21]

Summary

Both cancer and bacteria are complex to treat. Bacterial readily can become resistant to many of the common approaches to treatment, making a drug with a different mechanism of action

desirable. Current cancer treatments are to thank for the decreased death rate from cancer in the U.S., but these treatments still have severe side effects and are not always 100% effective are killing cancer. Nanotechnology may hold the key to solving both problems. Employing the use of MSNs to carry various drugs could help limit side effects from drugs that are toxic to healthy cells. The use of surfactants as antimicrobials could open the door for higher loading efficiencies and the ease of functionality could allow for a gatekeeping system to be attached for targeted release.

Chapter 2 - Understanding Gatekeepers

Gatekeepers are molecules that keep the cargo inside of the MSN pores. The gatekeeper may do this in a few ways. It may envelope MSN or coat it complete. It also may be attached to the surface of the MSN and sterically cover the pores. An advantage of using gatekeepers is that they can have specific modes of release which can greatly enhance the ability to actively target in-vivo.[7] While there are currently a vast number of gatekeepers being investigated, the majority can be divided into three main categories: pH dependent release, temperature or radiation release, and degradative release.

pH Dependent Release

In the field of drug delivery release of a drug caused by specific stimuli is considered to an advantage because it can allow for targeted treatment. One stimulus commonly considered is pH. This is because of the acidic environment found in tumor, inflamed tissues, lysosomes, and endosomes. Change in pH can trigger release of the cargo via different methods. There are pH cleavable molecules, pH soluble molecules, molecules that have conformational changes due to pH change, charge interactions change due to pH, and molecules that can change between hydrophilic and hydrophobic due to pH.[7]

Soluble Release

Quantum dots (QDs) are extremely small inorganic crystals measuring only a few nanometers in width.[24] QDs can be made from several different types of materials, giving them varying stabilities and characteristics. Some QDs are soluble under varying pHs, making them excellent gatekeepers for MSNs. The QDs essentially plug the pores of the MSN until they are in an acidic environment where they dissolve, releasing the cargo depicted in table 2.1.

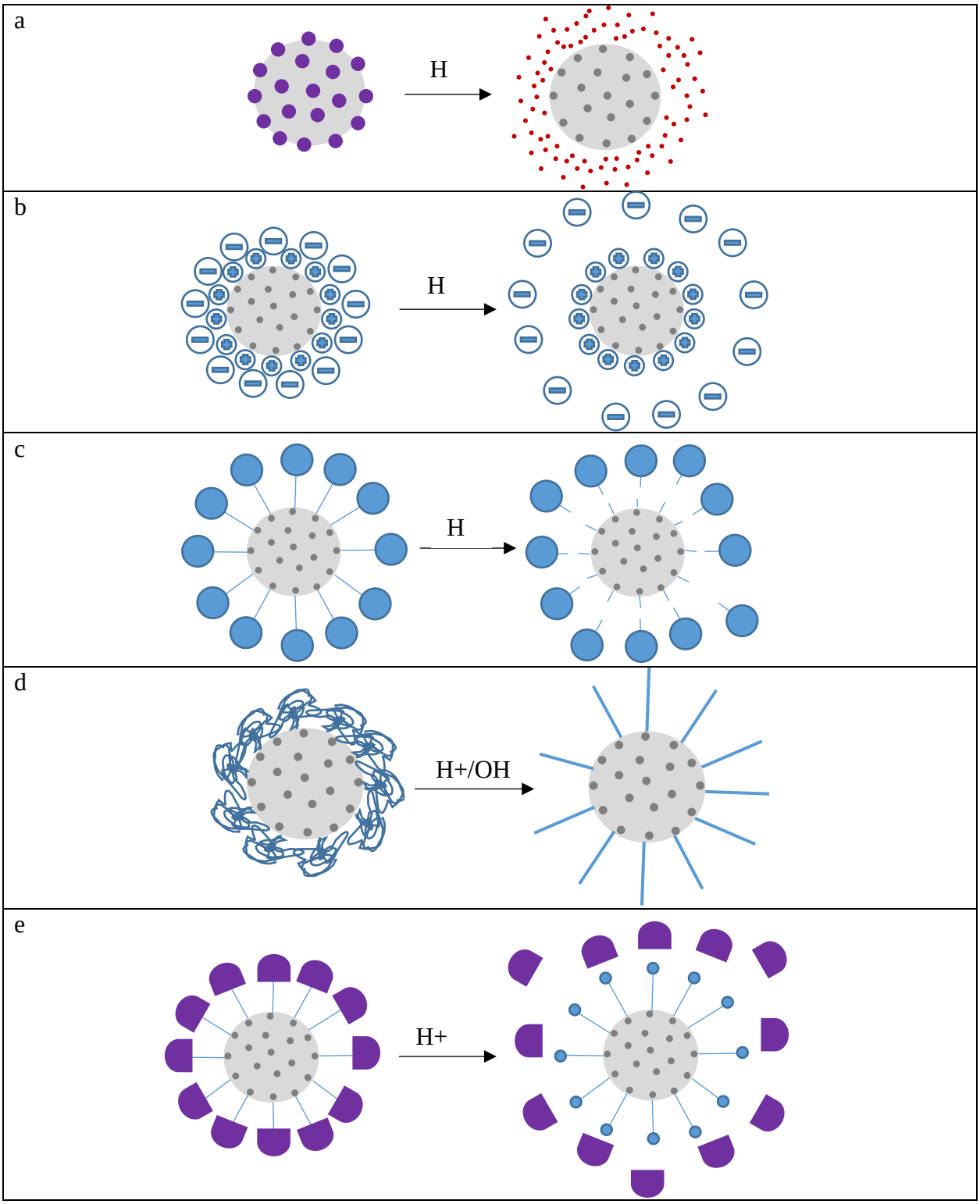

Table 2.1: Various types of pH-dependent gatekeepers. a. soluble gatekeeper, dissolves in acidic environment. b. electrostatic type gatekeeper, change interaction weakened in lower pH. c. acid cleavable linked gatekeeper. d. conformation change type gatekeeper e. guest-host system gatekeeper, caps vacate in acidic conditions.

One study utilized Zinc-oxide (ZnO) QDs as gatekeepers. ZnO QDs are broadly studied due to their biocompatibility and low cost. They are particularly of interest as gatekeepers for MSNs used to treat cancer due the anti-cancer characteristics of zinc ions.[25]

Guest-host release

Another common pH dependent gatekeeper method utilizes the concept of guest-host assemblies. Generally, the host molecule is a large cyclic molecule, while the guest is a much smaller molecule that can be held within the host.[26] When this concept is applied as a gatekeeper for MSNs the guest molecule is anchored to the MSN via a covalent bond. Because the guest molecule is small it does not impede on the drug release from the pores. Once the host molecule is introduced, however, its large, bulky nature sterically covers the pores keeping the drug inside. Once the host vacates, the drug is then released (depicted in table 2.1).[25] An example of theses host molecules is cyclodextrin (CD), a large cyclic molecule containing varying numbers of D-glucose units linked by 1,4-glucosidic residues.[26] CDs residues are hydrophobic, so their guests must be hydrophobic as well.[26] A study done by Zhang *et al.* in 2014 constructed an MSNs containing a variety of guest molecules capped with CDs for the potential treatment of bladder cancer. The host released the guest molecule in low pH. This study was then modified by another research group, attempting to make a dual functioning CD guest-host gatekeeper that could increase the toxicity of the MSNs by having the guest molecule be an anti-cancer reagent itself.[25]

Cleavable release

Additionally, pH can cause changes in electrostatic interactions. So if a MSN is enveloped with a molecule through a charged based interaction, the drop in pH can disrupt the interaction thus releasing the drug, as shown in table 2.1.[25] The most common approach to a pH dependent gatekeeper, however, is a molecule that is stable in a physiological pH of 7.4, but can be cleaved

under acidic conditions, such as that of a tumor or lysosome (illustrated in table 2.1). An example of this type of gatekeeper is described in the article published by The Royal Society of Chemistry, where a polymer bond to the MSN via an acid cleavable linker. The study utilizes poly(acrylic acid) homopolymer (PAA) to block the release of a well-known chemotherapeutic agent, doxorubicin (DOX).[7] The acid cleavable linker chosen, whose structure is shown in Figure 2.1, was 3,9-bis(3-aminopropyl)-2,4,8,10-tetraoxaspiro[5.5]undecane (ATU). ATU was linked via EDC/NHS coupling to MSNs that had previously been functionalized to contain a carboxylic acid group on their surface. Once the linker was attached the MSN was loaded with DOX and capped by allowing the MSNs to stir in a concentrated DOX for several hours, followed by the addition of PAA and EDC/NHS and stirred for several more hours. Control MSNs were also synthesized by attaching PAA directly to the MSN surface.[7]

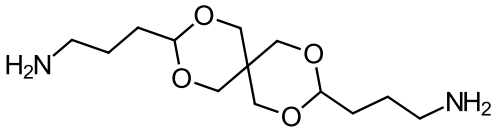

Figure 2.1: Structure of the acid cleavable linker, ATU

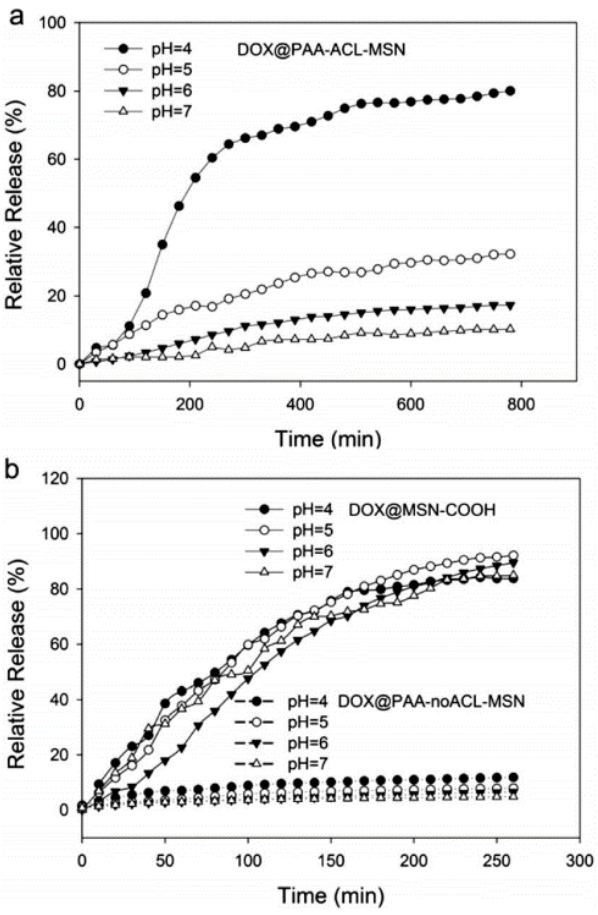

Figure 2.2: Release profiles of modified MSNs. a: profile for MSNs containing DOX and acid cleavable linked PAA. b: profile for control MSNs containing DOX. One without a gatekeeper and one without the acid cleavable linker.[7]

The drug release studies performed showed that the acid cleavable linker worked as intended. In Figure 2.2b, the MSNs without a gatekeeper (denoted DOX@MSN-COOH) exhibit spontaneous release at all pHs and the MSNs with PAA attached directly (denoted as

DOX@PAA-noACL-MSN) show little release regardless of pH. Above in Figure 2.2a, however, it is notable that the release of DOX increases with the decrease in pH. The highest percentage of release was at pH=4, but pH=5 was still three times that of the release at neutral.[7] The MSNs were then studied *in-vitro* to observe cellular uptake and release of DOX. Using confocal laser scanning microscopy (CLSM), the hypothesis that the modified MSNs would be localized in the lysosomes was proven correct. Lysotracker Blue was used to label the lysosomes of nasopharyngeal carcinoma cells (HNE-1). DOX has its own red florescence. In Figure 2.3, it is obvious from the merged image that the MSNs are localized in the lysosomes. It is also clear that red florescence increases over time, before eventually exiting the lysosomes and entering the cytoplasm. With the control MSNs, however, the red florescence remained in the lysosome even after a 24h incubation period, suggesting the non-cleavable gatekeepers held DOX inside while the cleavable gatekeepers allowed its release.[7] Similarly, cells' nuclei were dyed and CLSM was performed. The out was as expect, the DOX in the MSNs containing the cleavable linker reached the nucleus, while the DOX in the MSNs without the linker did not. Before moving to *in-vivo* studies, the cytotoxicity of the MSNs was determined using MTT assays. Both DOX loaded and unloaded MSNs were tested against HNE-1 cells. The

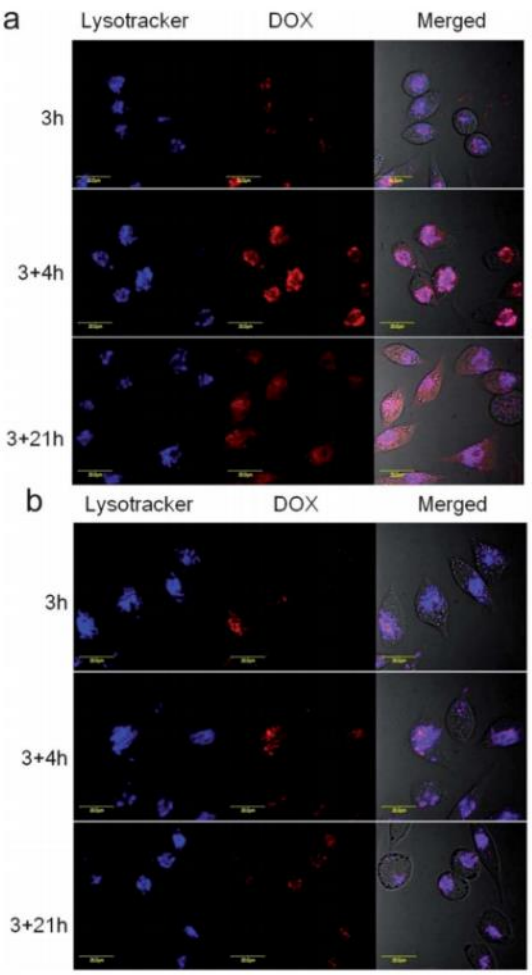

Figure 2.3: *In-vitro* cellular uptake study. a: confocal imaging of MSNs containing DOX and acid cleavable linked PAA. b: confocal imaging control MSNs containing DOX.[7]

unloaded MSNs showed biocompatibility, while the DOX loaded MSNs that contained the acid cleavable linker killed the cells substantially. The DOX loaded MSNs with the PAA directly attached showed 100%+ cell viability, continuing the proof of concept. Finally, an *in-vivo* experiment was conducted in which "HNE-1 tumor model bearing luciferase expressing activity"[7] was used. This allowed the scientists to observe the tumor using bioluminescent imaging while the mice were under anesthesia. With the various controls, the results were strikingly similar to that of the *in-vitro* testing. The DOX loaded, PAA gated MSNs that contained the acid cleavable linker were able to greatly reduce the growth of the tumor. They did not reduce the size as much as the free DOX, however, the weight loss of the mice was significantly less over the 6-day course when the mice had been treated with MSNs instead. This suggested the MSNs were overall less toxic and more targeted than the free DOX alone.[7]

Multi-function release

Sometimes multiple methods of pH-based release can be employed into a single gatekeeping system. A study done out of Northeast Normal University in Changchun, China, did this by not only modifying the CD gatekeeping system by placing tags on the CD cap, but also having the guest molecule attached to the MSN via a pH cleavable linker. The CD cap was tagged with two different molecules. One molecule was a targeting molecule, while the other was a florescent dye.[27] The guest molecule was attached to the MSN via a benzoic–imine linker that could be cleaved in acid conditions. The guest molecule itself was 1-adamantylamine, known for its anti-viral and other therapeutic effects. As a proof of concept, the MSNs were loaded with DOX.[27]

The release study showed at pH=5.3 the drug almost 90% of the drug was released over the course of 72h. This was almost 3-fold better than that of pH=6.8 and was at least 8-fold of that at the physiological pH of 7.4 (Figure 2.4).[27] As for the targeting agent used, either folic acid (FA)

or lactobionic acid (LA) were attached to the CD. With the multifunctional MSNs made, *in-vitro* studies were done. First, MTT assays were ran to determine cytotoxicity of the MSNs. The assays were ran for 24, 48, and 72h against HeLa cells. The major take away from the MTT assays was that the FA was a better targeting molecule, with cell viabilities being slightly lower than that of LA, and that when there is free FA available it will compete for binding.[27] Finally, confocal imaging was used to track the MSNs within HeLa cells. As expected, the FA tagged MSNs had the best cellular uptake. The imaging also showed that the florescence tagged CD caps remained in the cytoplasm while the DOX localized in the nucleus.[27] Overall, this study showed how more than one pH-based release system can be incorporated into a single NP gatekeeper for enhanced drug delivery.

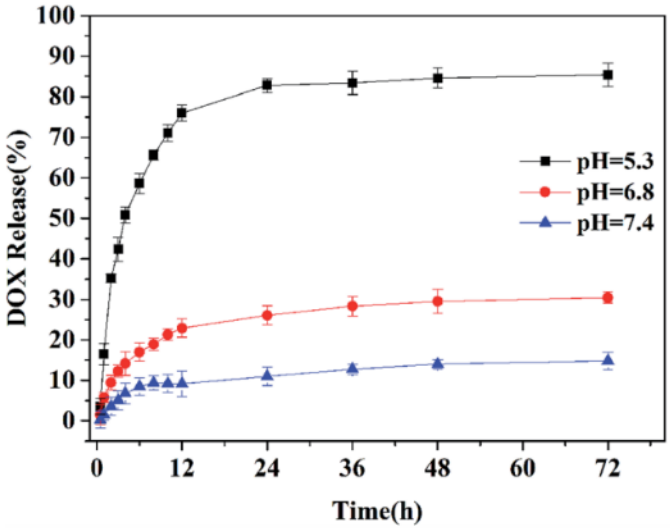

Figure 2.4:In-vitro release study at varying pH. Release of DOX from multifunctional MSNs at varying pH over 72 hours.[27]

Light irradiation release

Much like pH-dependent release, light irradiation can have multiple methods of release with the two most common being: photo-cleavable linkers and photothermal heating. Photo-cleavable linkers and photothermal heat for release have both been studied extensively. Taking their properties and incorporating them as MSN gatekeepers has opened the door for more diversity in release. Often, these methods are incorporated into dual- or even triple-stimuli release systems.

Single stimulus release

Near infrared light (NIR) is considered to have the deepest tissue penetrating ability, making it the most commonly used light for irradiation triggered systems. Recently, a gatekeeping system was developed utilizing reduced graphene (RGO) nanosheets as a capping agent. The system works by attaching alkyl chains to the MSN then loading with a model drug, DOX. These alkyl chains interact with the RGO through noncovalent interactions believed to be σ- π interaction and hydrophobic interaction.[28] In this single stimulus release system, NIR light (780) is utilized to disrupt these interactions and release the DOX. As proof of concept, the system was tested *in-vitro* against human hepatoma SMMC-7721 cells.[28]

First, a release study was performed to prove that the MSNs would release more efficiently at higher temperatures. This was first done in aqueous solution, increasing the local temperature. The results shown in Figure 2.5 clearly indicate that the expectation was correct with the release at 60^{o}C being more than 6 times that of room temperature release.[28] Next, to prove that these results could be achieved with NIR light, the MSNs were observed at room temperature under varying power densities of NIR light. Again, the results confirmed the hypothesis, with a higher cumulative release at the highest power density of 2 W/cm^2.[28] Using confocal imagining, they MSNs were tracked *in-vitro*. The lysosomes of the SMMC-7721 cells were dyed using Lysotracker blue and DOX was tracked from its red fluorescence. The cells were incubated with the RGO capped MSNs for 4h and 8h, then exposed to NIR irradiation with a power density of 2 W/cm^2 for 5 minutes.[28]

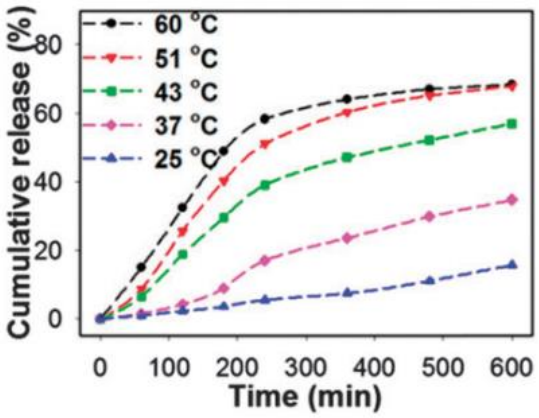

Figure 2.5: Release profile of RGO capped MSNs at varying temperature. MSNs were in aqueous solution.[28]

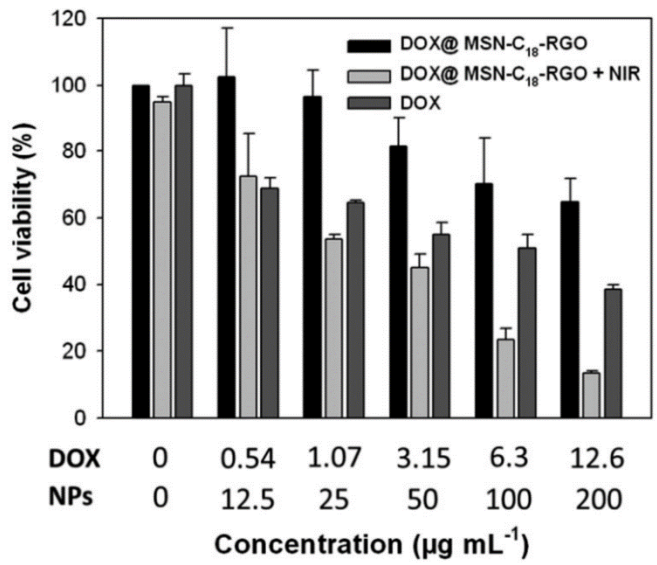

Figure 2.6: Cell viability after exposure to RGOMSNs+NIR, RGOMSNs, and free DOX.
SMMC-7721 cells incubated with varying concentrations for 48h. NIR group irradiated for five minutes after 1h of incubation.[28]

From the imaging it was clear that the MSNs likely accumulate in the lysosomes prior to DOX being released with much of the merged fluorescence overlapping at 4h and the red being more spread across the cell at 8h. Unfortunately, CLSM was not performed on cells that had been exposed to the MSNs, but that had not been exposed to NIR light. MTT assays were performed to quantify the cytotoxicity of the MSNs before and after irradiation (Figure 2.6). The assays confirmed that the MSN+5min irradiation had higher cytotoxicity that that of the non-irradiated group and the free DOX after 48h exposure to the MSNs/free DOX. The control group with concentration 0ug/ml showed that there was little death caused by the NIR irradiation itself.[28] These results proved that RGO could be used as a gatekeeper for MSNs with a triggered release from NIR irradiation.

Another single stimulus release system utilized the "light induced hydroxide ion emitter," malachite green carbinol base (MGCB), to cause a pH jump which allowed release of cargo inside the MSNs. In this study, i-motif DNA where used as the capping agent. MGCB was immobilized in the channels of the MSNs. $Ru(bipy)_3^{2+}$ molecules were loaded into the MSNs as a trackable dye.[29] Without light irradiation the DNA remained folded and blocked the pore of the MSNs, once exposed to UV light the DNA would unfold due to the increased pH and the dye could be release (similar to depiction in table 2.1-d). The release study showed that while in the dark the MSNs

only released about 10% of the dye over the course of 2h, but the MSNs exposed to UV light had a release of almost 90%.[29] Unfortunately, UV light has very low tissue penetration, greatly limiting the applications of these NPs.

Multi-stimulus release

In 2015, an article was published describing a dual-stimulus release system. The gatekeeper allowed differently sized cargo to be released by varying stimuli. The gatekeeper was again a guest-host system, only this time the CD cap was linked to the MSN by a photocleavable linker. The guest molecule was then chosen to a ferrocene.[30] With this model, two cargos were loaded into the MSNs: small size cargo p-coumaric acid (CA) and large size cargo Calcein. Calcein was loaded first, then the CD caps were attached, followed by loading of CA, and finally the ferrocene guest molecule. As shown in Figure 2.7, the ferrocene interaction with the host molecules could be disrupted with 1.5V of electro stimulation. This allowed the smaller cargo, CA, which can fit through the channel of CD to exit the MSN, while the large cargo remained trapped inside.[14] Once CA no longer showed release, the MSNs were washed with di-water and exposed to UV light, cleaving the CD caps and allowing the

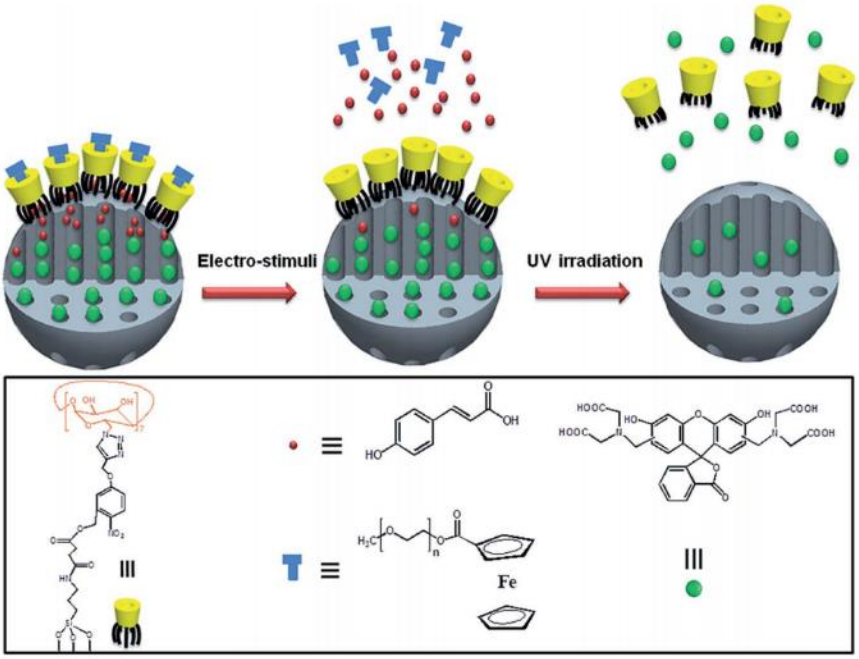

Figure 2.7: Schematic illustration of dual stimulus, guest-host gatekeeping system. MSNs linked via a photocleavable linker to cyclodextrin (yellow), loaded with p-coumaric acid (red) and Calcein (green). Capped with ferrocene (blue).[30]

release of Calcein.[30] This study shed light on the possibility combination therapy utilizing one NP. The biggest drawback is, as mentioned before, UV light does not have excellent tissue penetration limiting the use of these MSN *in-vivo*.

Exploiting inorganic nanoparticles as gatekeepers for MSNs can have many advantages. Taking advantage of the pH change in the cell can reduce the NPs. Also, the NPs can be reduced by molecules naturally occurring in the body. Recently, J. Wen *et al* combined these characteristics with the photo sensitive molecule: hematoporphyrin (HP).[25] The MSNs were loaded first with DOX then with HP. They were then capped with CeO_2 NPs as the gatekeeper making a tri-stimulus gated MSN. Once exposed to both the low pH environment within the tumorous cell and increased levels of glutathione (GSH), which is common in cancerous cells, the CeO_2 would be reduced. This re-exposes the HP molecules which can undergo a conformational change under light irradiation thus allowing enhanced release of DOX and O_2 production that has the potential for "photodynamic therapy" (illustrated in Figure 2.8).[25] Overall, this study along with others gave examples of potential gatekeepers with photo-driven releases. The largest

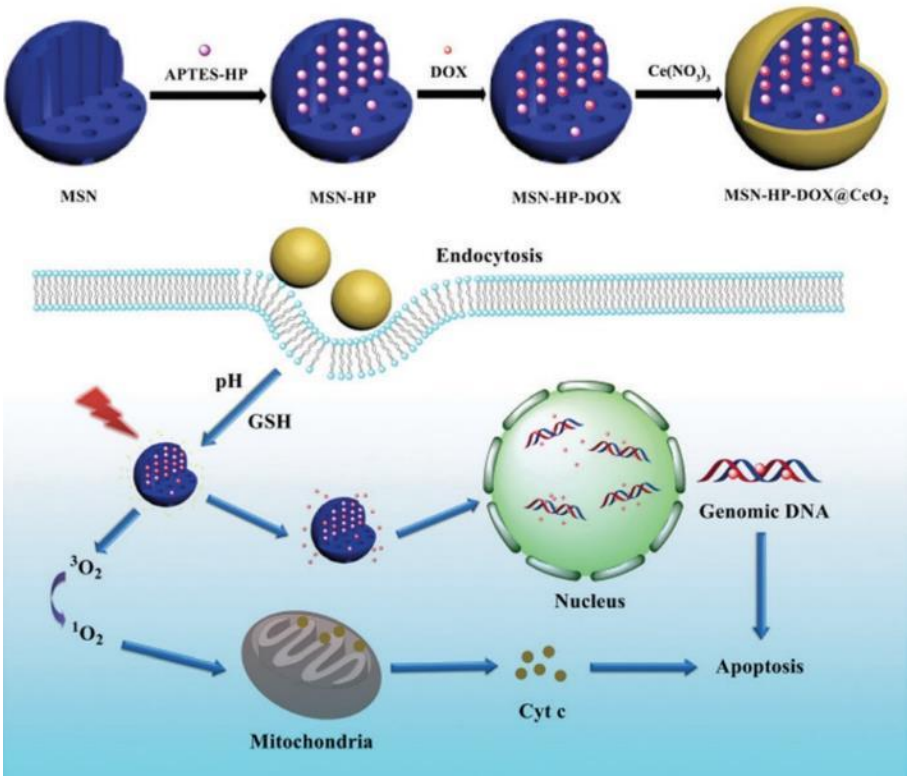

Figure 2.8: Schematic illustration of tri-stimulus gated MSN.[25]

disadvantage of these types of gatekeeper is the limitation of tissue penetration. The NPs are still exceedingly particle for the treatment of several diseases, but the breath of their scope is bound by this limitation.

Degradative release

Degradative release is the broadest category of gatekeeper. This includes any gatekeeper which is broken down or disrupted do to the presence of an enzyme or molecule found within the cell. The most common molecule is GSH, but it is not the only one used in bioresponsive systems. Lipid envelopes can also fall under this category depending on the nature of their breakdown. The main issue involved with enveloping MSNs in lipid layers is they tend to aggregate, which could lead to decreased biocompatibility.[31] Due to this, polymers, DNA templates, proteins/peptides, and NPs are more often explored.

Nanoparticle coating

Typically, NPs used as gatekeepers are prepared and then attached to the MSNs via a linker molecule. An example of this was seen in the CeO_2 gatekeeper described above. The CeO_2 could be reduced in the presence of GSH and work as a single stimulus, bioresponsive gate keeper as well.[24] One article described the use of DNA templating to form silver NPs (AgNPs) *in-situ* around the MSNs. This was accomplished by first functionalizing the MSNs with isocyanatopropyl groups, then grafting cytosine-rich DNA onto the MSN. Once the DNA template was in place the MSNs were loaded with a dye as a model drug, rhodamine 6G (Rh6G).[32] Then AgNPs were formed on the surface on the MSNs by placing them in HEPES buffer with Ag^+ ions in varying ratios. The TEM images make it clear that the more Ag^+ present, the larger the NPs are both in size and quantity (Figure 2.9). The size difference in the NPs allowed for the cargo to be released with

varying amounts of GSH, thus allowing these gatekeepers to be "tuned" for treatment. This effect was better quantified by performing a release study.[32] The capped MSNs were first placed in medium as a control and then the experimental group had 5.0mM of GSH added and the absorbance was read after incubation. Then a release profile was made by using different concentrations of GSH against all three NP gatekeepers. As expected the size of the AgNP gatekeeper inversely correlated to the amount of Rh6G release, shown in Figure 2.10.[32] These study will need to investigate the *in-vivo* properties of the AgNP gated MSN before firm conclusions can be draw about their applications.

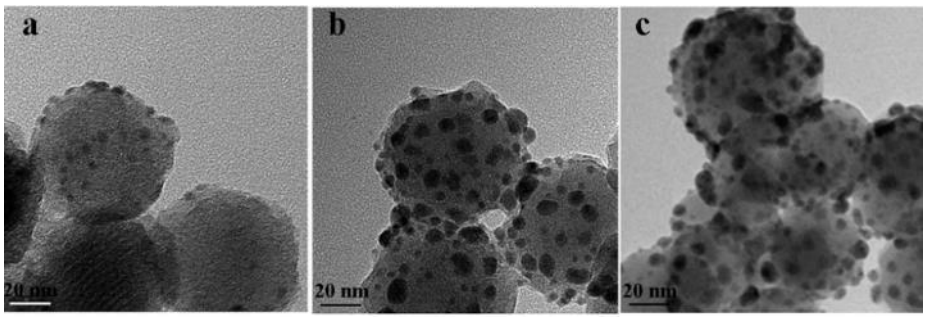

Figure 2.9: TEM images of MSNs capped with Silver nanoparticles. a: ratio of 20:1 Ag^+:MSN b: ratio of 40:1 Ag^+:MSN c: ratio of 80:1 Ag^+:MSN.[32]

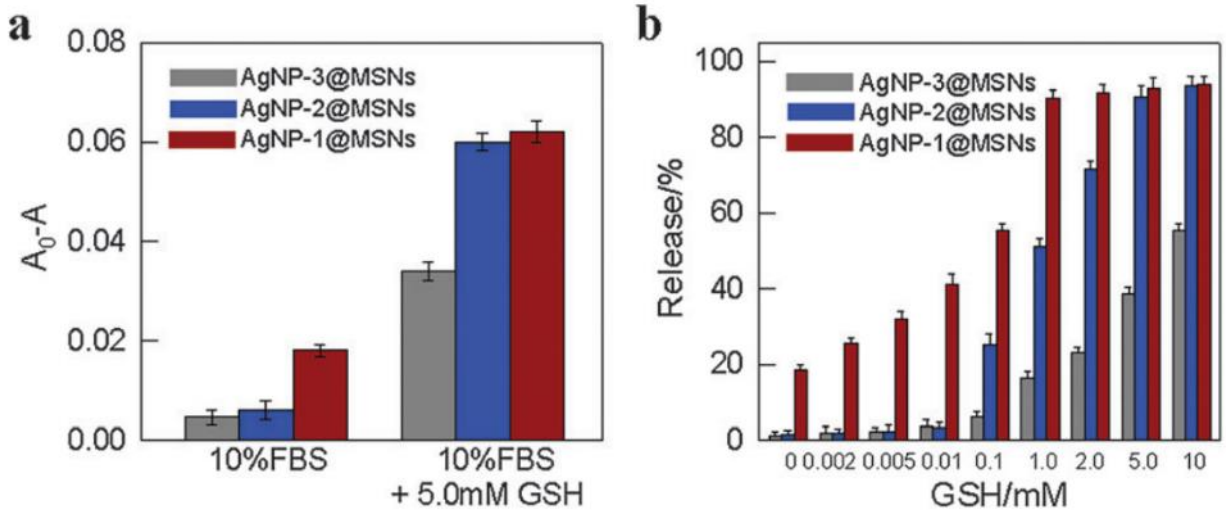

Figure 2.10: Release studies of AgNP gated MSNs

a: Absorbance spectra for varying size of AgNP gates. b: Release profile of the MSNs. AgNP-3@MSN correlates to the 80:1 ratio, AgNP-2@MSN correlates to the 40:1 ratio, and AgNP-1@MSN correlates to the 20:1 ratio.[32]

When using NPs as gatekeepers, the NP does not need to break down or be reduced in order to remove it if it is bound to the MSN by a cleavable linker. One study explores this by using ATP aptamer as the linker. Aptamers will interact with a targer molecule, in this case ATP, and disrupt the connection between the NP gatekeeper and the MSN. The study utlized gold NPs (AuNP) functionaized with ATP aptamers. These were linked to the MSN by an adenosine molecule anchored to the surface of the MSN. When the target molecule was presence the aptamer bound to it releasing the AuNPs from the surface and allowing the model drug (fluorescene) to escape.[33] TEM images show their proof of concept was successful. The AuNPs are bound closly to the MSNs without ATP present, and with ATP present few remain attached (Figure 2.11). The release studys gave the same results. They also tested if the gatekeepers were able to be triggered by other phosphate molecules including CTP, GTP, and UTP. From this is was confirmed that they gatekeepers were only triggered in the presence of ATP.[33] Altogether, this study is an excellent example of fine tuning a gatekeeping system that can be triggered by a specific biomarker. *In-vivo* testing still needs to be conducted to confirm the system will work within the body, but it does appear promising.

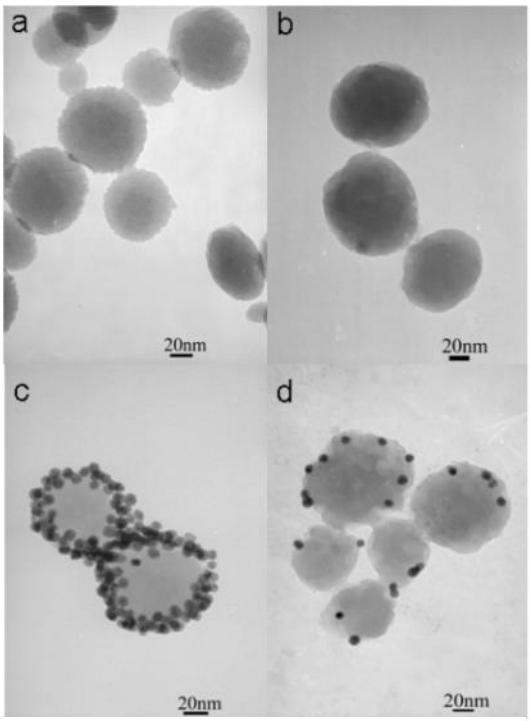

Figure 2.11: TEM images of MSNs.
a: MSNs with no modification. b: MSNs with adenosine anchors. c: MSNs with AuNP-aptamer cap. d: MSNs with AuNP-aptamer cap in the presence of ATP.[33]

Protein/peptide coating

Proteins and peptides can wonderful gatekeepers due to their diversity. The peptide can undergo a conformational change or be cleaved once it is inside the cell. Proteins can do the same and can

potentially be used in targeting specific cells as well and are inherently biocompatible. An example of a protein use was done by Liu *et al.* where phenylboronic acid (PBA) was conjugated human serum albumin (HAS). PBA was used as a targeting molecule, while HAS was the bioresponsive linker. In the presence of MMP-2, which is commonly overexpressed in tumor cells, HAS would break down removing the gatekeepers and releasing the drug.[25] This system was proven in *in-vitro* and *in-vivo* experiments.[25] Several other protein gatekeepers have been investigated, along with the use of a disulfide linker.

While proteins are biocompatible, they also often need to be isolated due to their complex nature. Instead, some scientists have chosen to investigate the use of peptides, or short strands of amino acids that often contain the crucial portions of the much larger proteins. To provide a brief example, the use of protease sensitive peptide was used as a gatekeeper. The peptide was long enough in length that when attached to the MSN its folded conformation blocked the pores of the MSN. The peptide was designed to have several spots that could be cleaved. Once a protease was introduced the peptide was cleaved in locations, allowing the drug to be release.[25] This is one of the simplest examples. Peptides can be modified to only release in the presence of very specific enzymes, making them an advantageous gatekeeper for targeted delivery.

Polymer coating

Polymers have also been explored as gatekeepers. This is not surprising considering polymers' coating abilities. Typically, polymers are broken down by the cell and that is how the cargo gets released from the MSNs. This is not the only type of release the are capable of. With intention in design, polymers can be pH, temperature, irradiation, or even ultrasound sensitive. Looking closer at the biosensitive polymers, they are often broken down to the reducing environment within the cell, specifically due to GSH. Once the polymer gatekeeper is in place it can also have targeting

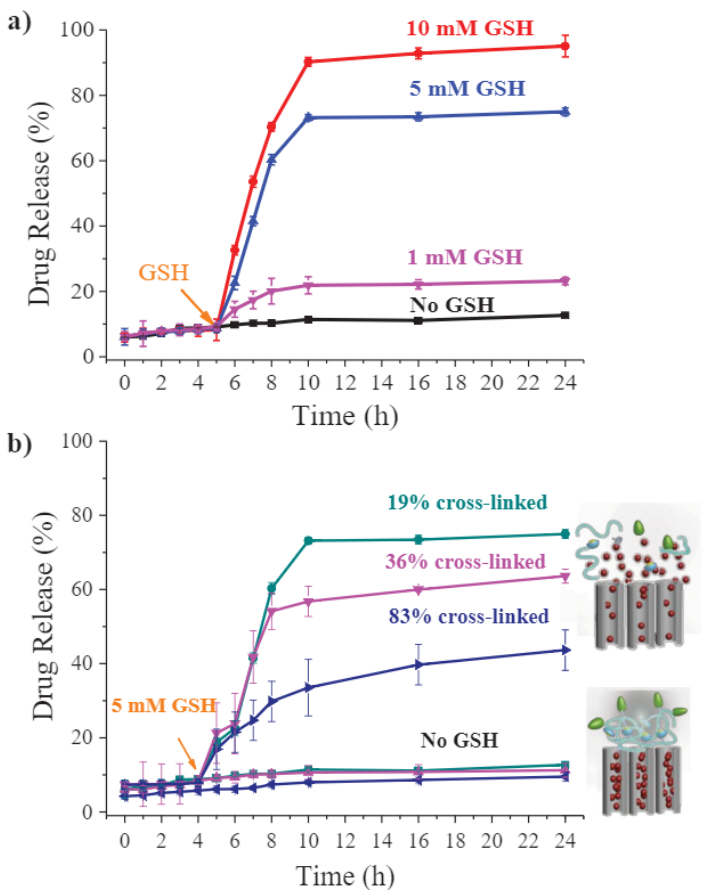

Figure 2.12: Release studies of polymer coated MSNs
a: polymer coated MSNs in the presence of varying concentrations of GSH b: polymer coated MSNs with different crosslinking densities in the presence of 5mM.[5]

molecules conjugated to it. An example of this method noncovalently coated MSNs in "biocompatible self-crosslinkable random copolymer containing pyridine disulfide hydrochloride (PDS) and poly-ethylene glycol (PEG) as side chains"[5] using a one-pot method. PEG was added to increase water solubility of the NPs. Cyclic (Arg-Gly-Asp-D-Phe-Cys) or cRGDfC was used as a targeting agent for cancerous cells and DOX was loaded as a model drug. The polymers broke down in the presence of GSH. The release studies, shown in Figure 2.12, proved that the more highly crosslinked polymers required more GSH to release the same amount of drug, allowing the MSNs to be customized to the treatment needs. After this, the polymer coating was tested on MSNs with a different morphology and the same result were observed.[5] Next the polymer coated MSNs were tested against a human nasopharyngeal carcinoma cell line (KB cells). To do so, a targeting molecule decorated polymer and a non-decorated polymer were used to encapsulate MSNs. Then CLSM and an MTT assay were used to determine the effectiveness of these gatekeepers. The CLSM made it clear that the targeting molecule greatly increased the ability of the MSNs to enter the cells (clear from the increased red fluorescence).

The MTT assay also reflected this showing a cell viability difference of nearly 20% at the highest concentration of MSNs. The cell viability assays can be seen in Figure 2.13. similar results were observed when then MSNs were loaded with cisplatin in place of DOX.[5] Overall, the *in-vitro* results of this study encourage more research of these tunable polymers coatings. They also emphasize why not only polymer gatekeepers, but degradative gatekeepers as whole are so diverse.

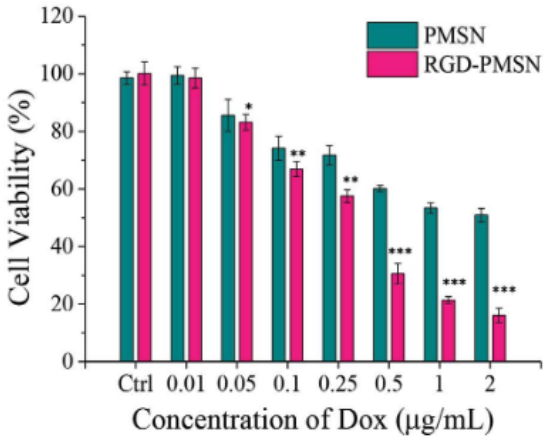

Figure 2.13: Cell viability assay of polymer coated MSNs. PMSN represents polymer coated MSNs that did not have the targeting molecule attached. RGD-PMSN are those that did have the targeting molecule attached.[5]

Summary

As summarized in this chapter, gatekeepers can be extremely diverse. They can provide triggered release under an array of methods including pH changes, light irradiation, and response or degradation to specific molecules within the body. Within each of categories there is more diversity still. There is degradation, conformer change, cleavability and more. Each having its own set of advantages and disadvantages. pH dependence for example could still result in release in healthy cells due to the acid nature of lysosomes. Light irradiation is greatly limited by the penetration depth of the given wavelength, but that does not render it useless. It could, for example, be used to treat melanoma where the penetration depth would be more than adequate. As for bioresponsive gatekeepers, they can be triggered by specific molecules or enzymes that are over expressed in cancerous cells, but these are naturally occurring in healthy cells as well, making the system less than 100% failproof. All of these modifications, even with their flaws, have higher specificity that the commonly used chemotherapeutic agents available today.

Through further investigation, it is possible to employ multiple of these methods into a single gatekeeper. A multi-stimulus system could improve specificity and biocompatibility further, creating an active targeting drug delivery system. The broader impact of these systems is not limited to cancer treatment. MSNs can be loaded with a variety of drugs, allowing them to treat an umbrella of diseases. The incorporation of smart gatekeepers could also allow drugs already used to be delivered with more accuracy, allowing smaller dosages to enter the body. Altogether, the use of MSNs as delivery vessels is become more and more promising with enhancements of gatekeepers.

Chapter 3 - MSNs Developed for Treatment of Bacterial Infections

Recently in the Bossmann group a one-pot method for MSNs was developed by Dr. Hongwang Wang. The method dramatically increased the loading efficiency of the NPs and opened the door for new loading procedures. This chapter will discuss the fine-tuning of benzalkonium chloride containing MSNs, proposal and synthesis of novel surfactants, construction of MSNs around these surfactants, as well as a gatekeeping system.

Preliminary studies and relevant background

Benzalkonium Chloride MSNs

Synthesis

To synthesize 100nm in diameter nanoparticles approximately 500mg of BAC is combined with 4.8ml NH_4OH (28-30%), 20ml of ethyl acetate and 300ml of D.I. water. This was stirred at room temperature for 10 minutes until a clear solution formed. Then 500µl of tetraethyl orthosilicate (TEOS) was added while stirring vigorously. The reaction mixture was heated to 60^oC and allowed to stir for 12 hours. Once the solution cooled to room temperature the white precipitant was collected using centrifugation (10000rpm, 10min), washed with approximately 5ml of D.I. water three times, and then washed with 5ml pure ethanol three times.

Next MSNs with NH_2-functionalized surfaces were synthesized. To synthesize 50nm nanoparticles 273mg of BAC was mixed with 350µl of 2M NaOH solution and added to 120ml of D.I. water. This solution was heated to 80^oC while stirring for 30 minutes. Then a mixture of 700µl TEOS and 100mg (3-Aminopropyl)triethoxysilane (APTES) was added dropwise. The reaction mixture was allowed to stir at 80^oC for 18 hours and then cooled to room temperature. Again, the white precipitant was collected using centrifugation (10000rpm, 10min), washed with 5ml D.I. water three times, and then washed with 5ml pure ethanol three times.

Changing the concentration of starting reagents and the length of time the reaction mixture was allowed to stir affected the size of the resulting MSNs. These MSNs were characterized using various methods. To remove the templating agent from them MSNs for control purposes, 500mg of the MSNs were stirred in a solution of 5ml of concentrated hydrochloric acid (HCl) and 45ml of absolute ethanol under reflux for 2 hours. The MSNs were then collected using centrifugation (10000rpm, 10min), and washed with D.I. water three times, and ethanol three times. The collected material was dried under high vacuum overnight and stored in a desiccator.

Characterization

The morphology and size of the MSN samples were characterized by Transmission Electron Microscopy (TEM) and Scanning Transmission Electron Microscopy (STEM). The TEM samples were prepared by immersing carbon-coated 200-mesh copper grids in the solution MSNs followed by washing the grids with dropwise chloroform and dried overnight in a desiccator. High resolution TEM are recorded on FEI Tecnai F20XT, 200kV; FEI, Hilsboro, OR. The hydrodynamic diameter and the zeta potential of the MSNs were measured on a ZetaPALS zeta potential analyzer (Brookhaven Instruments Corporation) by hydrodynamic light scattering (DLS) and laser Doppler electrophoresis. DLS measurements were recorded directly on MSN aqueous suspension at neutral pH.

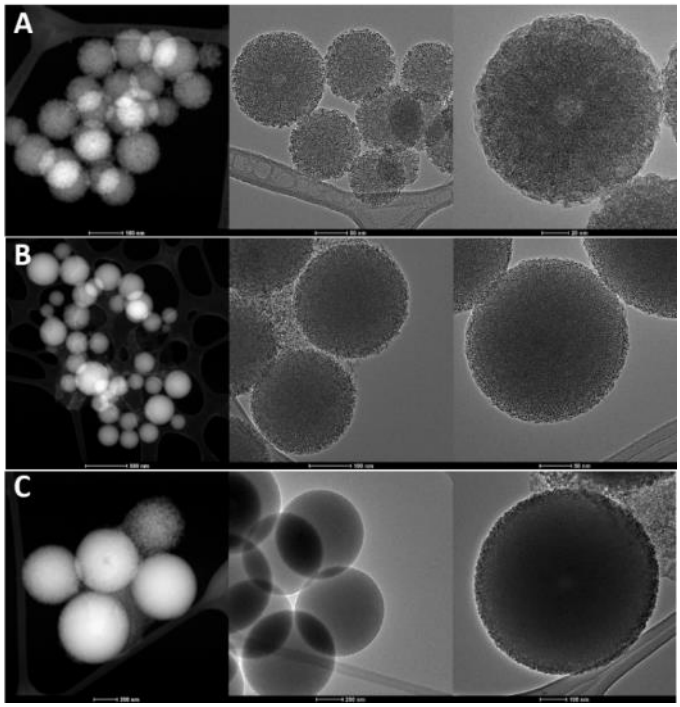

Figure 3.1: STEM and TEM of BAC templated MSNs: (A) 100nm MSNs, (B) 250nm MSNs, and (C) 750nm MSNs.

Thermogravimetric analysis (TGA) of MSNs were performed on a Shimadzu TGA-50 Analyzer. Approximately 5mg of each sample was heated under a stream of dry nitrogen (10 mL/min) from 25 °C to 700 °C at a heating rate of 5 °C/min.

The BAC templated MSNs (BACMSNs) without NH_2-functionalization were spherical in nature and had defined pores. Their size could be manipulated from 100 ± 15nm to 250 ± 20nm, and further to 750 ± 20nm by varying the concentration of BAC and/or silica precursor) of the BACMSNs were found to be 138 ± 10nm, 250 ± 15nm, and 741 ± 25nm respectively (Figure 3.2. Surprisingly, the zeta potential revealed the nanoparticles to have a large negative surface charge (ranging from -20mV to -50mV). This charge is not usually ideal for cell association. When attempting to load traditional MSNs with BAC, achieving high loading efficiency was difficult with the best results being around 1% (w/w). The BACMSNs however were found to have 16.2%, 19.2%, and 23.1% for the 100nm, 250nm, and 750nm MSNs respectively when analyzed using TGA (Figure 3.2).

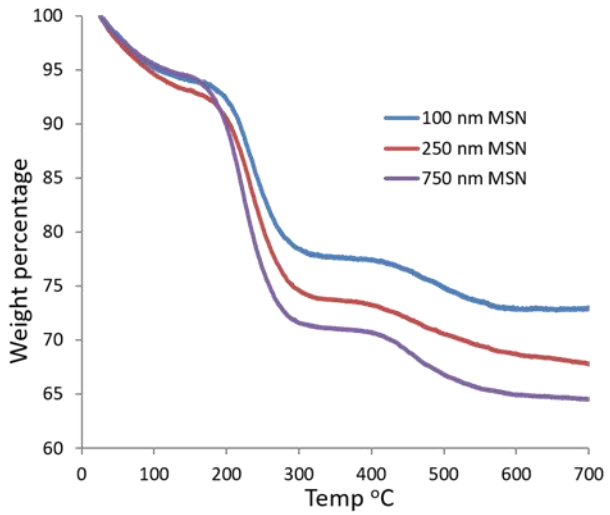

Figure 3.2: TGA of 100nm, 250nm, and 750nm BAC templated MSNs.

The spontaneous release was tested by adding 10mg of BACMSN to 10ml of Lennox broth (LB) and incubating at 37°C for 48 hours. The nanoparticles were collected using centrifugation (10000rpm, 10min), then washed with D.I. water. The recovered nanoparticles were lyophilized to dryness. By comparing the TGA results of the as prepared MSNs, we found 34.2%, 33.5%, and

42.5% of BAC leached out of the MSNs after 48 hours incubation for 100 nm, 250 nm, and 750 nm MSN respectively (Figure 3.3).

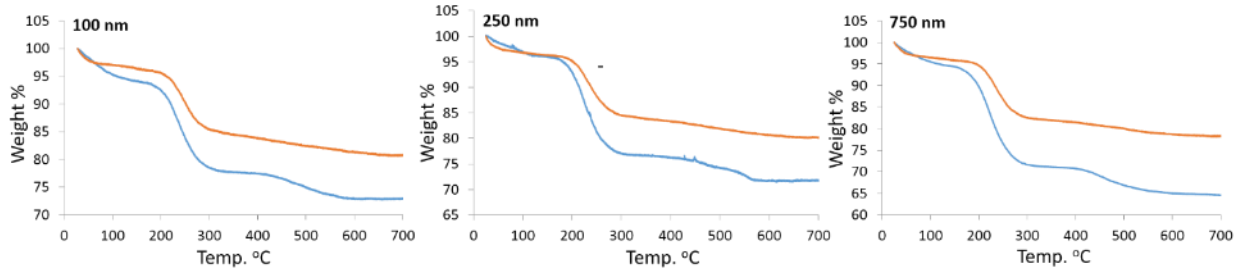

Figure 3.3: TGA of BACMSNs before (blue) and after (orange) incubation in LB broth

The APTES-added-BACMSNs were characterized in the same manner. The addition of APTES served to make functionalization of the resulting MSNs possible. It is necessary for introduction of functional moieties, such as gatekeepers, targeting antibodies, peptides, or dyes. The amino groups are usually graphed on the surface of MSNs by addition of APTES into MSN suspension under reflux condition. Once this reaction is complete the MSNs are washed several times to remove reactants. The BACMSNs, however, would lose BAC content during this process. That is why the APTES was mixed with the TEOS and used as one of the silica precursors. TEM and STEM characterization showed monodispersed spherical MSNs. The size of the particles again could be controlled by the concentration of BAC and/or silica precursors. By doubling the reactants concentration, the size of the particles was increased from 50 ± 5nm to 200 ± 10nm (Figure 3.4). Zeta potential measurements showed that the as synthesized MSNs possessed slightly positive surface charge which could be considered more ideal for a drug delivery vessel. A large positive surface charge was observed for acid-washed MSNs which confirmed the presence of amino group on the surface of MSNs prepared by this method. TGA showed the loading efficiency was over 20% for both 50nm and 200nm sized MSNs (Figure 3.5).

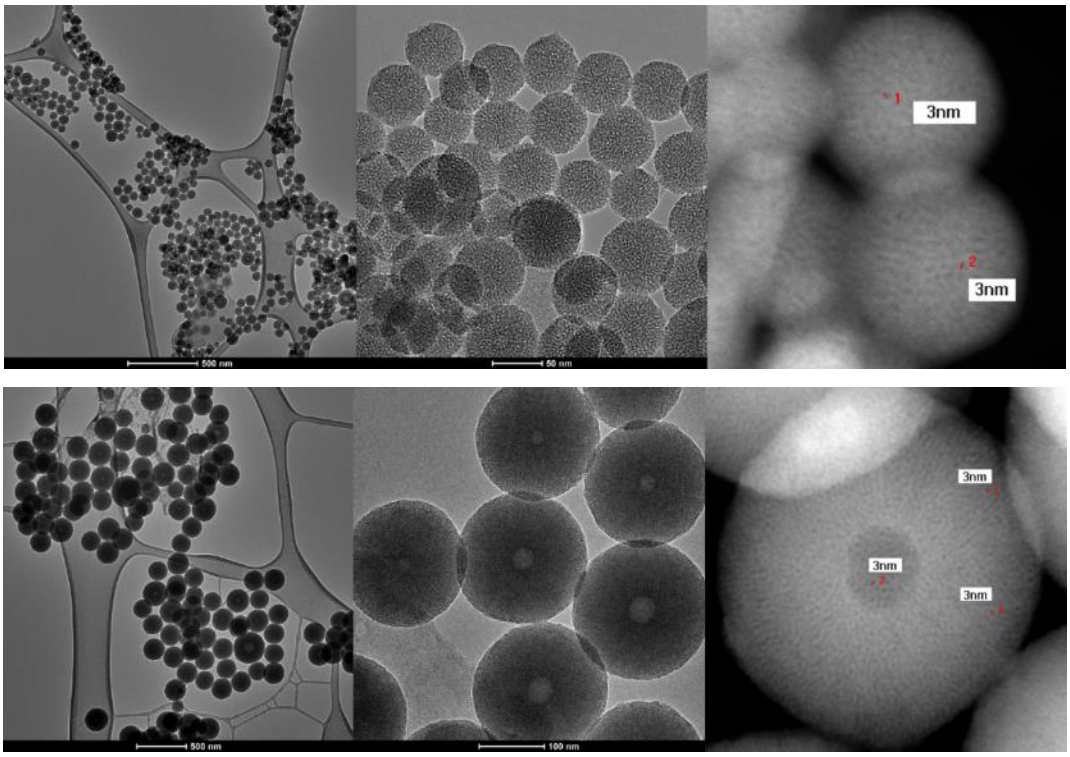

Figure 3.4: TEM and STEM for BACMSNs featuring amino groups on their surface.

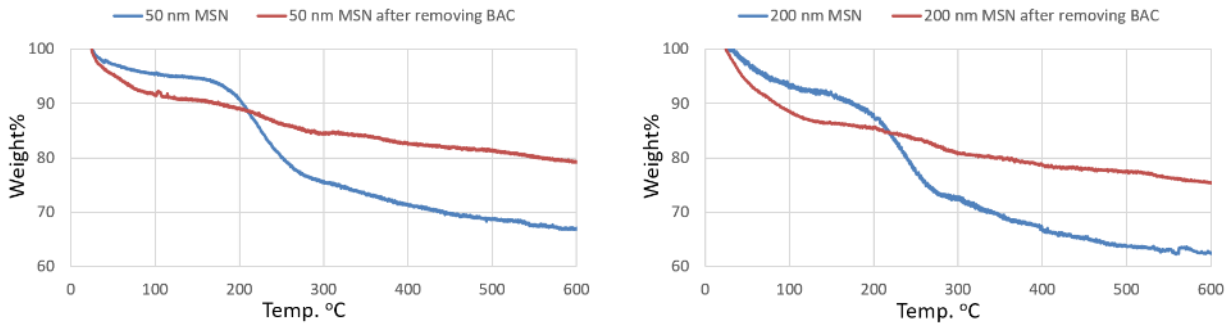

Figure 3.5: TGA of BACMSNs featuring amino groups on their surface, before (blue) and after (red) acid wash.

In-vitro studies

In-vitro testing began in the Bossmann lab. The BACMSNs were tested against *Micrococcus luteus.* This is a great module organism for multi-drug resistant bacteria because it is difficult to kill, but *M. luteus* is not considered dangerous to work with. A liquid culture of *M. luteus* was prepared by inoculating 100ml of LB with one isolated colony of *M. luteus.* The culture

was incubated at 37°C for 48 hours to allow growth. One solution of BACMSN, acid washed MSNs, and BAC only were prepared by dissolving 2mg of MSN or BAC in 10ml of D.I. water by sonication for 15 minutes at 25°C. These concentrated solutions were further diluted to obtain 50ml of two lower concentrations of 0.005 and 0.003mg/ml MSNs or BAC. After, 500mg of LB broth and 250mg of agar were added to each solution. Control LB agar solution was also prepared with no MSNs or BAC added. These solutions were autoclaved at 121°C for 30 min under 15 psi of pressure. Once cool enough to handle, the LB agar was poured into plastics petri dishes to let solidify. Plates were incubated at 37°C overnight to ensure they had not been contaminated. A liquid culture of *M. luteus* was diluted to $6x10^{-9}$ its original concentration. This was done to observe isolated, countable colonies. The petri dishes were inoculated using 100µl of the diluted solution. The dishes were incubated at 37°C for 48 hours to allow growth. After 48 hours of incubation, pictures were taken to compare growth, and isolated colonies were counted on the dishes that had growth. Growth was not observed at concentrations of 0.005mg/ml BACMSN and higher.

The minimum inhibitory concentration or MIC of a drug is the minimum concentration needed to inhibit growth of bacteria. The MICs of the BACMSNs against several strains of bacteria were determined in the Wolschendorf lab at the University of Alabama, Birmingham. The experiment utilized an OD600 experiment. To test susceptibility towards nanomaterials, individual colonies from plates were transferred into 3ml of MH-broth. From here cultures were grown for 6 hours while shaking at 37°C, then OD600-normalized in MH-broth to prepare the inoculum for the susceptibility assay. After preparing 2-fold dilutions in MH-broth on a 96-well plate, the nanoparticles reached a maximum final concentration of 250µg/ml to a minimum of 1.95µg/ml. The inoculum (OD600=0.002) was then added to the wells containing the nanomaterials for a final OD600 of 0.001. Test plates were incubated for 14 hours at 37°C. After which the bacterial growth

was examined by reading OD600 using a Cytation3 plate reader (BioTek). For measure of bactericidal activity, 5µl of the resuspended well-contents were spotted onto MH-agar and incubated overnight at 37°C prior scanning the plates with an Epson V800 Photo. Data were analyzed using Gen5 (v3.02) software (BioTek) and Excel. The results of this experiment can be summarized in the chart below (table 3.1). The BACMSNs had excellent results with *Staphylococcus aureus*, with MICs as low as 3.8µg/ml. Methicillin-resistant *S. aureus* (MRSA) also showed susceptibility with MICs ranging from 3.8-15 µg/ml. Unfortunately, *Pseudomonas aeruginosa*, gram-negative bacteria, showed no susceptibility to the drug. Although the MIC values were not as low as desired, the fact that *Acinetobacter baumanii* showed any susceptibility is exciting because *A. baumanii* is known for its multi-drug resistance.

Collection#	Strain	MIC
1510	*S. aureus*	3.8
1511	*S. aureus*	3.8
1513	*S. aureus*	3.8
1515	*S. aureus*	3.8
1471	*S. aureus* (Newman)	3.8
1508	*S. aureus* (MRSA)	15
1509	*S. aureus* (MRSA)	15
1512	*S. aureus* (MRSA)	7.5
1516	*S. aureus* (MRSA)	15
1517	*S. aureus* (MRSA)	7.5
1518	*S. aureus* (MRSA)	3.8
1520	*S. aureus* (MRSA)	7.5
1522	*S. aureus* (MRSA)	7.5
1523	*S. aureus* (MRSA)	15
1529	*S. aureus* (MRSA)	15
1300	*Pseudomonas aeruginosa*	250
1301	*Pseudomonas aeruginosa*	250
1302	*Acinetobacter baumanii*	15

Table 3.1: The minimum inhibitory concentration (µg/ml) of BACMSNs against various strains of bacteria.

Quaternary Amines

Single headed

Due to the outcome of the BACMSN *in-vitro* studies, other surfactants with biocidal or antimicrobial properties were investigated, starting with single-headed quaternary amines. Single headed surfactants are the oldest known surfactants. Their use varies largely depending on the length of the hydrophobic tail. Single headed cationic surfactants can also have two tails. An example of the simple synthesis of a single head, single tailed surfactant is shown below in Figure 3.6. This surfactant showed moderate activity toward *Escherichia coli* (gram-negative) and *S. aureus*. Surprisingly, this surfactant had great activity toward two different fungi species,

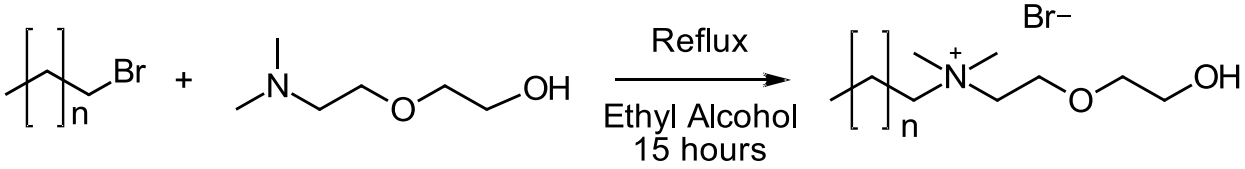

Figure 3.6: Synthesis of Single head cationic surfactants containing free hydroxyl group. n=6, 10, and 14 for total chain lengths of 8, 12, and 16 hydrocarbons.[23]

Aspergillus flavus and *Candida albicans.* When the free hydroxyl group of the head was not present, like the surfactant depicted in Figure 3.7, activity toward fungi was lost and only low-moderate activity against bacteria was observed, making it clear that the free hydroxyl group is of importance to activity.[23,36] This also called into question the lengths of the hydrophobic chains. In both cases there appeared to be a "cut off" length, meaning that activity increased as the chain length increased to a point. This cut off appeared to 12 carbons in length. Overall, single headed surfactants are some of the "simplest" surfactants, for this reason their activity is not spectacular and could likely be improved.

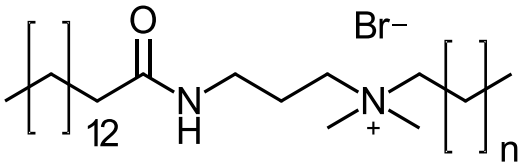

Figure 3.7: Structure of single head/double tailed cationic surfactants containing an amide. n=8, 10, and 14 for total chain lengths of 10, 12, and 16 hydrocarbons.[36]

Gemini Surfactants

Double headed surfactants are considered the stronger, better versions of their single headed predecessors. They are generally symmetrical molecules giving them the name "gemini." These molecules can be connected either with or without a spacer. Two types of gemini cationic surfactants were examined. Their structures are shown in Figure 3.8. They are close to the gemini equivalents to the two single head surfactants previously discussed.[22,23] One clear difference between the two gemini surfactants is that in one the hydrophobic tail is increased and in the other the hydrophobic spacer is increased. Both increase the hydrophobic nature of the surfactant and thus increase their activity. The amide containing compound even possessed activity toward fungi. The cut off effect was still observed for the amide containing compounds, but not for the compounds containing free hydroxyl groups. This may be because the length of the spacer did not exceed 12 carbons, which appears to be the "sweet spot". Again, it was observed that having a free hydroxyl group is superior for functionality making it a great candidate for further research.[22,23] When changing the head group of a surfactant it is important that the head is not too rigid. It commonly accepted that head groups containing more polar molecules (oxygen and nitrogen) are more active. Amides, however, can vary depending on tail components.[37] When increasing tail length, a common trend is observed. Increased tail leaded to a decreased MIC or better activity. Halogenated tails showed an increase in activity. The spacers for gemini surfactants

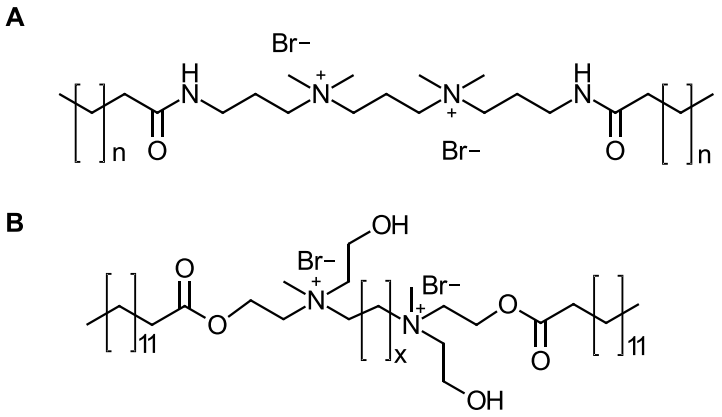

Figure 3.8: Structure of gemini cationic surfactants. A. gemini cationic surfactants containing amide groups where n=5, 9, and 13. B. gemini cationic surfactant containing free hydroxyl groups where x=1, 5, and 11 for total spacer lengths of 2, 6, and 12.[22,23]

can vary greatly as well. Spacers containing esters, like PEG, are suitable for antimicrobial compounds.[22,23,48] Double headed surfactants are not required to be symmetrical. Asymmetric or hetero-surfactants open the door to a plethora synthesizable compounds, which may lead to the discovery of stronger activity and better degradative abilities. This portion of the field is rapidly expanding as more attention is draw to the capabilities of double headed/two tailed surfactants.

Addition of semi-fluorinated carbon chains

One drawback of the cationic surfactants like BAC or the gemini surfactants described above was their lack of strong activity toward *P. aeruginosa*, a gram-negative bacterium. Gram-negative bacteria are more difficult to kill due to their double membrane. Using *P. aeruginosa* as a model, one study explored changing the hydrocarbon chains of standard gemini surfactants to semi-fluorinated carbon chains. The study found that the addition of the semi-fluorinated chains drastically decreased the MIC in comparison to the traditional surfactants.[38] This strategy could be used and tested against other gram-negative bacteria to see if it is equally as effective.

Rational Design of Novel Surfactants and Cleavable Gatekeeper

Surfactant Library

Taking into consideration the previous studies, a small surfactant library was proposed. The surfactant designs are located in Table 3.2. These designs combine the structure of BAC with new functional moieties that should increase the activity against gram-negative bacteria. In the preliminary studies it was observed that the free, terminal hydroxyl group increased the broad-spectrum activity. For this reason, all surfactants, excluding surfactants **G** and **H**, include at least one of these moieties. Also, it was discussed that Gemini surfactants have been more effective than their single headed counter parts, to test this theory both the single headed and double headed surfactant pairs were proposed. The pairs will be surfactants **A** and **B**, **C** and **D**, **E** and **F**, and **G**

and **H**. Surfactants **E-H** will explore the use of semi-fluorinated chains in broad-spectrum applications. It was hypothesized that surfactants **C** and **E-H** will shed light on the importance of the free hydroxyl group versus the semi-fluorinated chain. Surfactant **I** would investigate a triple headed molecule. These surfactants were also prosed to replace BAC within the MSN structure.

A 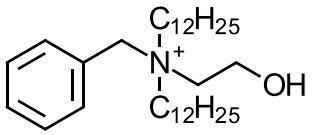	**B** 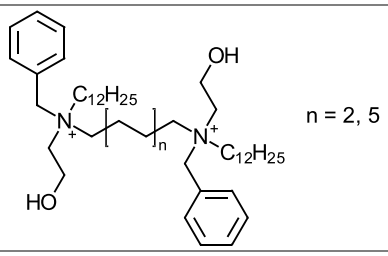
C 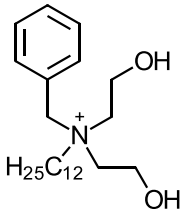	**D** 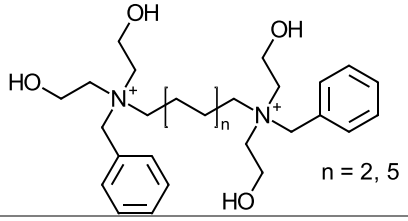
E 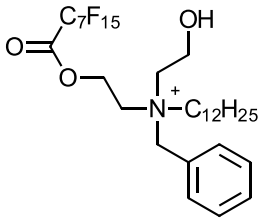	**F** 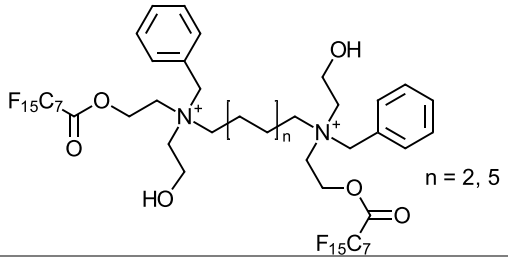
G 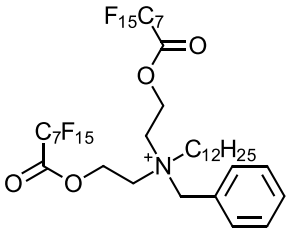	**H** 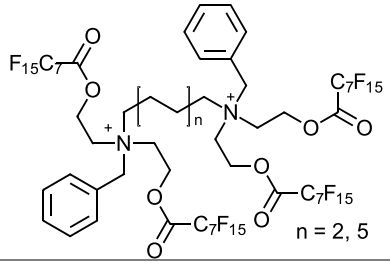
I 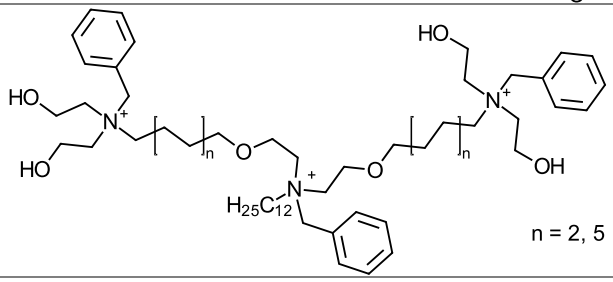	

Table 3.2: Potential surfactant variants for small surfactant library. Chloride counter ions omitted.

Gatekeeping System

After synthesis of the surfactants, the next logical step of the project would be to test their activity against multi-resistant bacterial strains. Then the surfactants with adequate activity would be incorporated into MSNs using a one-pot synthesis method modified from that of the BACMSNs. Finally, using the information gathered about gatekeepers the following peptide gatekeeper was proposed (Figure 3.9). The peptide contains two protease cleavage points. One is cleavable by cathepsin B and the other is cleavable by Matrix metallopeptidase 9 (MMP-9). The rational for these two cleavage points was that MMP-9 is often highly expressed in areas of inflammation which is the body's first response to infection[34]. Cathepsin B is a well-known, cysteine protease[35] which was chosen because it is found in the lysosomes of cells, including defense cells, which my take up the MSNs more rapidly. This is the "fail-space" plan, which increases the chance of release, even if the MSNs were to be endocytosed into the cell before cleavage of the gatekeeper occurred. The two cleavage points in the designed peptide are potentially able to be cleaved by either enzyme and other proteases that have weak affinity for the designed sequence. Typically, this non-specific trait may be disadvantageous, but in this case, it is an advantage because it increases the likelihood of release in the desired location because other proteases are upregulated during infection and/or pain. The peptide's design includes vancomycin anchored to the N-terminus of the chain via the free carboxylic acid on vancomycin labeled in red

Figure 3.9: Proposed gatekeeping system for anti-microbial MSNs containing protease cleavable, peptide linker.

in Figure 3.10. This large molecule is the major steric or "bulk" provider for the gatekeeper, keeping the cargo in place, but is also a well-known antibiotic that once cleaved can provide dual treatment. There have been documented cases when the free hydroxyl group of vancomycin was coupled with a peptide to improve drug activity[39,40], therefore it is assumed that the vancomycin will retain its activity even if a small portion of the peptide chain remains attached. The opposite end of the peptide would be covalently anchored to the MSN surface. The final product would be MSNs containing newly synthesized surfactants, coated with the cleavable peptide gatekeeping system.

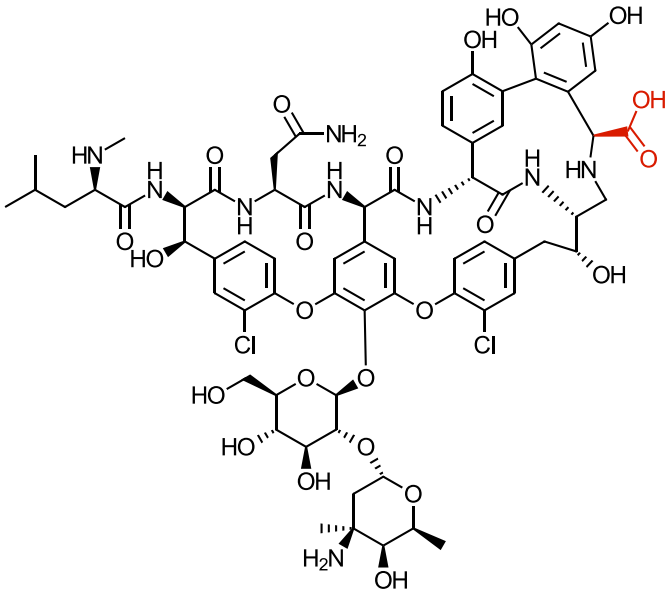

Figure 3.10: Structure of Vancomycin.

Using bioinformatic software the cleavage sequence for MMP-9 was determined to be Gly-Pro-Ala-Gly–Lue-Ala-Gly-Ala (GPAG-LAGA) with the cleavage point indicated by the large dash. The cleavage sequence for cathepsin B was determined to be Gly-Lue-Ala-Gly–Lue-Val-Gly-Gly (GLAG-LVGG). Then a combined, extended sequence with increased solubility was determined to be Gly-Ser-Lue-Ala-Gly–Lue-Val-Gly-Pro-Ala-Gly–Lue-Ala-Gly-Ala-Gly-Ser-Gly (GSGLAG-LVGPAG-LAGAGSG). The prediction software predicted an amorphous structure that should allow easy cleavage by MMP-9 and cathepsin B (Figure 3.11).[41]

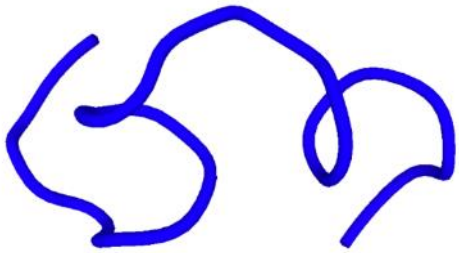

Figure 3.11: Predicted structure of protease cleavable linker.

Materials and Methods

Surfactant Synthesis

Of the proposed surfactants, four were successfully synthesized and characterized. These included SA, SB6, SB12, and SC. Two variant surfactants were also synthesized. These were denoted as Variant 1 (V1) and its Gemini counterpart, Variant 2 (V2).

Surfactant A (SA)

Surfactant A was synthesized following a method adapted from S.M. Shaban *et al.* (2016), in which 0.007mol N-benzylamino ethanol (N-BAE) and 0.021mol 1-bromododecane were dissolved in 100ml of absolute ethanol. The solution was refluxed for 24 hours. The solvent was then removed via rotovap. The yellow precipitate, N,N-didodecylbenzyl-2-hydroxyethan-1-aminium bromide, was washed two times with 5ml diethyl ether. After washing the precipitate was white. The product was recrystallized in ethyl acetate. The reaction scheme is shown below in Figure 3.12.

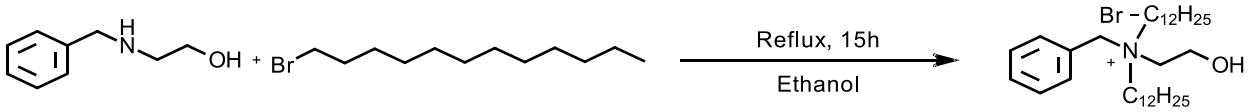

Figure 3.12: Reaction scheme for Surfactant A

Surfactant B-6 (SB6)

Again, a method adapted from S.M. Shaban *et al.* (2016) was employed. This time 2.285ml of 1-bromododecane and 0.755ml of 1,6-dibromohexane were dissolved in 35ml of absolute ethanol and brought to approximated 80^{o}C before adding 1.4ml N-BAE was added. The solution was the brought reflux and allowed to stir for 72 hours. After cooling to room temperature, the solvent was removed under vacuum and the gel like product, N,N'-bis(2-hydroxyethyl)-N,N'-dibenzyl-N,N'-didodecylhexan-1,6-diaminium bromide, was rinsed with diethyl ether. Recrystallization was attempted using a variety of solvents, all of which failed to recrystallize at

room temperature and at 0°C. So, the product was left slightly impure. The product was orange in color and gel-like.

Surfactant B-12 (SB12)

SB12 was synthesized following the same method described for SB6, but using 2ml of 1,12-dibromododecane in the place of 1,6-dibromohexane to produce N,N'-bis(2-hydroxyethyl)-N,N'-dibenzyl-N,N'-didodecyldodecan-1,12-diaminium bromide (SB12). The product was a deep orange in color and gel-like.

Surfactant C (SC)

SC was synthesized by dissolving 0.015mol of 1-bromododecane and 0.015mol of benzyl bromide in 50ml absolute ethanol. Once the solution was approximately 80°C and the solution was clear, 0.01mol of diethanol amine was added while stirring rapidly. The solution was brought to reflux and stirred for 48 hours. Once cool the solvent was removed under vacuum, the product was washed with diethyl ether, and then placed on the vacuum line overnight. Again, the product was a gel-like substance and light orange in color.

Variant 1 (V1)

Due to the reagents available a variant surfactant was synthesized by dissolving 960µl diethanol amine and 1-bromododecane in excess in 50ml of acetone. The solution was refluxed for approximately 72 hours while stirring. Once the solution was cool, the solvent was removed under vacuum and the product was rinsed with diethyl ether. The product was yellow in color and resembled dish soap.

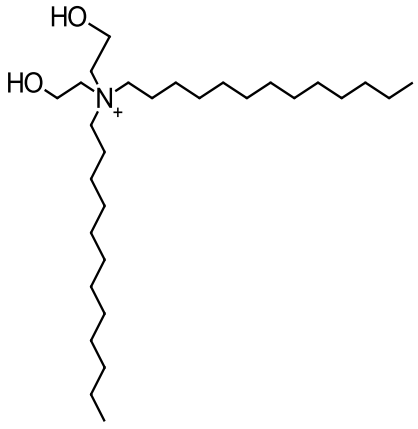

Figure 3.13: Structure of Variant Surfactant 1 (V1).

Variant 2 (V2)

For synthesis of V2, 0.01mol of 1-bromododecance and 3.7mmol of 1,12-dibromododecane were dissolved in 50ml absolute ethanol. Then 0.0151mol of diethanol amine was added to the flask. The solution was brought to reflux and stirred for 24 hours. Once the solution was cool, the solvent was removed under vacuum and the product was rinsed with diethyl ether. Again, the product was a translucent gel, but this time was slightly opaque.

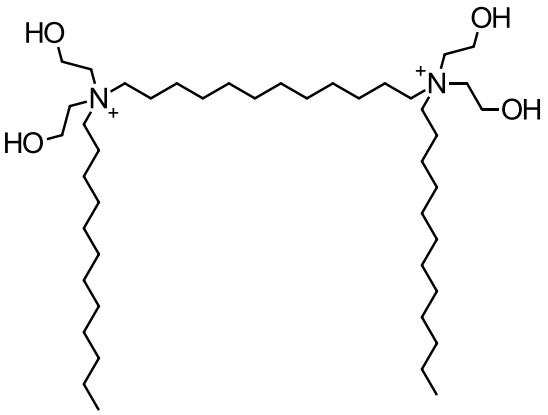

Figure 3.14: Structure of Variant Surfactant 2 (V2).

MSN Synthesis

As proof of concept, MSNs were first constructed around V1. V1 was chosen because it had better water solubility than other synthesized surfactants and had moderate activity against *Micrococcus luteus*. In 100ml diH_2O, 275mg of V1 was dissolved and 0.35ml 2M NaOH was added. This was stirred at 80^oC for 20 minutes. Then 700µl TEOS was added and the solution was stirred overnight. The cloudy white precipitate that formed was collected via centrifugation (10min, 10000rpm), then washed 3 times with 5ml of diH_2O. The product was then suspended in 10ml of diH_2O using sonication and frozen prior to being lyophilized.

The MSNs were also synthesized using a modified Tween 80 procedure. The a 5mg/ml surfactant in diH_2O solution was made. Then 5ml of this solution was placed in a flask with 1.5ml of 0.01M NaF. This solution was diluted to 50ml with diH_2O and heated to 60^oC. This solution was stirred for 15 minutes to allow for the formation of micelles. Then 500µl TEOS was added

dropwise. The solution was stirred for approximately 18 hours. Then the cloudy white precipitate was collected via centrifugation (10 minutes, 10000rpm). The precipitate was washed three times with 5ml diH_2O and three times with 5ml ethanol before being lyophilized.

Acid Wash Procedure

For controls, the MSNs were acid washed to remove the surfactant templates. This was done by taking approximately 30mg of the MSN and suspending them in a solution of 4ml absolute ethanol and 1ml concentrated HCl. This was refluxed with stirring for two hours. Once cool, the MSNs were collected via centrifuge (10min, 10,000rpm) then washed three times with diH_2O before being lyophilized.

Gatekeeper Synthesis

The gatekeeping system was synthesized by first synthesizing the peptide chain. This was done using solid phase peptide synthesis (SPPS). An insoluble resin loaded with glycine was swollen in methylene chloride (DCM). After removing the resin was then washed with 5ml of dimethylformamide (DMF). The first amino acid (F-moc protected) to be added, which is the second in the chain was weighed in a 1:3 molar ratio to the resin and HBTU, the coupling agent, was weighed in a 1:2.9 molar ratio to the resin. These were dissolved together in approximately 8ml of 1:23 N,N-Diisopropylethylamine (DIEA) in DMF and added to the peptide synthesis tube. This was swirled at room temperature for a half hour. Then drained and repeated. After the second half hour, the resin which now contained a two-peptide change was rinsed five times with 3-5ml DMF. Then 4ml of 20% diethylamine in DMF, the F-moc cleaving reagent, was added to the tube and swirled for 1 minute then drained. Another 4ml of 20% diethylamine was added and this time swirled for 10 minutes and drained. The resin was the carefully rinsed with DMF five times before adding the next amino acid in the same manner as the first. This process was repeated for each

amino acid in the chain from left to right until the chain read GSGLAGLVGPAGLAGAGSG-Resin.

Vancomycin contains a free carboxyl acid group. Taking advantage of this vancomycin was dissolved in a 1:2 ration in 1:23 DIEA in DMF with 1:2.9 ratio of HBTU. This was allowed to stir was the final F-moc group was removed from the N-terminal of the peptide. After the peptide chain was rinsed carefully with DMF the solution was added and allowed to stir overnight. Once the reaction was complete the solution was removed, and the peptide chain was washed five times with DMF and then five to six times with DCM before adding the resin cleaving cocktail (95% trifluoroacetic acid, 2.5% TIPS buffer, and 2.5% diH_2O). The cocktail was allowed to swirl for 3 hours. During this time the resin and all side chain protecting groups were removed. The solution was then squeezed into 10ml cool diethyl ether. The precipitate was collected via centrifugation (10min, 10000rpm) and washed three times with cool diethyl ether before being dissolved in 10ml of diH_2O and lyophilized. The vancomycin containing peptide was characterized by HPLC and mass spectroscopy.

Dynamic Light Scattering (DLS) and Zeta Potential

The hydrodynamic diameter and the zeta potential of the MSNs were measured on a ZetaPALS zeta potential analyzer (Brookhaven Instruments Corporation) by hydrodynamic light scattering (DLS) and laser Doppler electrophoresis. DLS and Zeta potential measurements were taken of MSNs in aqueous suspension at neutral pH. Generally, for DLS, 50µl of a 1mg/ml stock would be diluted to 1ml using double distilled water and then read. For Zeta potential 50-80µl of a 1mg/ml sample stock would be diluted to 1.4ml using double distilled water before inserting the meter for reading.

Thermogravimetric Analysis (TGA)

The TGA of MSNs were performed on a Shimadzu TGA-50 Analyzer. Approximately 5mg of each sample was heated under a stream of dry nitrogen (10 mL/min) from 25 °C to 700 °C at a heating rate of 5 °C/min. The data was converted from milligrams lost to weight percent lost.

Transmission Electron Microscopy (TEM) and Scanning Transmission Electron Microscopy (STEM)

TEMs and STEMs were carried out in the Microscopy and Analytical Imaging Laboratory at University of Kansas with the assistance of Dr. Prem Thapa. Several images were taken for each sample.

Bacterial Studies

For studies against *Micrococcus luteus* the experiments were set up by dissolving the surfactant at varying concentrations into 25g/L Lysogeny broth (LB) containing 1% Agar. Then the solution was autoclaved (121 C, 20 minutes) and poured into plastic petri dishes. Each concentration had three replicas made. Once cool, 10µl cultured *M. luteus* was spread on the surface and incubated at 37ºC for 48 hours. Colony forming units (CFUs) where then observed. For the purposes of these trials, growth was denoted as "+" and no growth was "-" and counted as "+" if any of the replicas showed growth.

For studies against methicillin-resistant *Staphylococcus aureus* (MRSA), the surfactants were sent to our sent to our collaborators at UAB and performed in the same manner described in Chapter 3 – Relevant Background and Studies. Minimum inhibitory concentrations were reported in mg/ml. These studies were performed in solution.

High Performance Liquid Chromatography (HPLC)

Peptide purity was determined using HPLC (Ultimate 3000, Thermo scientific). The crude peptide was dissolved in distilled water at a concentration of 1.0 mg/ml. After running a blank, 20µl of the solution was filtered using 0.2µM nylon filters and then injected into the HPLC column (Thermo AcclaimTM 300, C18, 3µm, 2.1 x 150mm). The flow rate was maintained at 0.30 mL/min using a binary mixture. A: water containing 0.10% TFA, B: acetonitrile with 0.10% TFA. Gradient: 1-16min: 20% - 80% B, 16-20min: 80% B. The wavelength used was 205nm.

Results and Characterization

Surfactants

NMR

^{1}H-NMRs were collected for each surfactant and can be seen in Appendix A. The spectra were compared to the simulated NMRs. The real NMRs were slightly shifted due to micelle formation, even in DMSO, and also had a few peaks that were due to the protons being different environments within the micelles and the ones that may have truly been free in solution. There were also small peaks near 9ppm in some of the spectra. These were assumed to be due to water that associated with the molecules.

Fourier-transform infrared spectroscopy

FTIR was also taken for each surfactant. The FTIRs were used to confirm the functional groups present in the surfactant. Below is the FTIR for SA. The spectrum is not extremely clean, but an alcohol peak can be seen at 3300cm^{-1} and the aromatic region is correct. The typical bromo-alkane peaks are also not obviously present, suggesting the starting material is not present.

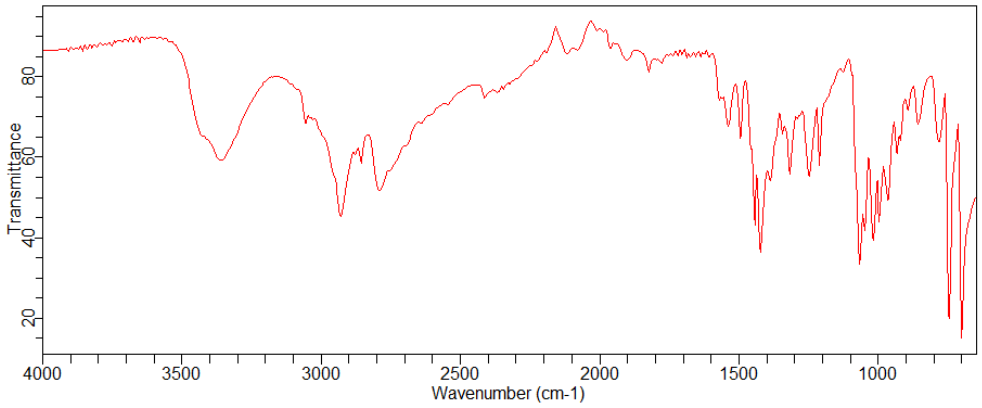

Figure 3.15: IR Spectrum of Surfactant A.

Mass Spectroscopy (MS)

Mass spec. was also used to characterize the surfactants synthesized. MS was performed by the Core Center at University of Kansas Medical. The calculated molecular weights are shown in the table below. The mass spectra for each surfactant gave the expected molecular peak which are shown in the figures following the molecular mass table. The fragmentation peaks also confirmed the molecules synthesized where the desired products.

Surfactant	***Calculated Molecular Weight with Counter Ions***	***Calculated Molecular Weight without Counter Ions***
SA	568.75g/mol	488.85g/mol
SB6	883.01g/mol	723.21g/mol
SB12	967.17g/mol	807.37g/mol
SC	444.49g/mol	364.59g/mol
V1	522.68g/mol	442.78g/mol
V2	875.03g/mol	715.23g/mol

Table 3.3: Calculated Molecular Weights of Synthesized Surfactants with and without Counter Ions.

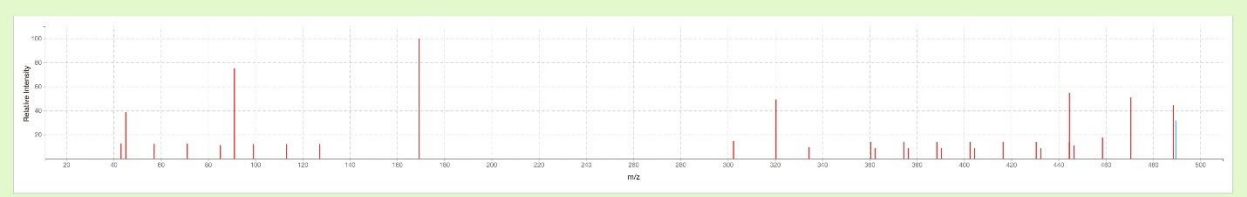

Figure 3.16: Mass Spectroscopy Data for Surfactant A.

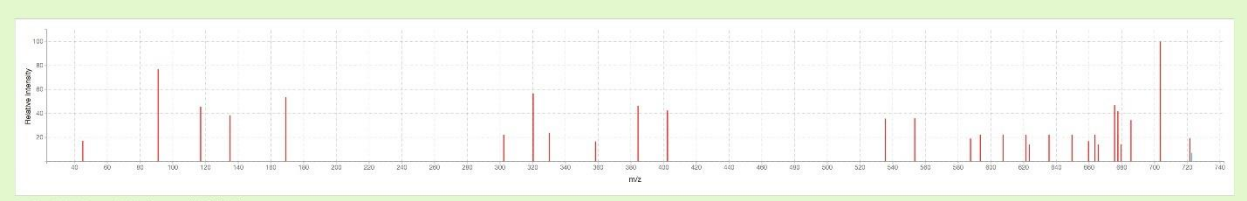

Figure 3.17: Mass Spectroscopy Data for Surfactant SB6.

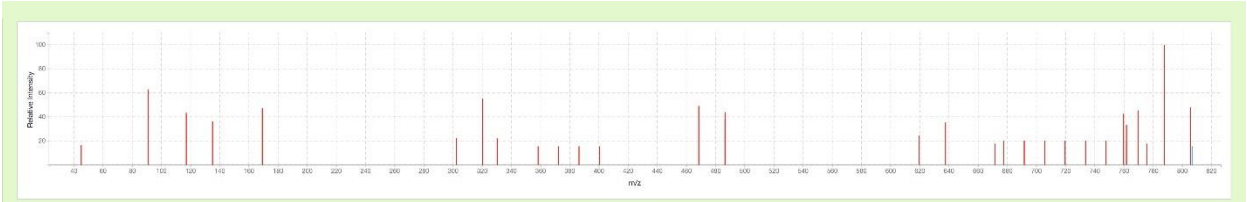

Figure 3.18: Mass Spectroscopy Data for Surfactant SB12.

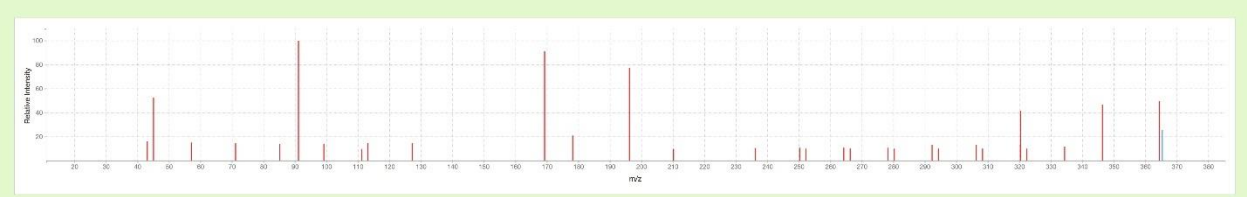

Figure 3.19: Mass Spectroscopy Data for Surfactant C.

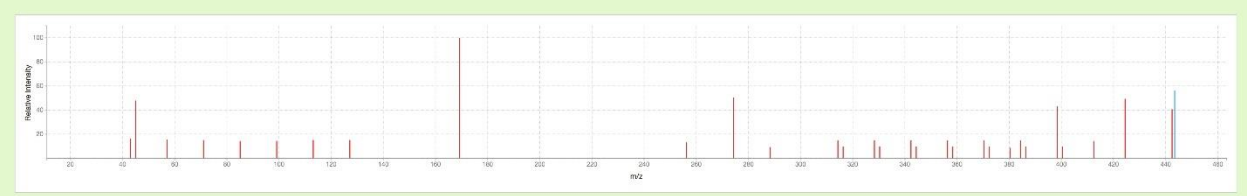

Figure 3.20: Mass Spectroscopy Data for Surfactant V1.

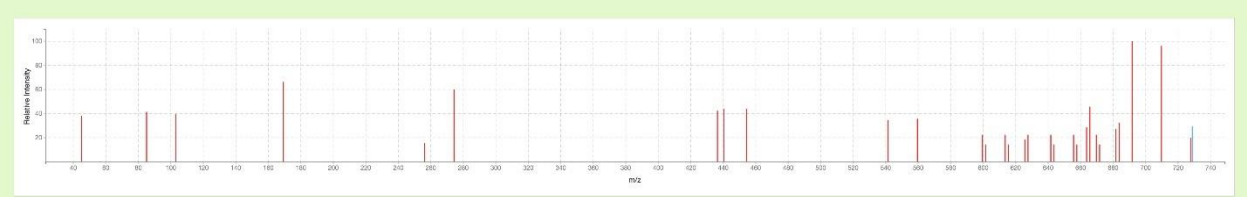

Figure 3.21: Mass Spectroscopy Data for Surfactant V2.

Bacterial Studies

The results for various surfactants against *M. luteus* are summarized in Table 3.3. As expected the Gemini surfactants SB6, SB12, and V2 had the best activity. This confirmed the assumption that Gemini surfactants have increased activity. The synthesized surfactant with the best activity was SB12 which showed activity at concentrations as low as 0.01mg/ml against *M. luteus.* It was assumed that surfactants that did not kill at 1.0mg/ml would not kill at lower concentrations. The 1.0mg/ml trials were repeated twice to ensure growth was observed and then further concentrations were not tested.

	1.0mg/ml	***0.5mg/ml***	***0.3mg/ml***	***0.1mg/ml***	***0.05mg/ml***	***0.01mg/ml***	***0.005mg/ml***
SA	+*	+	+	+	+	+	+
SB6	-	-	-	+	+	+	+
SB12	-	-	-	-	-	-	+
SC	+*	+	+	+	+	+	+
V1	-	-	-	+	+	+	+
V2	-	-	-	-	-	+	+

Table 3.4: Activity of Synthesized Surfactants Against *Micrococcus luteus*.
Growth indicated as "+" and absence of growth indicated as "-".

The surfactants were then sent to UAB for testing against MRSA. The MICs against MRSA directly correlated to those against *M. luteus.* SA and SC showed the lowest activity and SB12 and

V2 showed the best activity. Unfortunately, the best activity was still approximately 10 times that of the common MRSA treatment, Vancomycin.[42]

	SA	*SB6*	*SB12*	*SC*	*V1*	*V2*
MIC (mg/ml)	2.8	0.15	0.027	0.85	0.32	0.038

Table 3.5: Minimum Inhibitory Concentrations of Synthesized Surfactants against Methicillin-Resistant *Staphylococcus Aureus.*

Gatekeeping System

Of the gatekeeping system, the peptide linker was successfully synthesized and an attempt to bind it to vancomycin was performed.

HPLC

The HPLC of the crude peptide indicated that the purity of the peptide would be good enough to move forward to the anchoring of MSNs. There were minor impurities, but the presence of one major peak indicated the successful synthesis of the peptide and coupling of vancomycin.

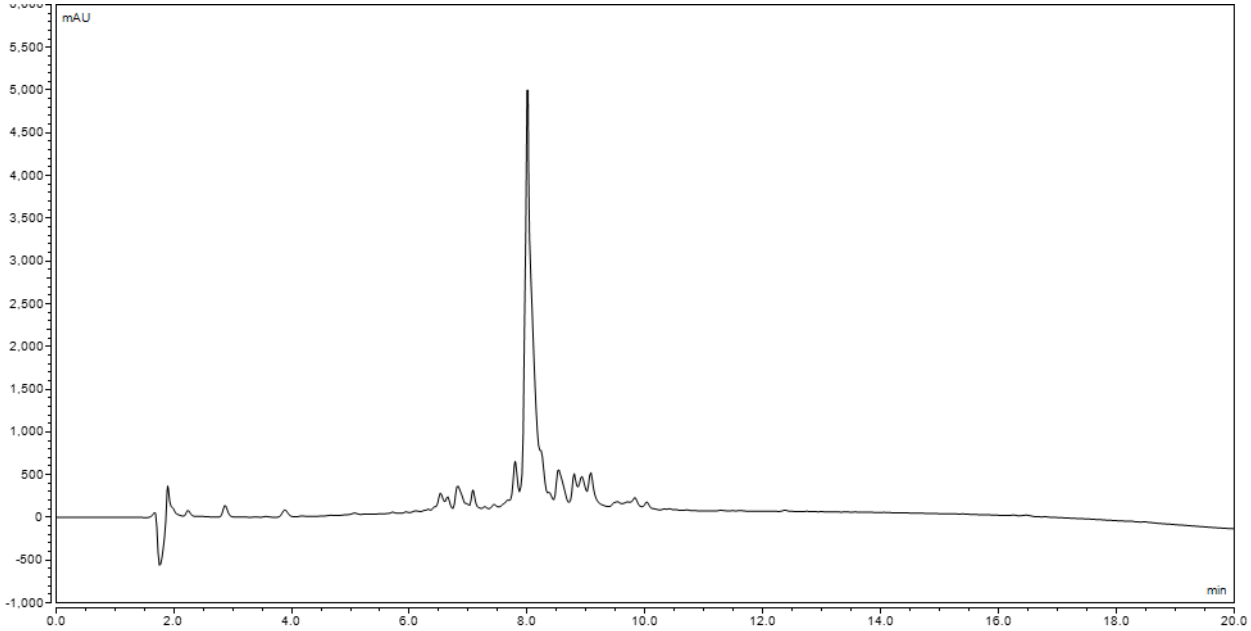

Figure 3.22: HPLC of Gatekeeping Peptide Linker Attached to MSN.

Mass Spectroscopy (MS)

MS was used to determine if vancomycin had truly been attached to the peptide chain. Using a molecular weight calculator at genscript.com the molecular weight of the peptide without vancomycin was determined to be 1468.62g/mol ($C_{62}H_{102}N_{19}O_{22}$). The molecular weight of vancomycin is 1449.3g/mol. Considering that the coupling occurs with a loss of water, the final molar mass was expected to be 2899.84g/mol. The LC-MS showed a major peak around 940. This was not anticipated, but the peak near 2878.46g/mol indicated the desired product after the loss of one terminal glycine unit. This implied vancomycin had successfully been attached to the peptide. The peak at 2822.48g/mol is consistent with a further loss of C4H6 fragment from leucine.

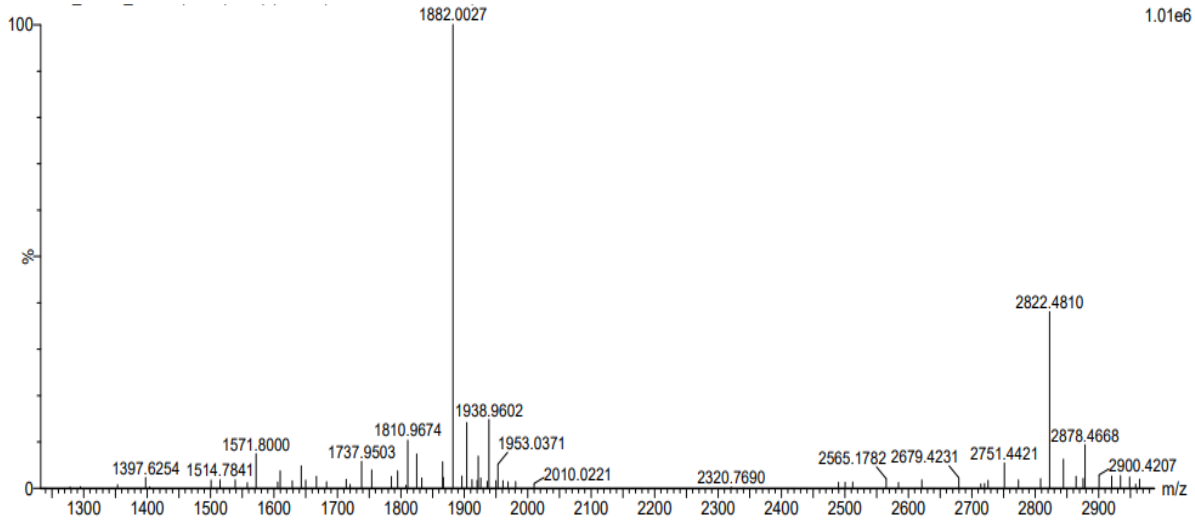

Figure 3.23: Mass Spectroscopy Data for Vancomycin Conjugated Peptide Chain

MSNs

MSN characterization is accomplished using several methods. For the purposes of these studies TGA, DLS, Zeta potential, and TEM. These analyses confirmed the presence of a silica scaffold, as well as incorporation of surfactant.

TGA

The TGA of the MSNs catalyzed by either NaOH or NaF showed differing weight loss patterns. This was the first indication that the morphology of the two samples may be different. Both MSNs had patterns that appeared to follow the weight-lost pattern of the surfactant alone. This was good indication that V1 had successfully been incorporated into the mesoporous structure.

V1MSNs catalyzed with NaOH

In Figure 3.16, the first notable feature is the solvent loss from 0-100ºC. The next is that there is a distinct difference between the control MSNs and the V1-MSNs. This indicated loading. Finally, in the temperature range 100-400ºC the V1-MSNs follow the same pattern as V1 alone. This suggests that V1 is what is loaded into the MSN structure. From the data collected, the weight

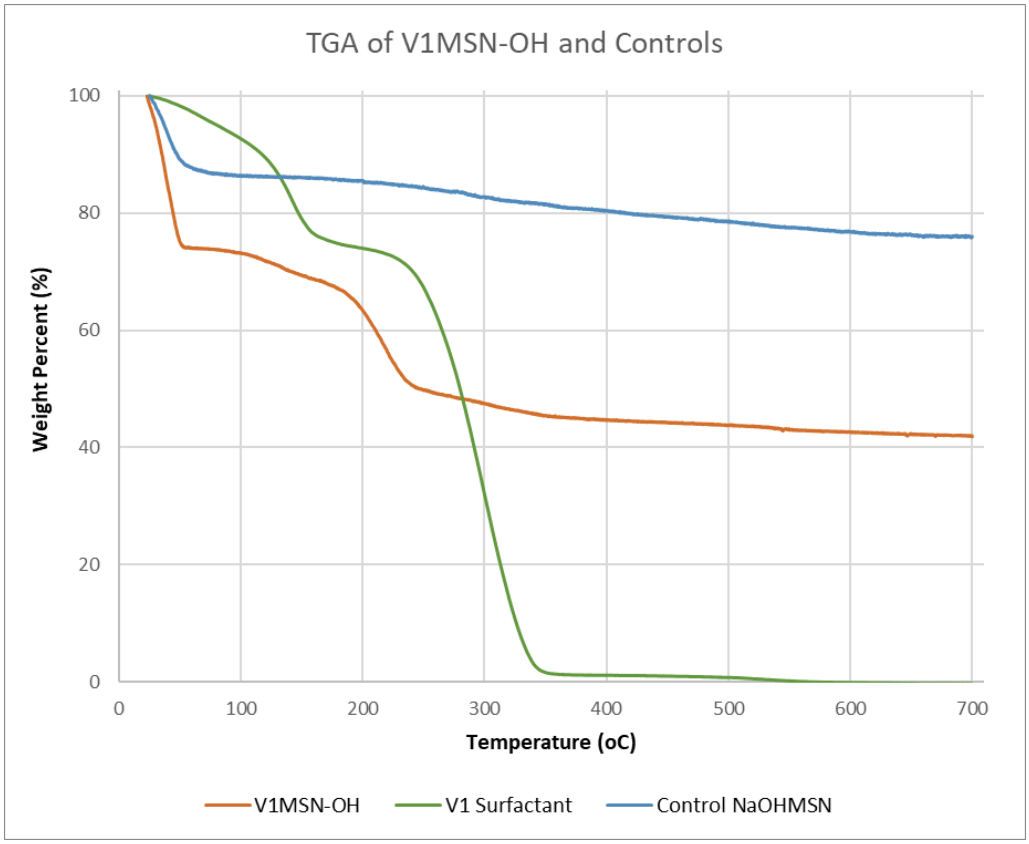

Figure 3.24: TGA of NaOH Catalyzed V1-MSNs, V1 alone, and Acid Washed Control MSNs.

percent lost can be calculated. Using the control measurements, a “truer” calculation can be made. These calculations are summarized in Table 3.5. The loading efficiency was over 20% (w/w).

Surfactant		Control NaOH MSN		V1MSN-OH	
Weight loss		Weight loss		Weight loss	
Temp		Temp		Temp	
0-700		0-700		0-700	
	100.3		24.0		58.2
0-100		0-100		0-100	
	7.3		13.7		26.8
100-600		100-600		100-600	
	92.8		9.5		30.5
100-400		100-400		100-400	
	91.5		5.9		28.4

Table 3.6: Summarized Calculations for TGA of TGA of NaOH Catalyzed V1-MSNs, V1 alone, and Acid Washed Control MSFs.

V1MSNs catalyzed with NaF

Again, the same statements held true for the TGA of NaF catalyzed V1-MSNs. One notable feature present in V1-MSN-Fs and their control counterpart had a weight loss at approximately 500^{o}C. This was evidence that V1-MSN-Fs have a different morphology than V1-MSN-OHs. The weight lose pattern that correlated to V1 was much smaller, showing a lower loading efficiency (Figure 3.17). The calculations summarized in Table 3.6 agree with this, giving a loading efficiency of approximately 5%(w/w).

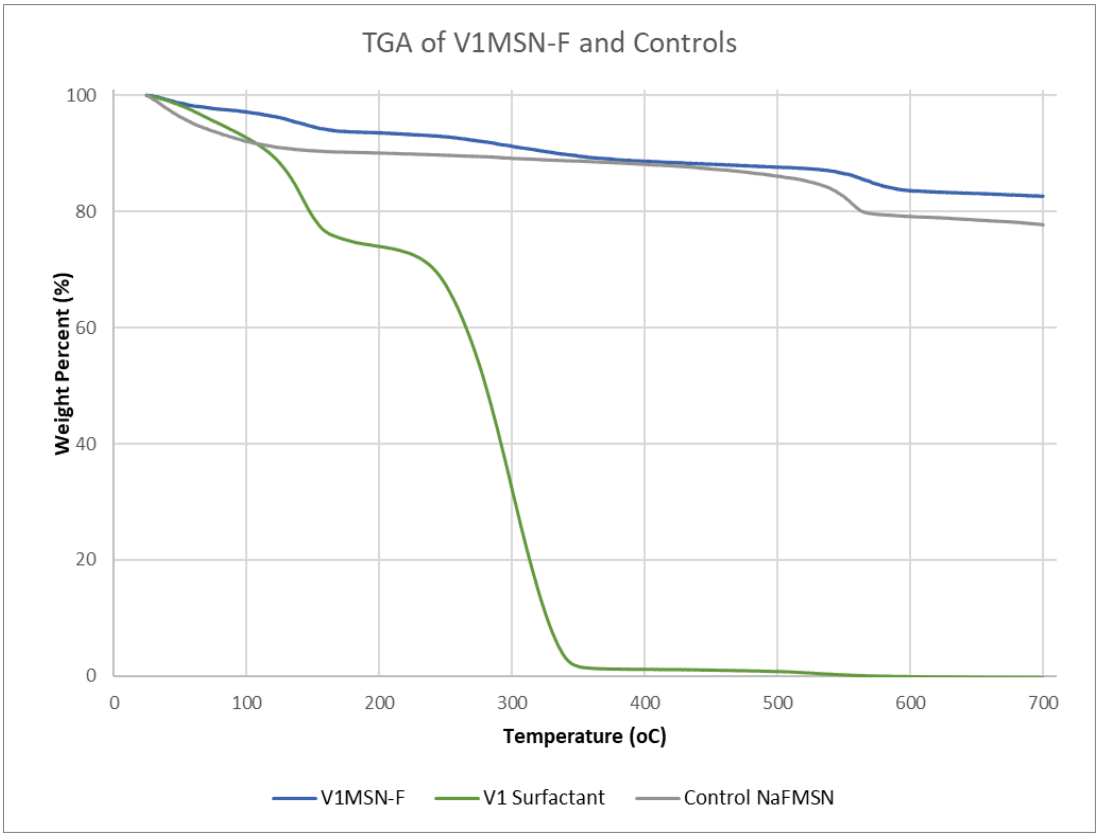

Figure 3.25: TGA of NaF Catalyzed MSNs, V1 Surfactant Alone, and Acid Washed V1-MSN-F Control.

Surfactant		Control NaF MSN		V1MSN-F	
Weight loss		Weight loss		Weight loss	
Temp		Temp		Temp	
0-700		0-700		0-700	
	100.3		22.3		17.3
0-100		0-100		0-100	
	7.3		7.9		2.8
100-400		100-400		100-400	
	91.5		3.9		8.5
500-600		500-600		500-600	
	0.9		6.9		4.1

Table 3.7: Summarized Calculations for TGA of NaF Catalyzed MSNs, V1 Surfactant Alone, and Acid Washed V1-MSN-F Control.

DLS

Not surprisingly, the DLS results for the two types of MSNs varied greatly. Both exhibited sizes larger than expected, which may be due to aggregation.

V1MSNs catalyzed with NaOH

The DLS reveled two distinct populations for the NaOH catalyzed MSNs seen in Figure 3.18. The first population was around 430nm in diameter. The other population was around 1200nm in diameter. This was assumed to be due to clustering of 2 nanoparticles together (400nm*3 = 1200nm). Although, these assumptions could not be verified without use of TEM.

Figure 3.26: DLS Results for NaOH Catalyzed V1-MSNs.

V1MSNs catalyzed with NaF

There was only on population for the NaF catalyzed MSNs. This can be seen in Figure 3.19. The population had a massive diameter size of approximately 4100nm. This was assumed to be due to aggregation rather than being the true diameter of the nanoparticles.

Figure 3.27: DLS Results for NaF Catalyzed V1-MSNs.

Zeta Potential

Zeta potential is the measurement of the surface charge of the nanoparticle. When the zeta potential is either greatly positive or greatly negative less aggregation generally occurs. This observation has been made many times in the Bossmann Laboratory.

V1MSNs catalyzed with NaOH

The Zeta potential for the NaOH catalyzed MSNs was negative, but with an average of only around -20mV it is reasonable to believe some clustering can take place. The Zeta potential graph, as well as the individual run readings and average can be observed in Figure 3.20.

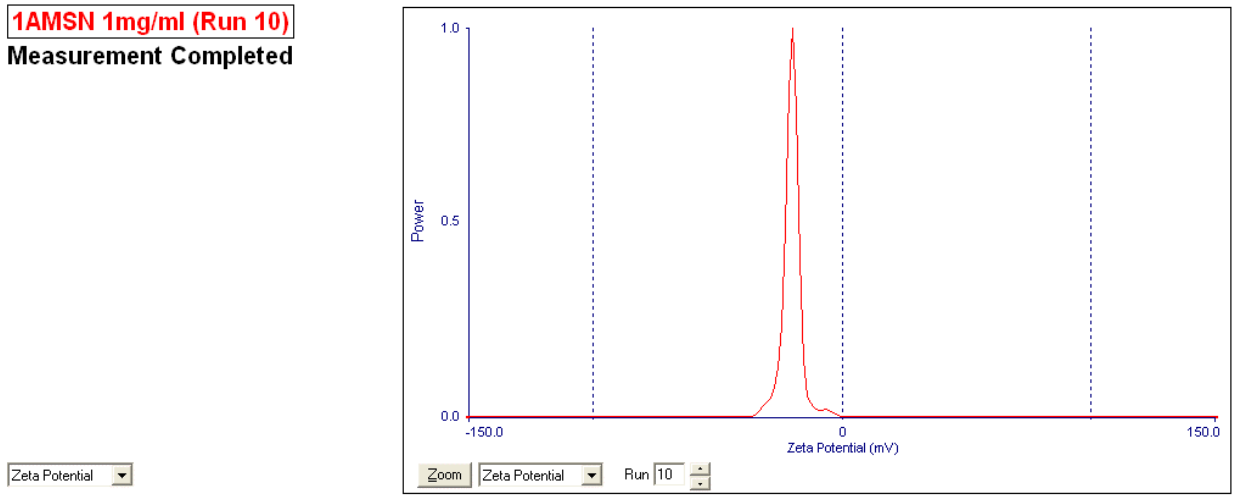

Run	Zeta Potential (mV)	Half Width (mV)
1	-21.09	5.62
2	-16.11	3.86
3	-21.13	2.96
4	-23.00	5.15
5	-22.61	2.80
6	-24.04	3.09
7	-18.24	2.63
8	-24.47	5.77
9	-21.91	2.71
10	-19.69	2.71
Mean	-21.23	3.73
Std. Error	0.83	0.41

Measurement Parameters:	
Conductance	= 1 µS
Current	= 0.14 mA
Electric Field	= 15.47 V/cm
Sample Count Rate	= 1433 kcps
Ref. Count Rate	= 1282 kcps

Figure 3.28: Zeta Potential Results for NaOH Catalyzed V1-MSNs.

V1MSNs catalyzed with NaF

The Zeta potential for the NaF catalyzed MSNs was nearly neutral with an average of 3.66mV. The neutral surface charge could explain the aggregation that lead to the extremely large diameter reading from DLS. The graph and individual trial runs fort Zeta potential can be seen in Figure 3.21.

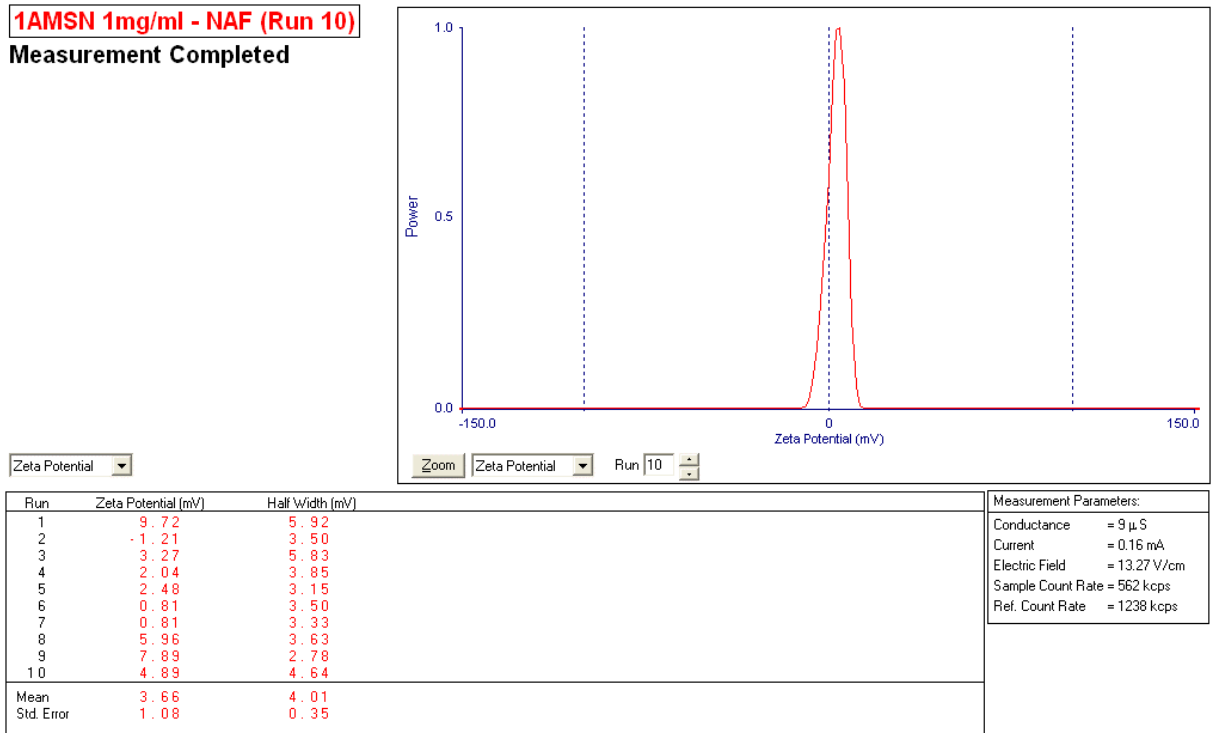

Figure 3.29: Zeta Potential Results for NaF Catalyzed V1-MSNs.

TEM

TEM and Scanning TEM (STEM) were used to visualize the structural differences between the NaOH catalyzed and NaF catalyzed MSNs. The results also were used to determine porosity and aggregation.

V1MSNs catalyzed with NaOH

The TEM images revealed that the NaOH catalyzed V1MSNs had a spherical shape and were approximately 20-50nm in size which can be seen in Figure 3.22 and Figure 3.23. The MSNs greatly aggregated. They also localized into secondary structures resembling bubbles. It is speculated that this was due to the surfactant being released and forming bubbles while sonicated that the MSNs clung to. The STEM showed that these structures were porous as expected. Overall, these TEM results were what was desired. The only surprising outcome was the amount of aggregation. From the Zeta potential it was expected that the MSNs would aggregate less.

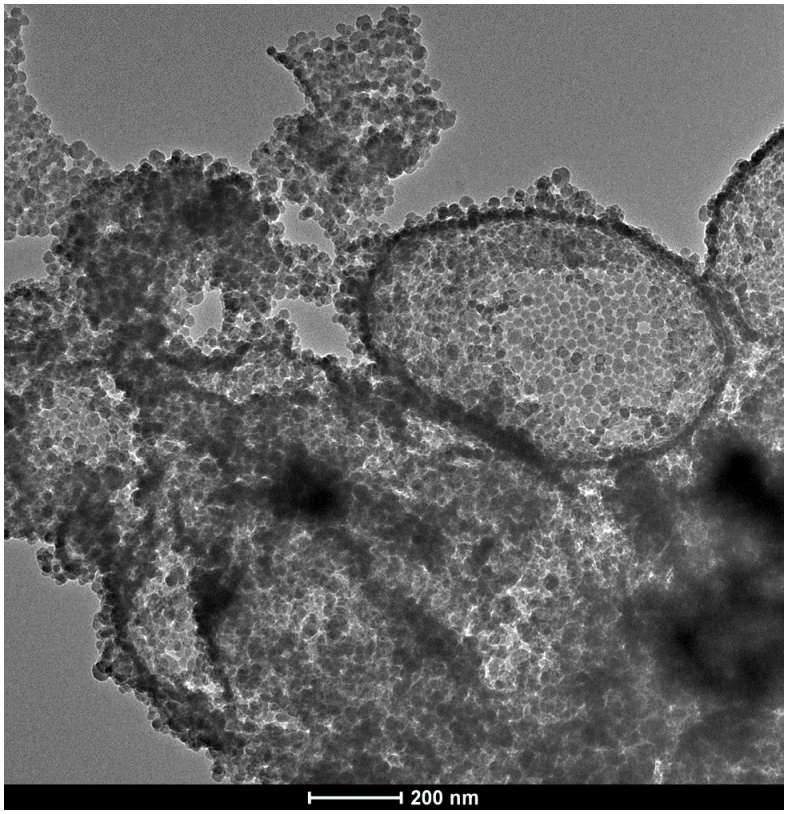

Figure 3.30: TEM of V1MSN-OH and Secondary Structures

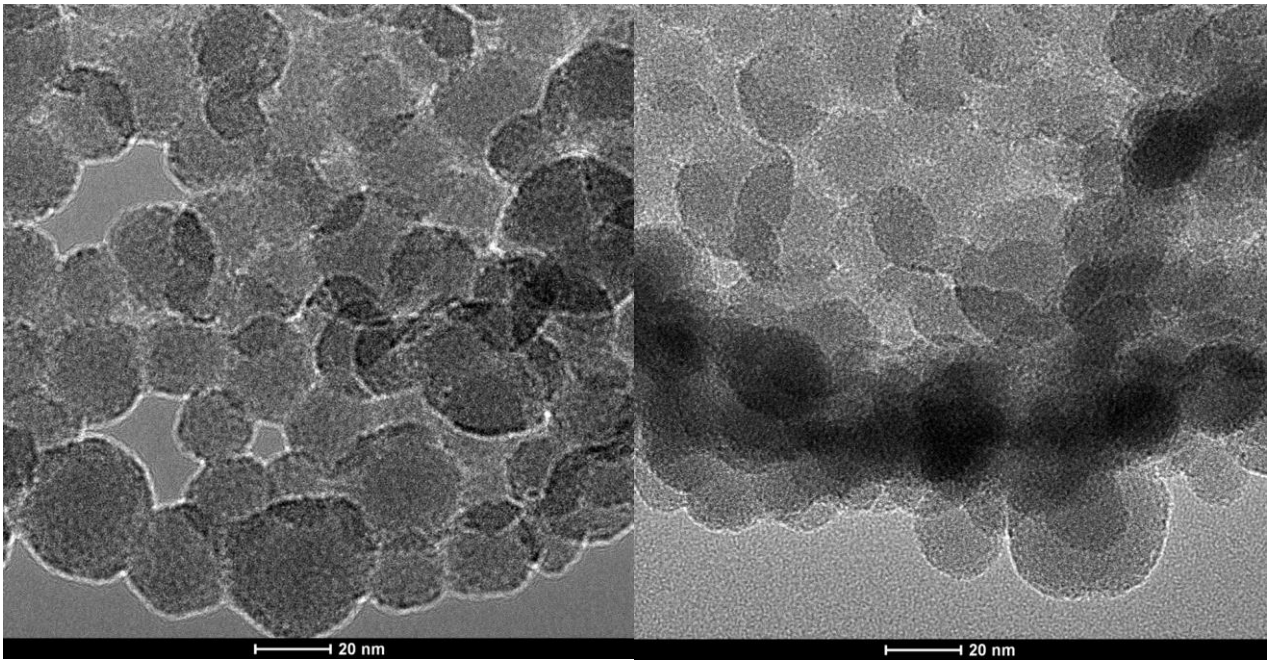

Figure 3.31: TEM of V1MSNs Catalyzed by NaOH

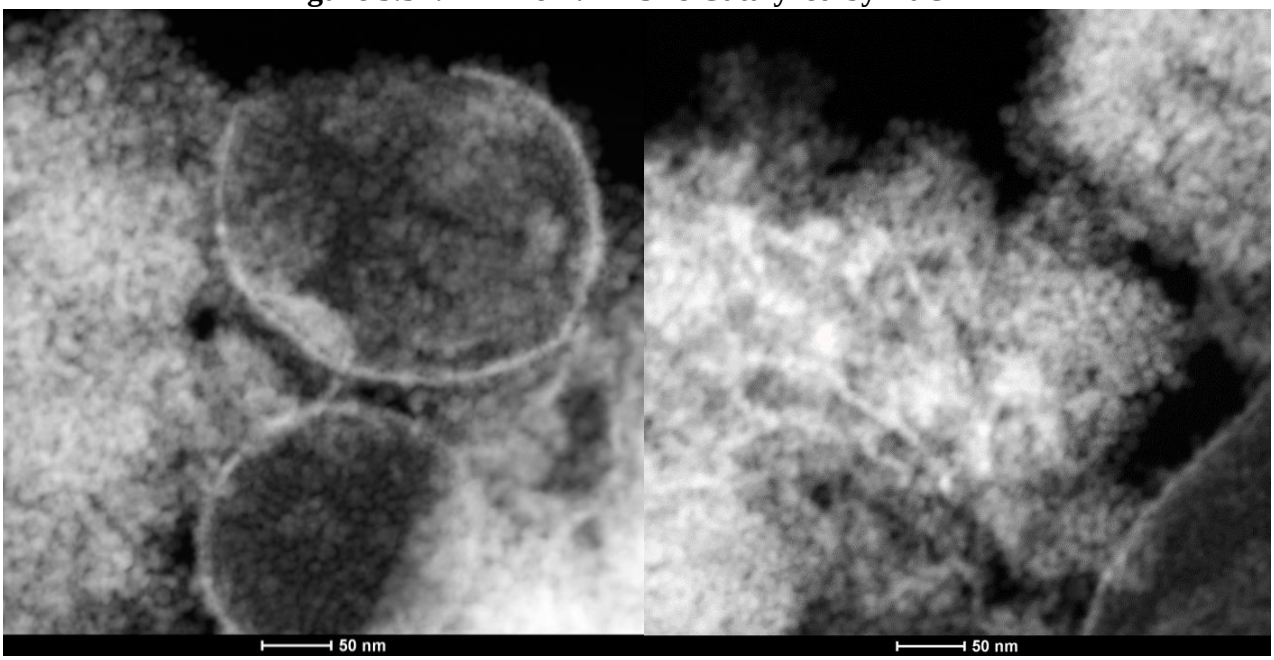

Figure 3.32: STEM of V1MSNs Catalyzed by NaOH

V1MSNs catalyzed with NaF

The TEM images for V1MSN-F had two different morphologies present. There were structures that resembled mesh (meso-mesh) and then there were large spheres. The meso-mesh

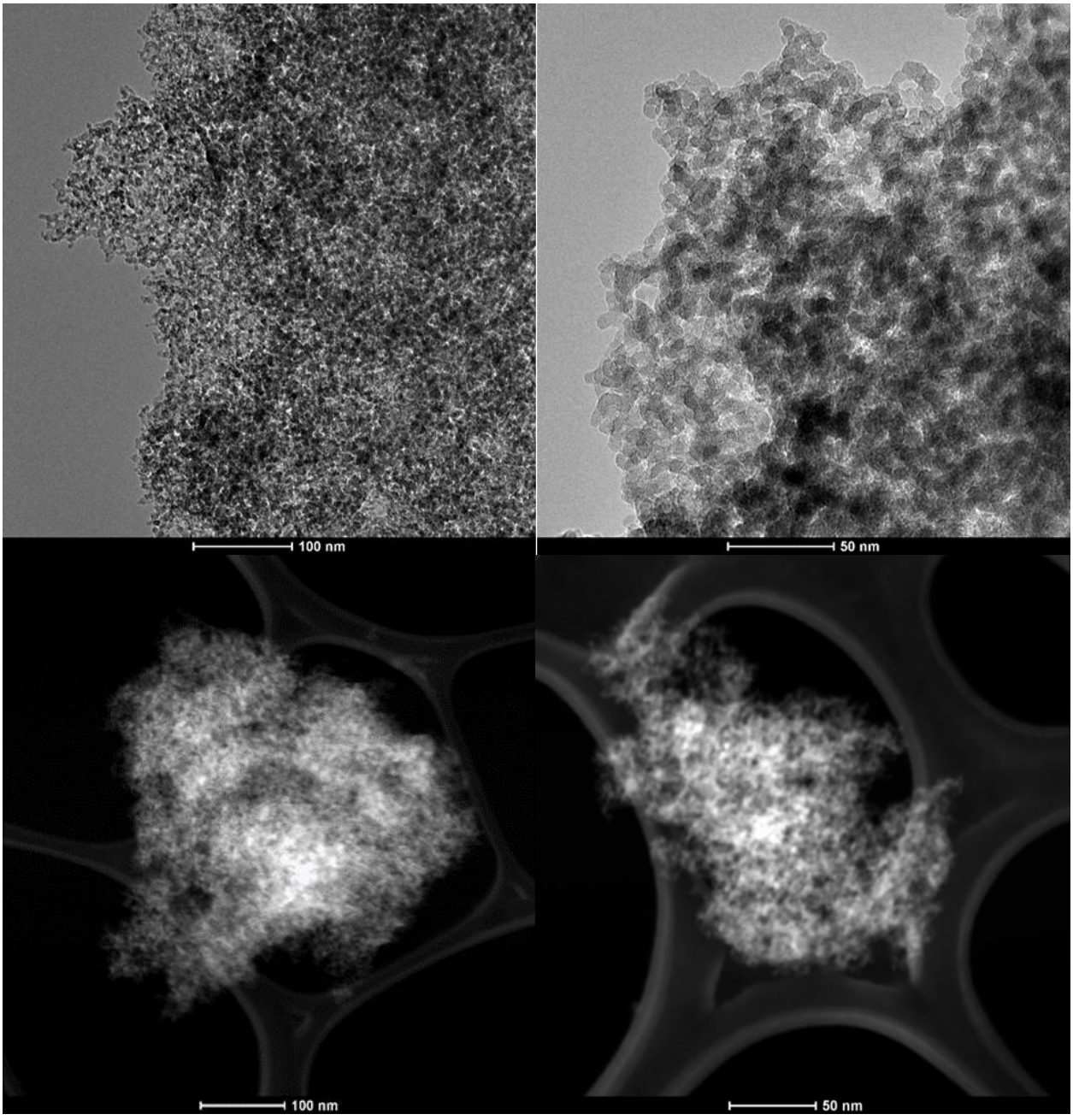

Figure 3.33: TEM and STEM of the Mesh-Like Mesoporous Silica Nanostructures, "Meso-Mesh" of V1-MSN-F.

was porous when looking at the STEM. This is clear from the black pores showing thought the white structure. The clusters of meso-mesh varied in size from under 50nm to 2μm. The

nanospheres ranged in size from 400nm to 2μm. Looking closely at the edge of the spheres it is believed they may be porous as well. The spherical structures were anticipated, but the meso-mesh was not. Looking at the mesh, it is possible that several tiny nanoparticles are clustering together. This would not be as surprising given that the zeta potential was relatively neutral, which can lead to aggregation. These TEM images also confirm that the large diameter readings were due to aggregation as the particle size was not uniform and no single particle had a diameter of 4000nm. Aggregation is not surprising because the Zeta potential was nearly neutral. The nanospheres are

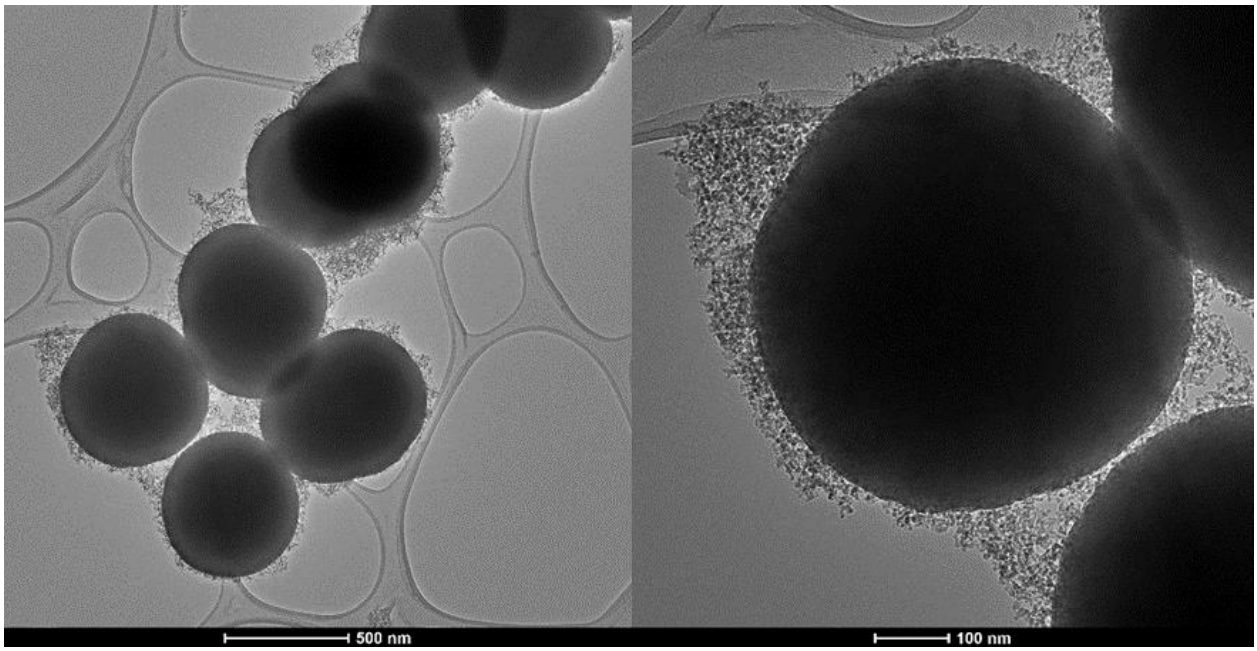

Figure 3.34: TEM images of spherical nanostructures within V1-MSN Sample.

larger than anticipated as well, but this may be able to be fine-tuned by changing the concentration of surfactant to begin the reaction. This is what was done for the BACMSNs and worked nicely.

Discussion

In this chapter the synthesis of four novel surfactants, their MICS, and their incorporation into mesoporous nanostructures was discussed. The results indicated that the expected surfactants had been synthesized. These surfactants had low to moderate activity against MRSA, with the best activity being that of SB12 at 0.027mg/ml. V1 was successfully incorporated into MSNs of two

different morphology. The NaOH catalyzed synthesis resulted in much lower yields, but had less aggregation, a high loading efficiency, and a more uniform structure. NaOH synthesized MSNs had spherical, porous structures that aggregated in bubble like secondary structures. The NaF synthesized MSNs had both mesoporous mesh-like structures (meso-mesh) and more uniform spheres. The meso-mesh and nanospheres both varied in size. The synthesis of the gatekeeping system for these MSNs was also discussed. Considering this synthesis is a new method, it is not surprising that it did not turn out exactly as anticipated. Luckily, it has been observed that manipulation of the starting reagents can greatly affect the size of the resulting structures. Therefore, with some fine-tuning, the desired size and uniformity should achievable. The di-cleavable peptide was successfully synthesized. Vancomycin was also successfully anchored to the N-terminal using a newly established method.

Future Work

Moving forward with the project, the gatekeeping system will be anchored to the surface of BACMSNs as proof of concept. Once the system is anchored the gated MSNs will be tested against *M. luteus* in solution to determine if the system is successful. Two versions of the peptide without Vancomycin will also be synthesized and anchored to the MSN to determine if the peptide alone will act as a gatekeeper. Vancomycin will also be anchored to the "cleaved" peptide variants to prove it is still active with these peptides attached. These MSNs are hoped to be applied to modern medicine in several ways including use as oral antibiotics and as preventive, slow-release antibiotics that can be placed at the site of surgery to protects patients for days or weeks to come.

Chapter 4 - MSNs Developed for Cancer Treatment

Previously in the Bossmann laboratory an anti-cancer peptide was developed by Dr. Jing Yu. Due to its non-specific nature MSNs were implemented as a carrier vessel. Unfortunately, the loading efficiency was extremely low. In chapter the history of the peptide and its uses, various methods of building the MSN directly around the peptide, and creating a gatekeeping system will be discussed.

Preliminary studies and relevant background

Development of SA-K_6L_9-AS

The predecessor of SA-K_6L_9-AS was an antimicrobial peptide developed in 2002 as an antimicrobial peptide called K_6L_9.[43] The name referred to the six lysine and nine leucine residues. The hydrophobic and polar nature of the peptide allowed it to disrupt the membranes of both gram-positive and gram-negative bacteria *in-vitro* in a serum-free environment. The peptide was virtually inactive in the presence of enzymes Trypsin and Proteinase K which quickly broke down the peptide.[43] With this in mind, the group chose to synthesize and test several diastereomers of K_6L_9 with varying amounts of D-amino acids. D-amino acids are not naturally occurring, so they often are more stable in physiological conditions. The best diastereomer was the peptide they called D-K_6L_9 with the structure LK*L*LK*K*L*LK*KLL*K*LL-NH_2 where the D-amino acids are denoted by italics and underline.[44] D-K_6L_9 appeared promising due to both its activity toward four gram-positive and four gram-negative bacteria in serum and its stability. It was determined that the mechanism of action was through membrane depolarization.[44] This discovery implied that the peptide may be active toward more than bacteria alone. Thus, leading to the investigation of D-K_6L_9 against cancerous cell lines.

A known trait of cancerous cells is that they exhibit a negative change on the surface of the membranes while healthy cells do not.[44,45] There are two reasons thought to be the main contributors to this occurrence: enrichment of phosphatidylserine in the outer membrane leaflet and secretion of lactate anions due to the Warburg effect.[45-47] The enrichment of phosphatidylserine helps the cancer cells avoid detection from the immune system because these molecules are non-immunogenic.[44] One of the most notable differences in the metabolism of cancer cells is the elevation glycolysis and less reliance on mitochondria for production of ATP.[45] The byproduct of glycolysis is lactate, which is then excreted by the cell. This excretion of lactate leads to the negative cell on the surface of the cell, as well as the acidic environment found within tumors.[45] A depiction of the secretion of lactate anions can be seen below. The negative charge allows for the cancer cells to be targeted by molecules containing positive residues/charges.

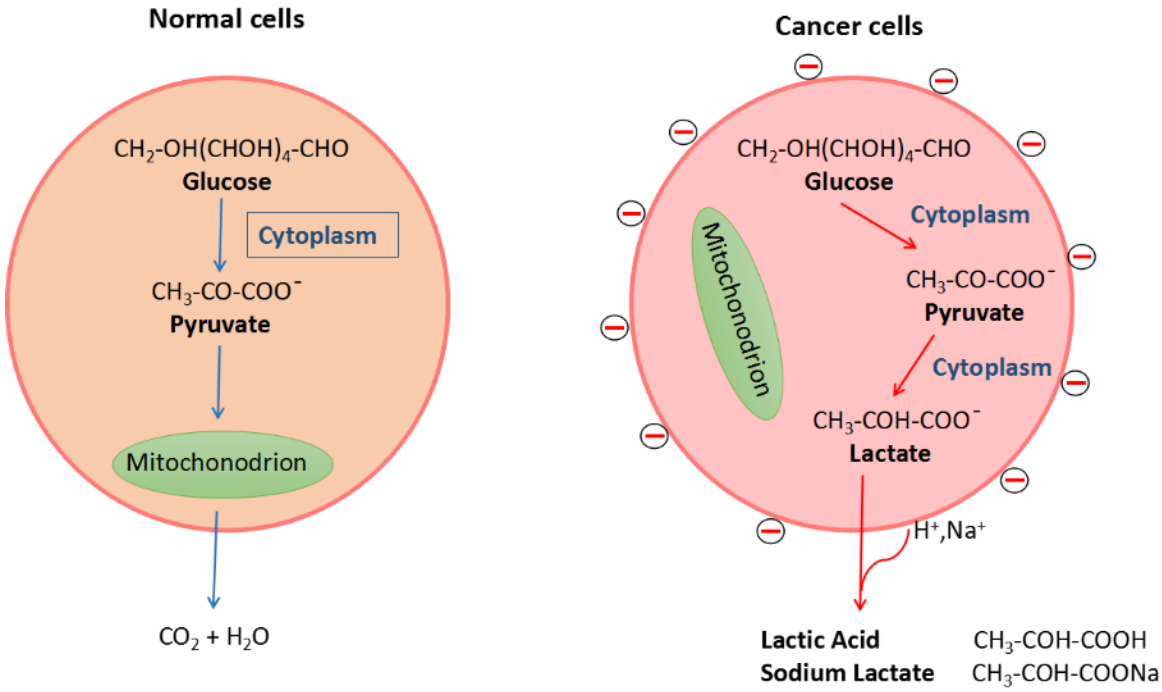

Figure 4.1: Illustration depicting the upregulation of glycolysis and the subsequent extraction of lactate leading to a negative charge in cancerous cells.[45]

By 2006 it was established that D-K_6L_9 was active against multiple types of cancer, however the peptide was not selective and killed healthy cells showing systemic toxicity.[43,44] Confocal imaging using CL1 pancreatic cancer cells and a fluorescent dye was utilized to determine the mechanism of cell death. From the images in figure 4.2, it was determined that the peptide was interacting with the membrane of the cells, further proving the group's proof of concept.[43] Further, it was believed that cell death occurred through a necrotic mechanism because of data obtained from histopathology and cell permeability studies. D-K_6L_9 was able to depolarize the transmembrane potential and rupture the membrane. This was clear from release of a cell encapsulated dye into solution.[43]

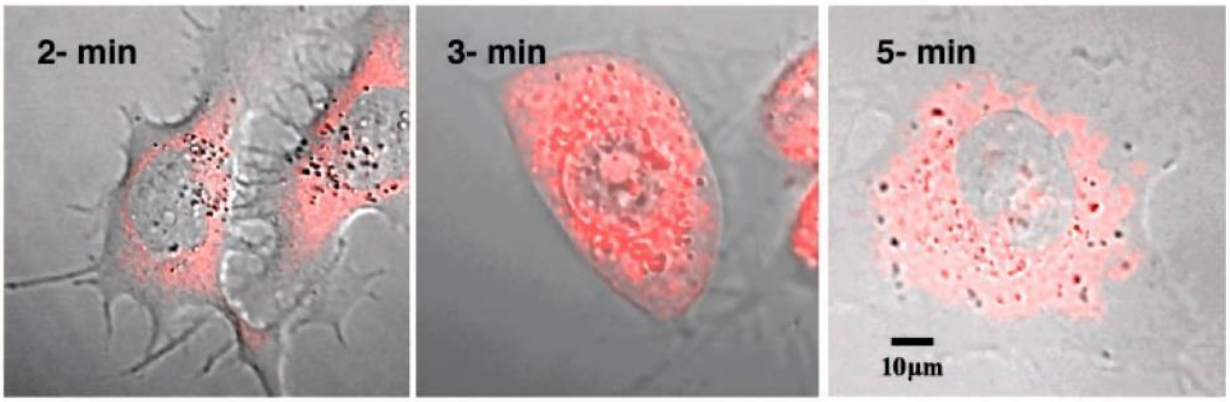

Figure 4.2: Confocal microscopy images of CL1 pancreatic cancer cells after 2 min., 3 min., and 5 min. of incubation with rhodamine-labeled D-K_6L_9.[42]

Using the information discovered by Shai, *et al.* Dr. Jing Yu of the Bossmann laboratory at Kansas State University sought to enhance the properties. According to recent studies, it was determined that necrotic cell death is an advantageous in killing cancer cells because the release of cancer neoantigens which can be recognized by dendritic cells can trigger an immune response.[48-50] A more through explanation of the cancer-immunity cycle can be found in Appendix B. The improvement of D-K_6L_9 aimed to amplify the necrotic mechanism and toxicity of the therapeutic peptide by increased targeting of organelles.[51] Along with this, increased solubility and

the ability to differentiate the lysine and leucine residues via NMR were also desired. This was accomplished with the addition of four amino acids to the peptide change: a serine and an alanine on each end. The new chain read SA-LK*L*LK*K*L*LK*KLL*K*LL-AS. Through extensive NMR studies it was determined that SA-D-K_6L_9-AS did not retain an alpha-helical structure as predicted by software, in contrast it was much more amorphous shown in figure 4.3.[51]

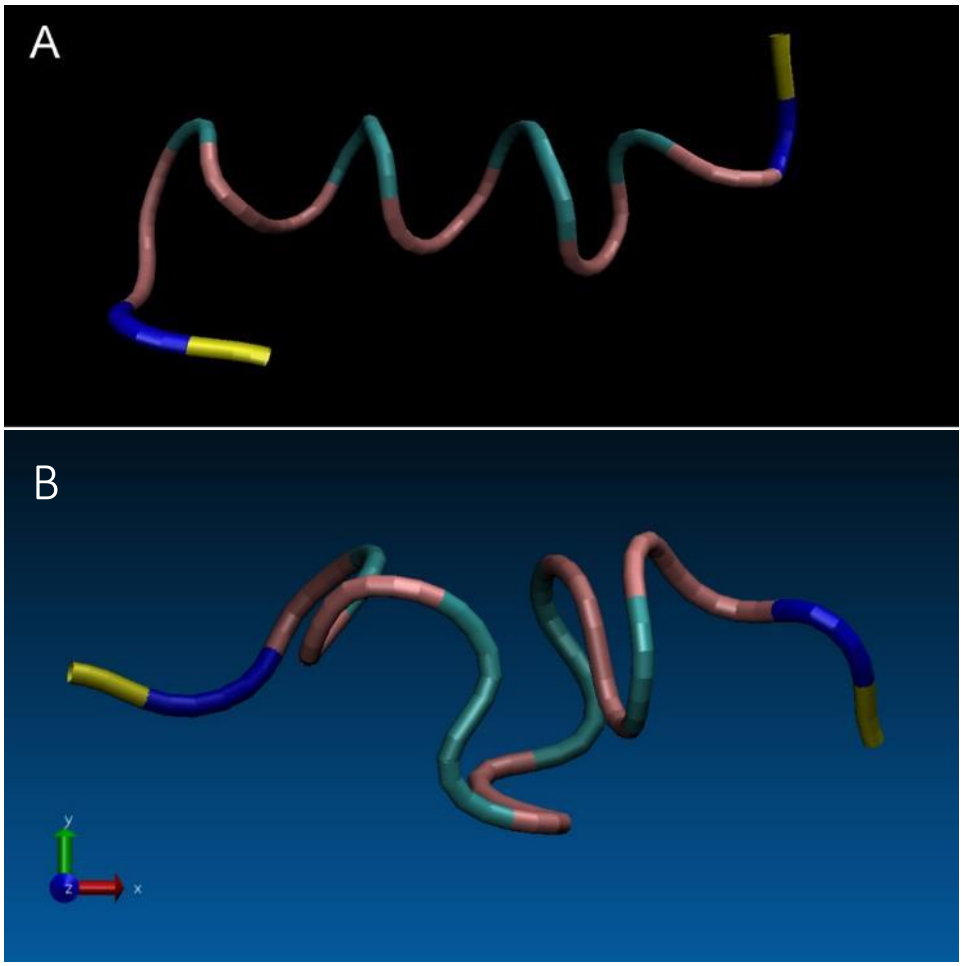

Figure 4.3: A. Predicted Folding of SA-D-K_6L_9-AS structure, as calculated by PEPstrMOD B. Most Probable Folding of SA-D-K_6L_9-AS in DMSO(D_6) based on lowest number of NOE violations and a total energy as calculated by CNS.[51]

The toxicity of the improved peptide was then tested. As expected the toxicity had increased dramatically, being eight times more toxic to GL26 cells than D-K_6L_9. Using confocal imaging it was determined that this increased toxicity came from the ability of the peptide to also target the mitochondrial membranes as well. This was clear from the overlapping fluorescence

from the dye attached to the peptide and the dye that stained the mitochondria (figure 4.4). D-K_6L_9 only was able to target the cell membrane.[51] This also increased necrotic cell death which should benefit the cancer-immunity cycle. Unfortunately, the peptide remained unselective in its targeting, making a nanocarrier necessary.

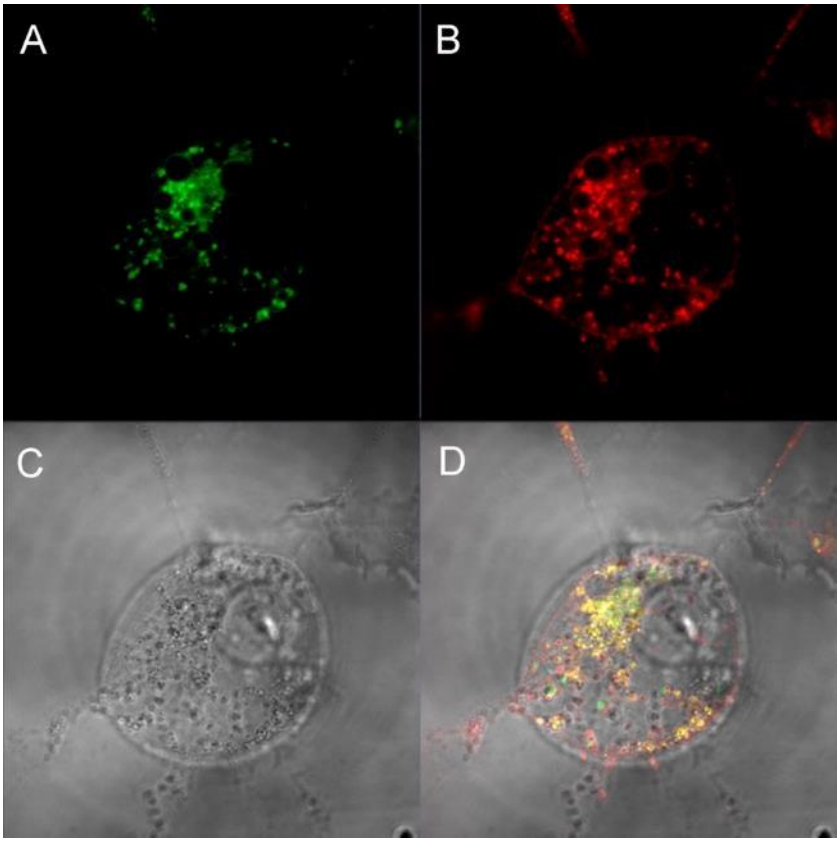

Figure 4.4: Fluorescence microscopy of GL26 stained with Mitotracker Green FM, treated with 3μM of Rhodamine B labeled SA-D-K_6L_9-AS for live confocal imaging.[51] A. Green fluorescence for Mitotracker Green FM. B. Red fluorescence for Rhodamine-B labeled SA-D-K_6L_9-AS. C. Bright field image. D. Overlap of (A) (B) and (C). 400x magnification. Picture captured at 20min after monitoring

Proposed Gatekeeping System for Anti-Cancer MSNs

As well established within this thesis it is well known that MSNs exhibit a slow release of their cargo over time. Due to the unselective nature of SA-D-K_6L_9-AS this is not desirable. To combat this, a gatekeeping system was proposed. In this system, the MSNs loaded with peptide would first have iron oxide nanoparticles imbedded in polyvinylpyrrolidone (PVP) and dopamine

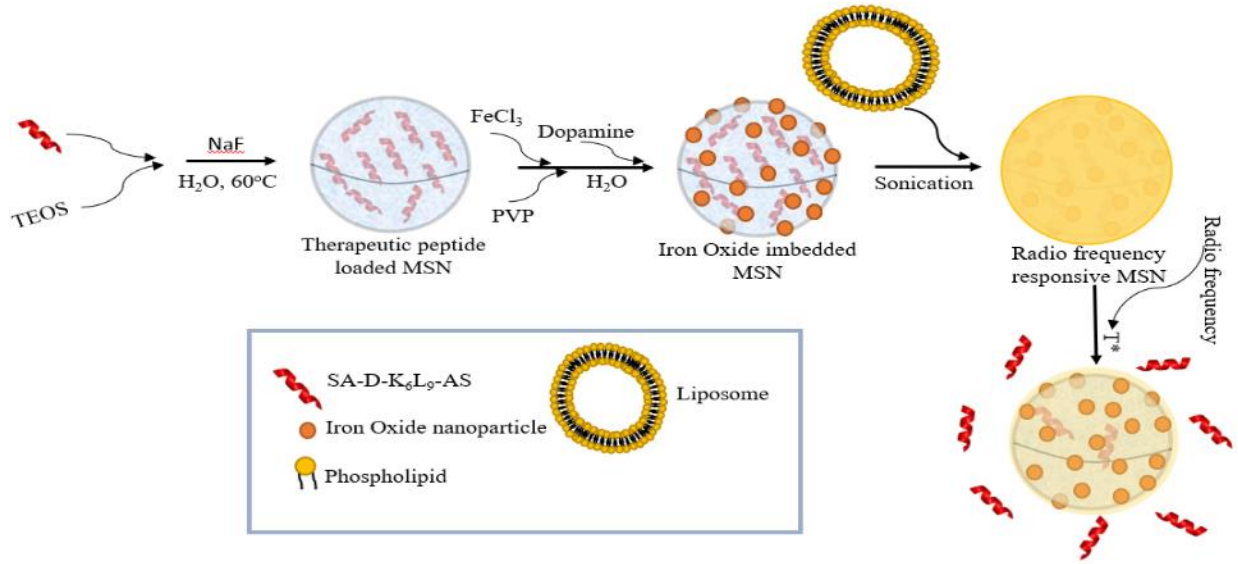

Figure 4.5: Diagram of the proposed method for synthesizing radio frequency responsive MSNs and their triggered release.

on their surface. Then a lipid layer made from three lipid components would be used to envelope the MSNs. This lipid layer could be disrupted and release the product when the it is hit with the correct non-invasive radio frequency causing temperature increase. The temperature increase is due to the vibration of the iron oxide nanoparticles.

Materials and Methods

Synthesis of SA-K_6L_9-AS Variant

The peptide chain was modified to contain a "lego" peptide or a portion of a peptide that will bind to itself and make a self-assembling peptide. The lego peptide chosen was RARA-DADA. Where the positively charged arginine side chains will interact with the negatively charged aspartic acid side chains. The new sequence reads RARADADA-SA-LK*L*LK*K*L*L**K*KLL*K*LL-AS. Solid phase synthesis was used as descried in Chapter 3 – Gatekeeper Synthesis to synthesis the peptide.

MSN Synthesis

Synthesizing the MSNs directly around the peptide proved to be more challenging than anticipated. The original procedure using NH_4OH at the catalyst was problematic because the peptide precipitated out of solution in basic conditions. For this reason, new methods were explored.

Ammonium Hydroxide Catalyzed

In this method approximately 100mg of peptide was dissolved in 70ml of diH_2O. Then 9600µl of 28-30% NH_4OH and 7ml ethyl acetate were added. When this occurred, the peptide precipitated out. The solution with peptide was allowed to sit for six days as the peptide slowly re-dissolved. Once the solution was clear, 200µl TEOS was added with stirring at 80°C. The solution was stirred for 24 hours, but little precipitate formed. The solution was then allowed to sit at room temperature without stirring for one week at which point the white precipitate was collected via centrifugation (10 minutes, 10000rpm). The precipitate was washed three times with 5ml diH_2O and three times with 5ml ethanol before being lyophilized.

Tween Entrapment with Sodium Fluoride Catalyst

The tween encapsulation technique followed a modified version of a previously reported procedure.[52] The method uses Tween 80 which is a non-toxic, nonionic surfactant and emulsifier that is commonly used in foods and cosmetics, to entrap the peptide within its micelle before the silica scaffold is constructed.[53] This was done by placing 10ml of Tween 80 aqueous solution (10mg/ml), 5ml of aqueous peptide (2mg/ml), and 1.5ml of 0.01M NaF in a flask and diluting to 50ml with diH_2O. This solution was stirred for 15 minutes to allow for the formation of micelles. Then 500µl TEOS was added dropwise. The solution was stirred for approximately 18 hours. Then the cloudy white precipitate was collected via centrifugation (10 minutes, 10000rpm). The

precipitate was washed three times with 5ml diH_2O and three times with 5ml ethanol before being lyophilized. Then the procedure was repeated using Rhodamine B labeled peptide.

Control Tween MSNs

Control MSNs were synthesized using the Tween method. This performed by placing 10ml of Tween 80 aqueous solution (10mg/ml) and 1.5ml of 0.01M NaF in a flask and diluting to 50ml with diH_2O. This solution was stirred for 15 minutes to allow for the formation of micelles. Then 500µl TEOS was added dropwise. The solution was stirred for approximately 18 hours. Then the cloudy white precipitate was collected via centrifugation (10 minutes, 10000rpm). The precipitate was washed three times with 5ml diH_2O and three times with 5ml ethanol before being lyophilized.

Sodium Fluoride Catalyzed

After considering the fact the peptide being used should self-assemble, the procedure was modified to exclude Tween 80. This was done by dissolving 25-50mg of Rhodamine B labeled peptide in 45ml diH_2O. Then 1.5ml of 0.1M NaF was added and the solution was diluted to 50ml with diH_2O. This solution was stirred for 15 minutes to allow for the peptide to self-assemble. Then 500µl TEOS was added dropwise. The solution was stirred for approximately 18 hours. Then the cloudy white precipitate was collected via centrifugation (10 minutes, 10000rpm). The precipitate was washed three times with 5ml diH_2O and three times with 5ml ethanol before being lyophilized. This procedure was repeated using unlabeled peptide, but the yield was approximately half the amount.

Control Sodium Fluoride Catalyzed

Control MSNs following the NaF catalyzed procedure were attempted. 1.5ml 0.1M NaF was diluted to 50ml with diH_2O. The solution was stirred at room temperature while adding 500µl

of TEOS. After 24 hours no precipitate had formed. The solvent was slowly evaporated to be sure product would not form. After 24 hours of slow evaporation, no precipitate formed.

Iron Oxide Nanoparticle Coating

Iron Oxide Nanoparticles have previously been synthesized by Dr. Hongwang Wang in the Bossmann Group. In this procedure, 66mg of Polyvinylpyrrolidone (PVP, molecular weight: 10000 g/mol) was dissolved in 8.8mL of D.I. water with vigorous stirring. Then 0.2mL of FeCl3 aqueous solution (100 mg/mL) was then added to the PVP solution, and further stirred at room temperature for 60 minutes. Next, 1mL of dopamine aqueous solution (10mg/mL) was added to the above solution. The reaction mixture was further stirred at room temperature for 24 hours, and then transferred to a dialysis membrane bag (molecular weight cutoff 8000) and dialyzed against 3L of D.I. water for 24 hours. The solution that was left in the dialysis bag was transferred to a centrifuge tube and lyophilized to dryness overnight.

To incorporate the iron oxide nanoparticles onto the MSNs a one-pot method was employed without the use of dialysis. First, 25mg of NaF catalyzed, Rhodamine B labeled-peptide loaded MSNs, 33mg PVP, and 10mg $FeCl_3$ were dispersed into 17.6mL diH_2O with the aid of sonication. The reaction mixture was stirred at room temperature for 90 minutes to ensure the even disperse of iron precursor into the channel of MSNs. Next, 0.5mL dopamine aqueous solution was added to the dispersion and stirred at room temperature for 24 hours. The MSNs entrapped with iron oxide nanoparticles were collected by centrifugation (10min, 10000rpm).

Lipid Bilayer Envelope

The next step of the gatekeeping system implemented a lipid bilayer envelope around the iron oxide imbedded MSNs. This was done following a previously published procedure.[54] The thermo-responsive lipid bilayer will be composed of DPPC/DSPC/Chol/DSPE-PEG2000 at a

molar ratio of 65:5:25:5. The mixture was dissolved in chloroform at 5mg/ml. After a lipid film was formed the chloroform was removed using rotary evaporation. Then, 25mg of the MSNs described above were dispersed on top of the lipid film and the lipid film was re-hydrated for 15 minutes at 37 °C. The suspension was then sonicated to fuse the lipid bilayers and MSNs. The resulting MSNs were collected by centrifugation (10min, 10000rpm) and lyophilized.

Cell Viability Assays

Cell viability was tested utilizing a colorimetric assay modified by the Dr. Troyer lab. First a stock solution of 5mg/ml methylthiazolyldiphenyl-tetrazolium bromide (MTT) in 1XPBS was made. The stock was aliquoted out and frozen until ready for use. The three cell lines: GL26, B16F10, and NSC, were plated in 96-well plates at approximately 15,000 cells/cm^2. GL26 and B16F10 require 10% fetal bovine serum in RPMI (10% FBS RPMI). NSC cells require Neural Stem Cell medium (NSC medium). The plates were incubated at 37^{o}C for 24 hours. At this time, the medium was removed and replaced with 100µl respective medium and varying concentrations of 2mg/ml reagent in 1XPBS. The final concentrations of the wells were: 0mg/ml (100µl medium, 100µl 1XPBS), 0.01mg/ml, 0.05mg/ml, 0.10mg/ml, 0.25mg/ml, 0.50mg/ml, 0.75mg/ml, and 100mg/ml. Each reagent had three replicas of each concentration.

The plates were then returned to the incubator for either 24 hour and 48 hours. At the given time, the plates were removed and the medium and reagent were suctioned off. All wells were rinsed once with 100µl of 1XPBS to remove settled MSNs. Then 10µl MTT stock per 100µl medium was added back into all wells (110µl per well) and incubated for 4 hours. Then 100µl of 10% SDS in 0.01M HCl was added to all wells and incubated overnight.

The absorbance was read at 550nm and 690nm using UV/Vis plate reader (Synergy H1 micro-plate reader BioTek, Winooski, VT) and analysis software Gen5 v2.05 (BioTek Winooski,

VT). The difference (A_{690}-A_{550}) was used to create the cell viability assays. Sample calculations can be found in Appendix B – Sample Cell Viability Assay Calculations.

	1	2	3	4	5	6	7	8	9	10	11	12	
A	SPL1:1 0	SPL1:1 0	SPL1:1 0	SPL2:1 0	SPL2:1 0	SPL2:1 0	SPL3:1 0	SPL3:1 0	SPL3:1 0	SPL4:1 0	SPL4:1 0	SPL4:1 0	Well ID Conc/Dil
B	SPL1:2 0.01	SPL1:2 0.01	SPL1:2 0.01	SPL2:2 0.01	SPL2:2 0.01	SPL2:2 0.01	SPL3:2 0.01	SPL3:2 0.01	SPL3:2 0.01	SPL4:2 0.01	SPL4:2 0.01	SPL4:2 0.01	Well ID Conc/Dil
C	SPL1:3 0.05	SPL1:3 0.05	SPL1:3 0.05	SPL2:3 0.05	SPL2:3 0.05	SPL2:3 0.05	SPL3:3 0.05	SPL3:3 0.05	SPL3:3 0.05	SPL4:3 0.05	SPL4:3 0.05	SPL4:3 0.05	Well ID Conc/Dil
D	SPL1:4 0.1	SPL1:4 0.1	SPL1:4 0.1	SPL2:4 0.1	SPL2:4 0.1	SPL2:4 0.1	SPL3:4 0.1	SPL3:4 0.1	SPL3:4 0.1	SPL4:4 0.1	SPL4:4 0.1	SPL4:4 0.1	Well ID Conc/Dil
E	SPL1:5 0.25	SPL1:5 0.25	SPL1:5 0.25	SPL2:5 0.25	SPL2:5 0.25	SPL2:5 0.25	SPL3:5 0.25	SPL3:5 0.25	SPL3:5 0.25	SPL4:5 0.25	SPL4:5 0.25	SPL4:5 0.25	Well ID Conc/Dil
F	SPL1:6 0.5	SPL1:6 0.5	SPL1:6 0.5	SPL2:6 0.5	SPL2:6 0.5	SPL2:6 0.5	SPL3:6 0.5	SPL3:6 0.5	SPL3:6 0.5	SPL4:6 0.5	SPL4:6 0.5	SPL4:6 0.5	Well ID Conc/Dil
G	SPL1:7 0.75	SPL1:7 0.75	SPL1:7 0.75	SPL2:7 0.75	SPL2:7 0.75	SPL2:7 0.75	SPL3:7 0.75	SPL3:7 0.75	SPL3:7 0.75	SPL4:7 0.75	SPL4:7 0.75	SPL4:7 0.75	Well ID Conc/Dil
H	SPL1:8 1	SPL1:8 1	SPL1:8 1	SPL2:8 1	SPL2:8 1	SPL2:8 1	SPL3:8 1	SPL3:8 1	SPL3:8 1	SPL4:8 1	SPL4:8 1	SPL4:8 1	Well ID Conc/Dil

Figure 4.7: Sample Layout of 96-well Plates for Cell Viability Assays.

	Sample 1			Sample 2			Sample 3			Sample 4			
	1	2	3	4	5	6	7	8	9	10	11	12	
A	1.145	1.103	1.152	1.166	1.109	1.144	1.149	1.174	1.234	1.213	1.257	0.924	550
	0.045	0.045	0.046	0.046	0.047	0.049	0.049	0.048	0.05	0.05	0.052	0.047	690
	1.1	1.058	1.106	1.12	1.062	1.095	1.1	1.126	1.184	1.162	1.205	0.877	Delta
B	0.831	0.676	0.757	0.887	0.842	0.99	1.299	1.061	1.082	1.025	1.006	0.821	550
	0.051	0.051	0.05	0.05	0.048	0.05	0.052	0.051	0.05	0.05	0.05	0.048	690
	0.78	0.625	0.707	0.837	0.794	0.94	1.247	1.01	1.033	0.975	0.955	0.773	Delta
C	0.805	0.72	0.686	0.606	0.624	0.749	1.138	0.95	0.861	0.916	0.878	0.662	550
	0.052	0.051	0.053	0.052	0.053	0.054	0.058	0.057	0.056	0.057	0.059	0.057	690
	0.753	0.669	0.633	0.554	0.572	0.695	1.08	0.893	0.805	0.86	0.82	0.605	Delta
D	0.26	0.169	0.228	1.051	1.091	1.13	0.863	0.873	0.94	0.999	0.985	0.726	550
	0.058	0.057	0.057	0.064	0.064	0.064	0.061	0.061	0.062	0.061	0.06	0.058	690
	0.202	0.112	0.171	0.987	1.027	1.066	0.802	0.812	0.878	0.938	0.924	0.667	Delta
E	0.186	0.12	0.108	0.146	0.109	0.11	0.877	0.755	0.811	0.894	0.826	0.803	550
	0.057	0.057	0.058	0.061	0.061	0.062	0.07	0.07	0.078	0.072	0.072	0.072	690
	0.129	0.063	0.05	0.085	0.048	0.048	0.807	0.685	0.733	0.822	0.754	0.731	Delta
F	0.148	0.116	0.113	0.113	0.112	0.112	0.838	0.874	0.787	1.024	0.975	0.863	550
	0.069	0.069	0.068	0.069	0.069	0.069	0.081	0.08	0.081	0.078	0.077	0.075	690
	0.079	0.048	0.045	0.044	0.043	0.043	0.757	0.794	0.706	0.947	0.897	0.788	Delta
G	0.108	0.12	0.118	0.118	0.12	0.119	1.027	0.944	0.915	1.175	1.148	0.942	550
	0.07	0.07	0.071	0.073	0.074	0.075	0.097	0.095	0.106	0.093	0.095	0.09	690
	0.038	0.049	0.047	0.045	0.046	0.044	0.93	0.849	0.809	1.082	1.053	0.852	Delta
H	0.124	0.129	0.128	0.132	0.128	0.128	0.862	0.866	0.906	1.147	1.124	1.065	550
	0.081	0.082	0.082	0.083	0.083	0.082	0.119	0.111	0.129	0.096	0.099	0.096	690
	0.043	0.047	0.046	0.049	0.046	0.045	0.744	0.756	0.777	1.051	1.025	0.969	Delta

Figure 4.6: Sample Results for Cell Viability Assays.

Results and Characterization

All synthesized MSNs were characterized using Dynamic Light Scattering (DLS), Zeta potential, thermogravimetric analysis (TGA), and transmission electron microscopy (TEM) with the assistance of Joe Hammer and Sonia Barrett. DLS, Zeta Potential, and TGA were run in the same manner described in Chapter 3 – Materials and Methods. TEMs were run in the Electron Microscopy Lab out of Kansas University with the assistance of Dr. Prem Thapa.

Peptide Loaded MSNs

Peptide loaded MSNs (P-MSNs) and Rhodamine B labeled-peptide loaded MSNs (R-MSNs) were synthesized with and without Tween 80. For sake of clarity those synthesized with Tween 80 will be referred to as Tween P-MSNs or Tween R-MSNs.

DLS

DLS was used as a starting point in determining the effective diameters of each MSN.

P-MSNs

P-MSNs had an average effective diameter of nearly 2000nm. There were two distinct populations. One was 3330nm and the other was around 300nm. This suggested that there was aggregation in the sample. Potentially, the MSNs could be clustering in groups of three or more from these results. DLS results can be observed in Figure 4.8.

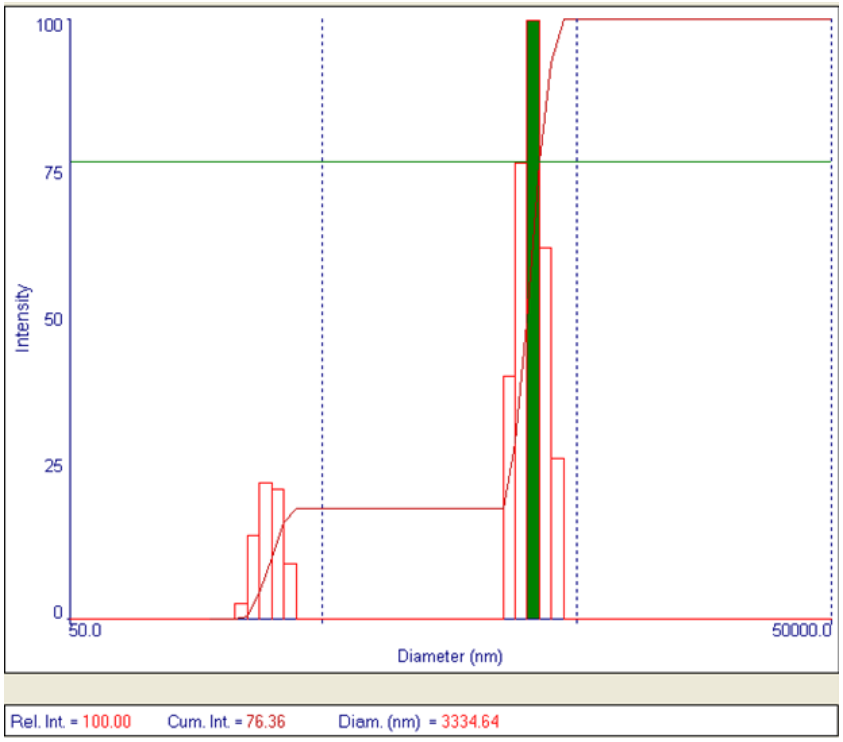

Figure 4.8: DLS of P-MSNs.

R-MSNs

The DLS for R-MSNs showed to major populations as seen in Figure 4.9. The major population was large at approximately 3200nm. The smaller population was around 200nm. It was assumed that the major population was due to aggregation.

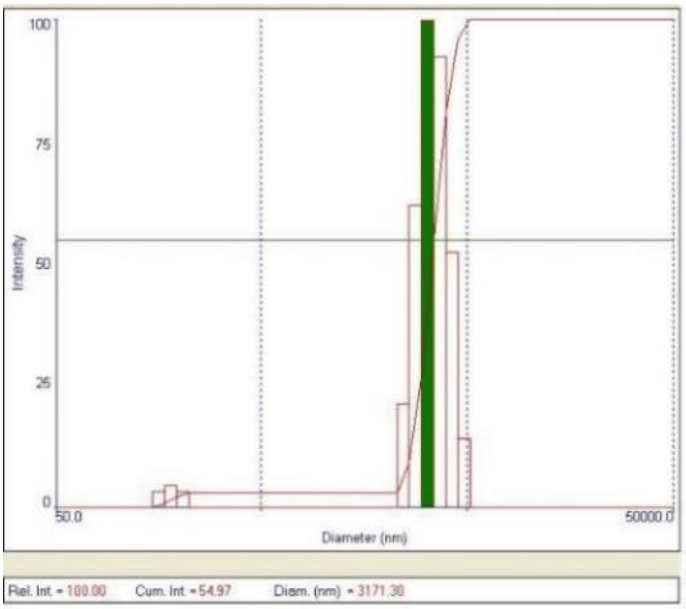

Figure 4.9: DLS of R-MSNs.

Tween P-MSNs

The DLS of Tween P-MSNs showed two major populations. The first population was approximately 450nm and the second was nearly 3200nm. Again, this suggests that the MSNs were aggregating greatly. The MSNs were also assumed to be larger than anticipated given that the smaller population measured close to half a micron.

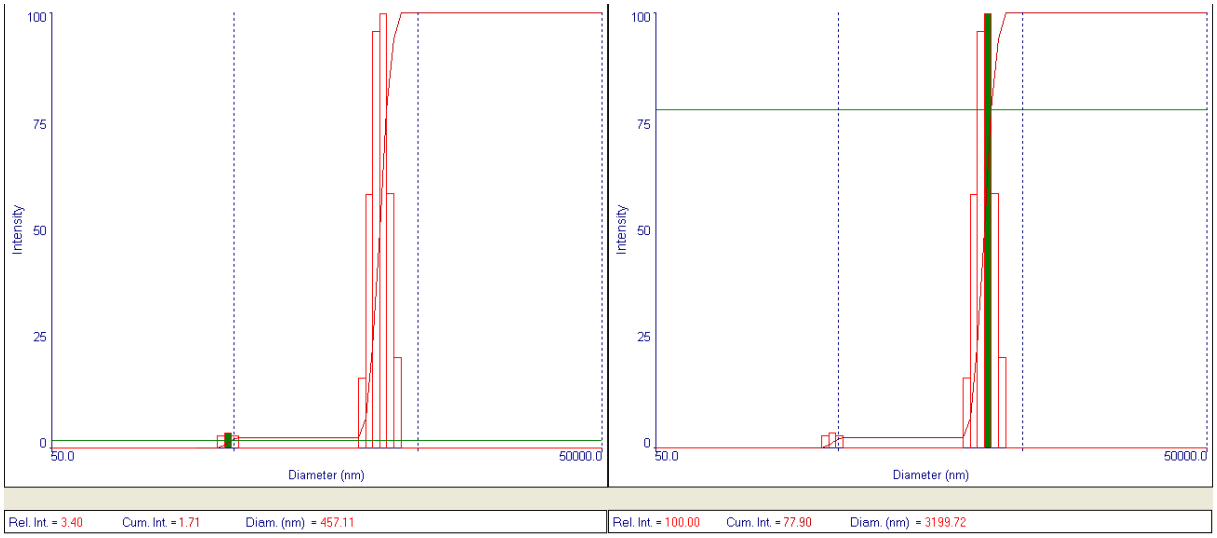

Figure 4.10: DLS of Tween P-MSNs.

Tween R-MSNs

The Tween R-MSNs also showed to populations (Figure 4.11). The smaller population was still large at about 1600nm. This was the most likely due to aggregation, not assumed to be the true value.

Figure 4.11: DLS of Tween R-MSN.

Zeta Potential

Zeta potential was measured to determine the surface charge of the MSNs. This information is important for resulting aggregation and cell studies.

P-MSNs

The Zeta potential for P-MSNs was barely positive at approximately 3mV. This is very close to neutral and would explain the DLS results that had large population sizes.

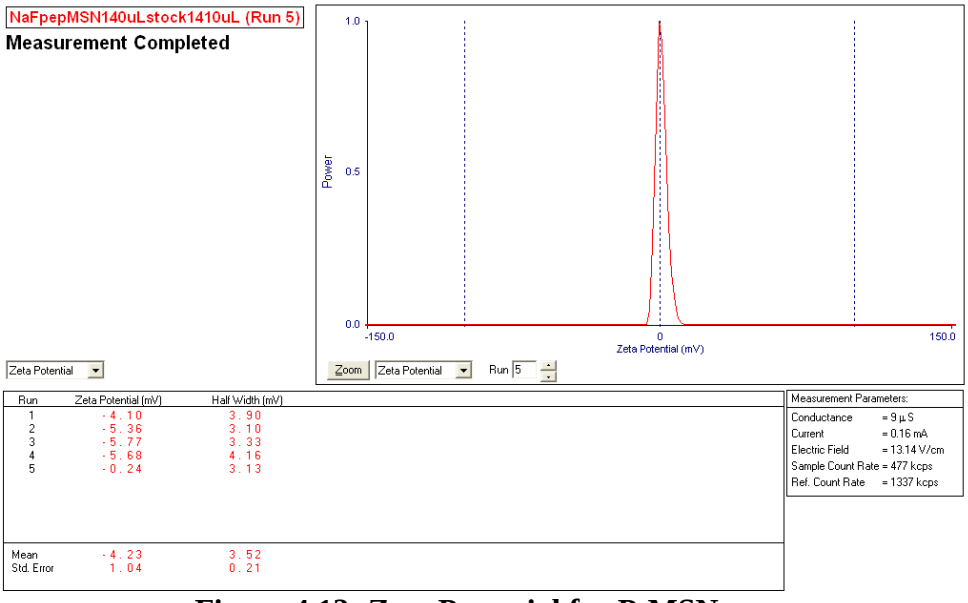

Figure 4.12: Zeta Potential for P-MSNs.

R-MSNs

There Zeta potential was extremely close to neutral which would like lead to aggregation.

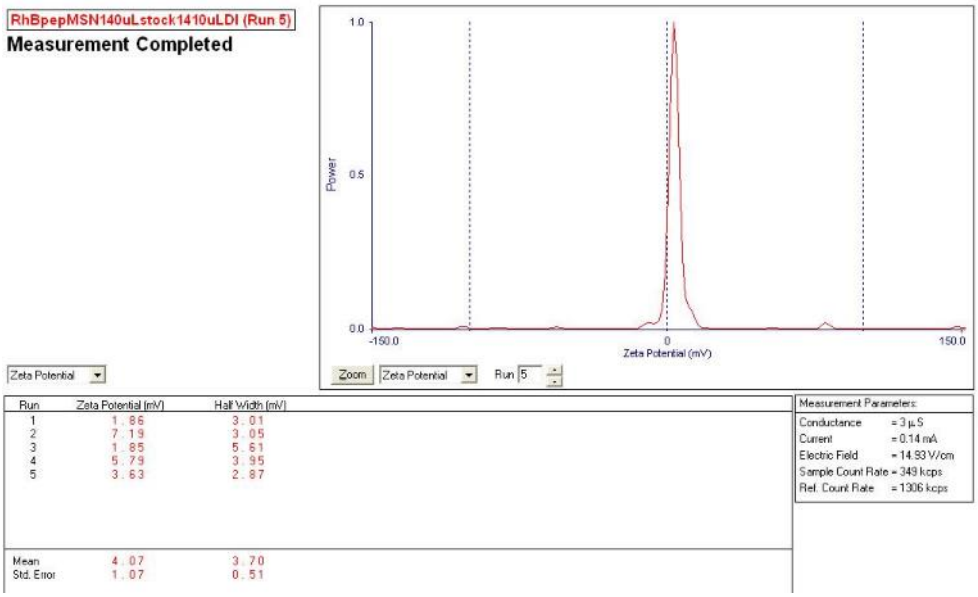

Figure 4.13: Zeta Potential of R-MSNs.

Tween P-MSNs

The Zeta potential for Tween P-MSNs was again found to be less neutral at approximately -18mV. This was not as neutral as expected considering that the DLS showed what was assumed to be aggregation. It is possible aggregation still occurs.

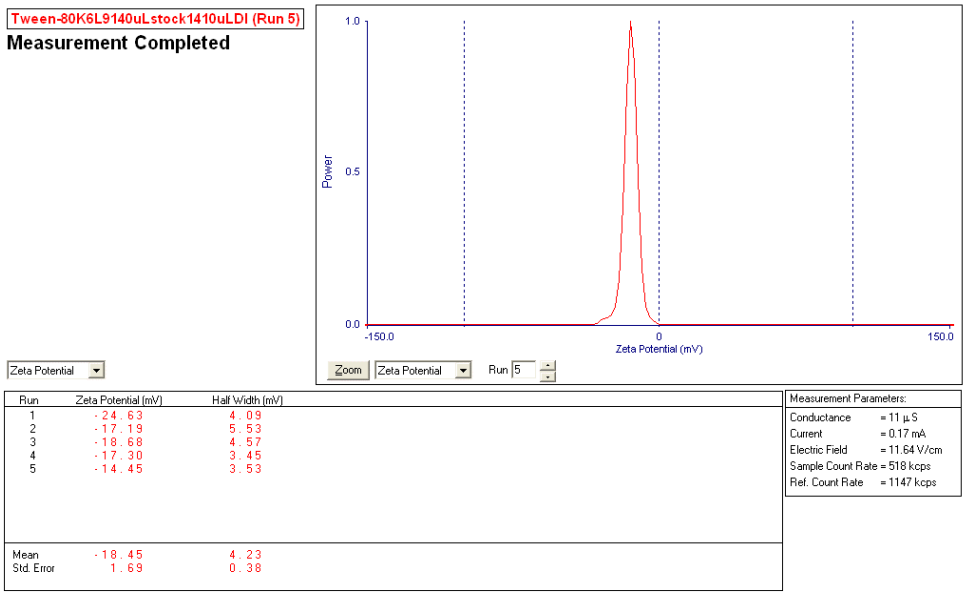

Figure 4.14: Zeta Potential of Tween P-MSNs.

Tween R-MSNs

There Zeta potential for Tween R-MSNs was more negative around -20mV. This did not completely explain the large DLS diameter readings. TEM images were necessary to determine the true size and morphology of the structures.

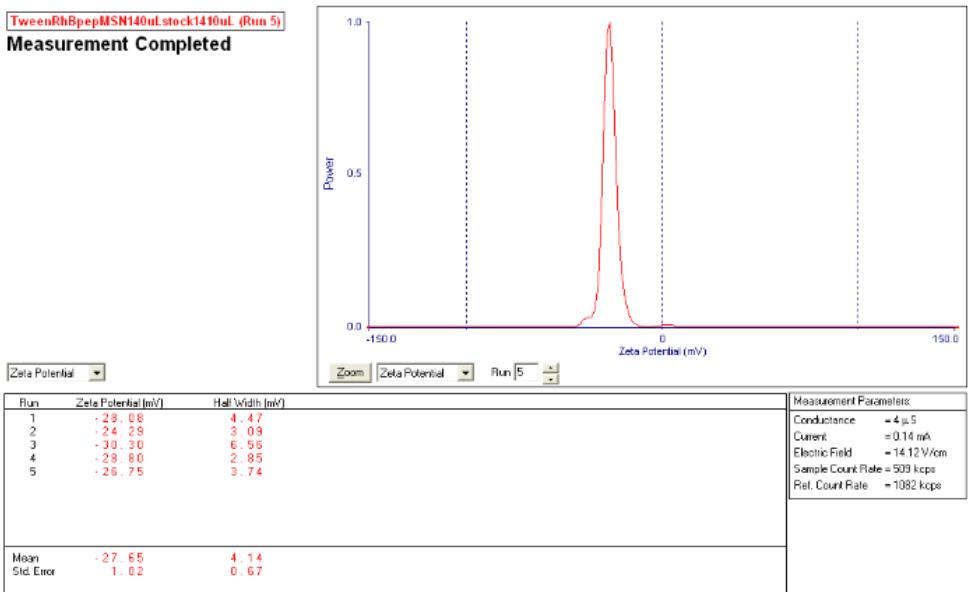

Figure 4.15: Zeta Potential of Tween R-MSNs.

TGA

TGA was ran to determine the loading efficiency of each MSN.

P-MSNs

Looking at the TGA data in Figure 4.16 and Figure 4.17, the weight lost from 100-500^{o}C was due to loaded material and likely from the peptide (given the same temperature range). The loading efficiency was determined to be about 3.5% (w/w). A summary of the data used can be found in Table 4.1 This is still a success considering the loading efficiency of peptide into MSN post-synthesis was only around 1%.

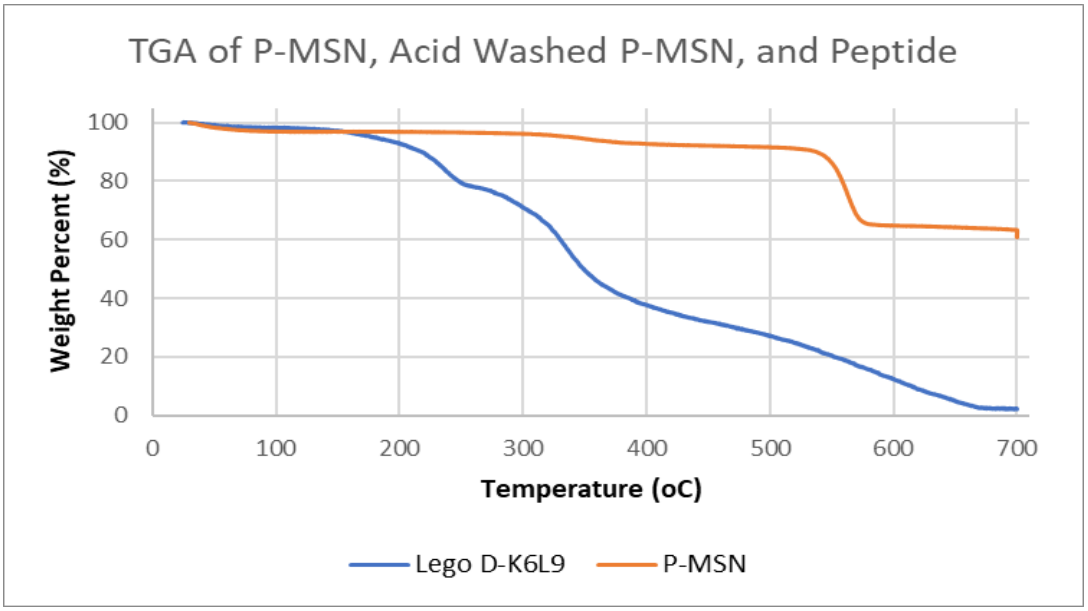

Figure 4.17: TGA of P-MSN and Peptide.

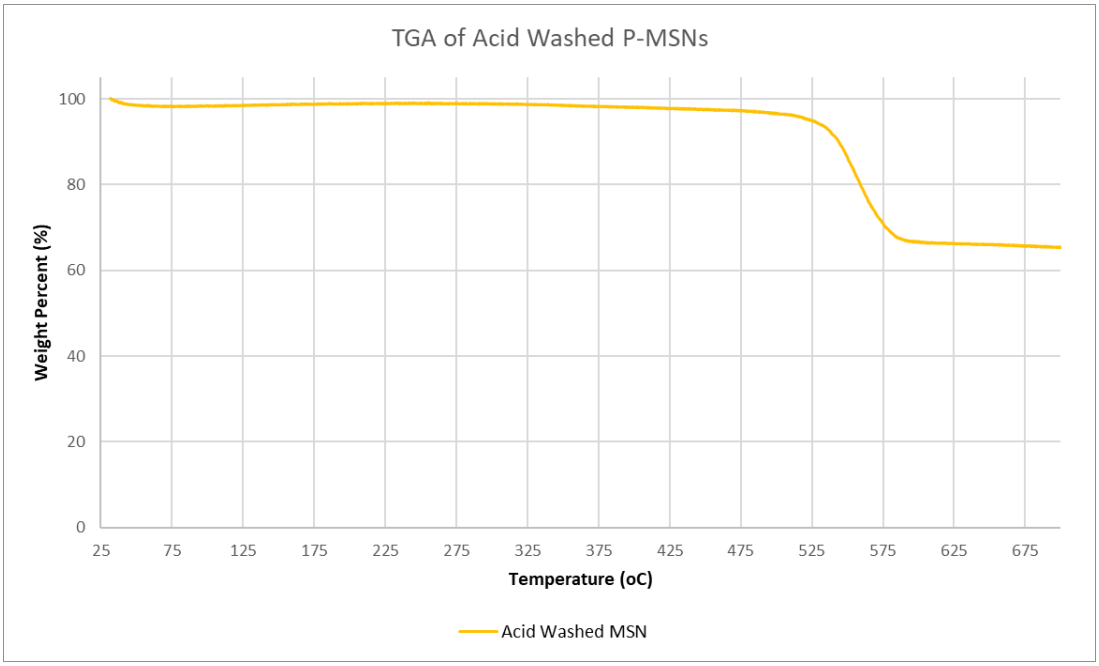

Figure 4.16: TGA of Acid Washed P-MSNs.

	Peptide		*Control*		*P-MSN*	
Temp. Range (°C)	100-500		100-500		100-500	
Exact Temp, Wt %	100.0157	96.95543	100.0199	98.33155	100.0206	96.96505
Exact Temp, Wt %	500.0384	24.95283	500.0352	96.50185	500.0641	91.60806
Weight Percent Lost		72.0026		1.829692		5.356992

Table 4.1: Summation of TGA Data Calculations.

R-MSNs

The TGA results of R-MSNs indicated about 3% loading efficiency. This is close to the P-MSNs. Given the yield was much higher than that of the P-MSNs, it can be assumed that having the hydrophilic rhodamine B attached to the end of the peptide helped form better micelles to build around resulting in a higher yield of MSNs.

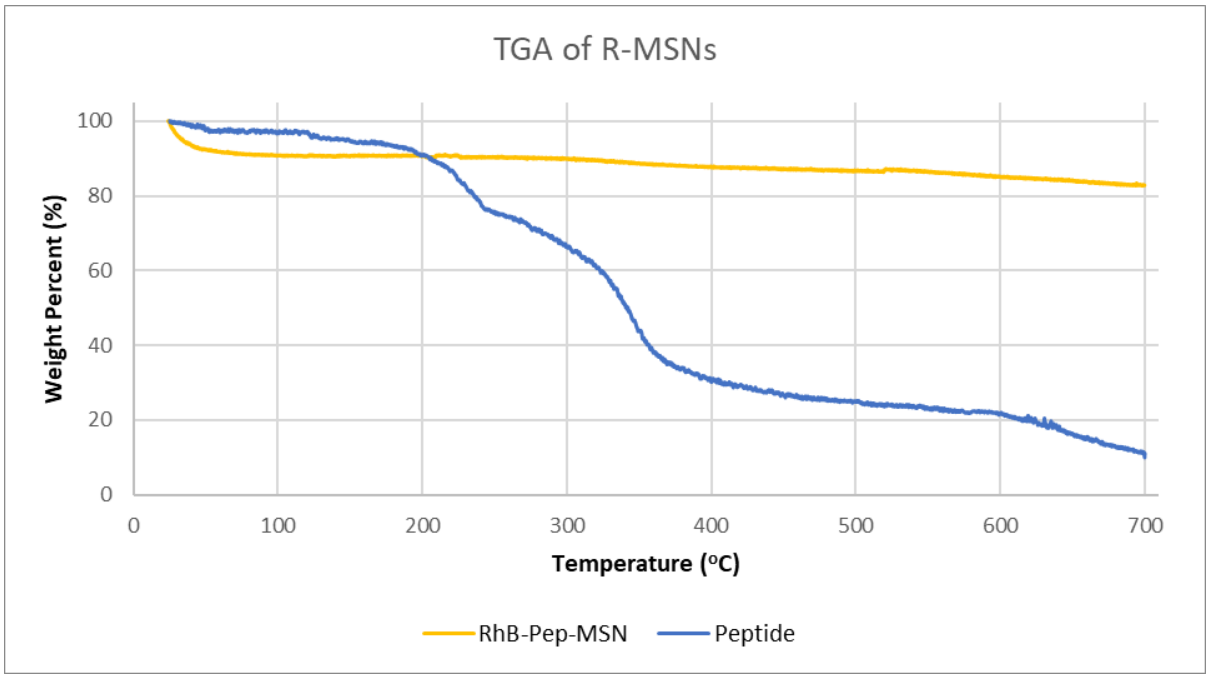

Figure 4.18: TGA of R-MSN and Rh. B-labeled Peptide.

Control Tween MSNs

Control Tween MSNs were run to determine the amount of Tween 80 typically entrapped in the MSNs without the addition of peptide. The calculations showed the weight lost from 100-500^{o}C was 37% and the total weight lost from the MSN from 100-700^{o}C was about 42%. The shape of the TGA curve can also be used to help determine if peptide was successfully loaded. If the shape of the curve differs then Tween 80 was not added alone. Looking at the comparison of

the three TGA curves below, it is clear that both the Tween P-MSN and Tween R-MSNs differ in pattern.

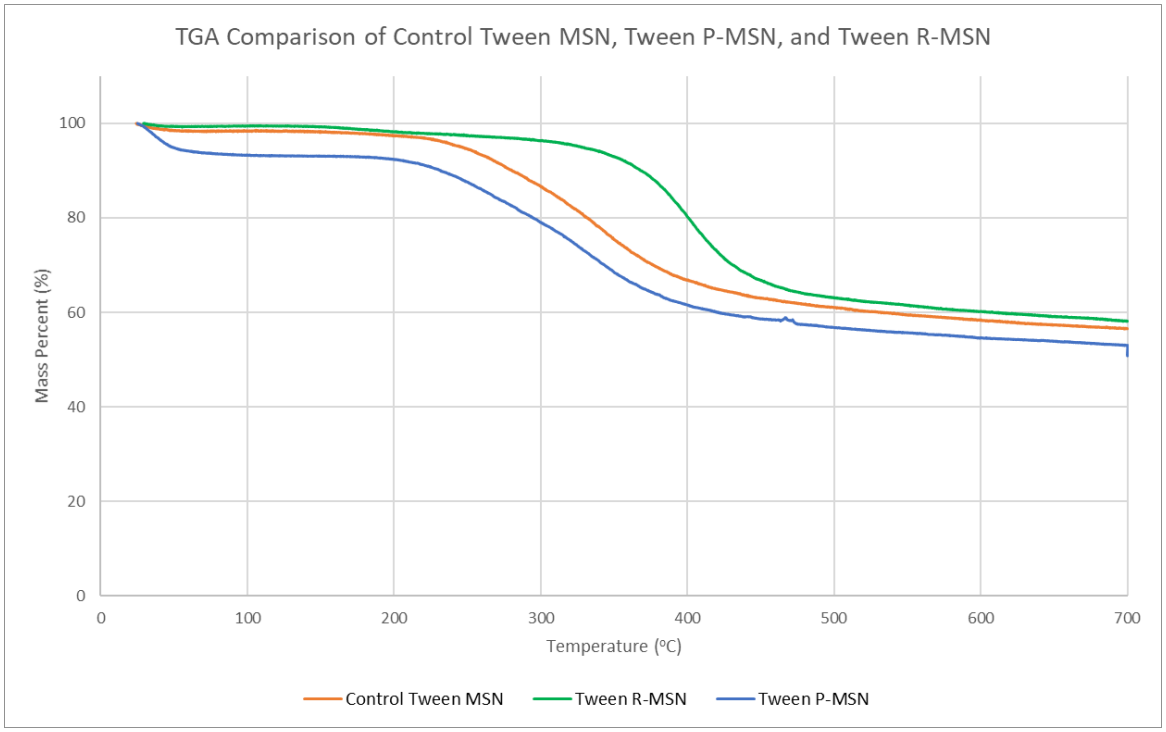

Figure 4.19: TGA Comparison of Control, Tween P-MSNs, and Tween R-MSNs.

Tween P-MSNs

The TGA for Tween MSNs showed a 36.5% loading efficiency. This was not completely peptide, as some of this was Tween 80. Considering the ratio of peptide to tween during synthesis

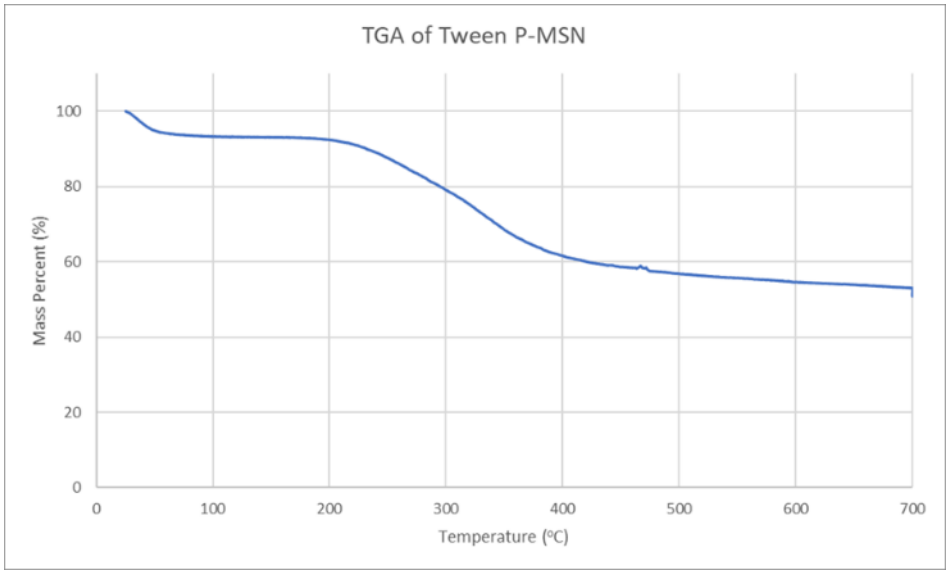

Figure 4.20: TGA of Tween P-MSN.

was 1:10, the true peptide loading was likely closer to 3.6%. This is approximately the same as the P-MSN loading efficiency. The loading efficiency being slightly lower than that of the control suggested that when the non-labeled peptide self-assembles and/or is trapped in the Tween 80 micelle, solvent is also incorporated. This is evident from the much larger solvent loss from 0-100ºC.

Tween R-MSNs

The Tween R-MSNs exhibited a similar TGA to that of the Tween P-MSNs. This suggested a similar morphology and loading efficiency. The loading efficiency was calculated to be to be approximately 36.2% from 100-500ºC. The assumption can be made that one tenth of this loading is peptide resulting in approximately 3.6% loading of Rhodamine-B labeled peptide. It is notable that the weight drop occurred at a later temperature than that of the control. There is also a distinct difference in weight loss from temperatures 100-300ºC of approximately 3% further suggesting a loading efficiency of around 3% peptide. It is also notable that the was not a large solvent lost prior to 100ºC as was seen in the Tween P-MSNs. This suggested the incorporation of Rhodamine-B to the peptide either changed the way that it self-assembles or the way it is entrapped by Tween 80.

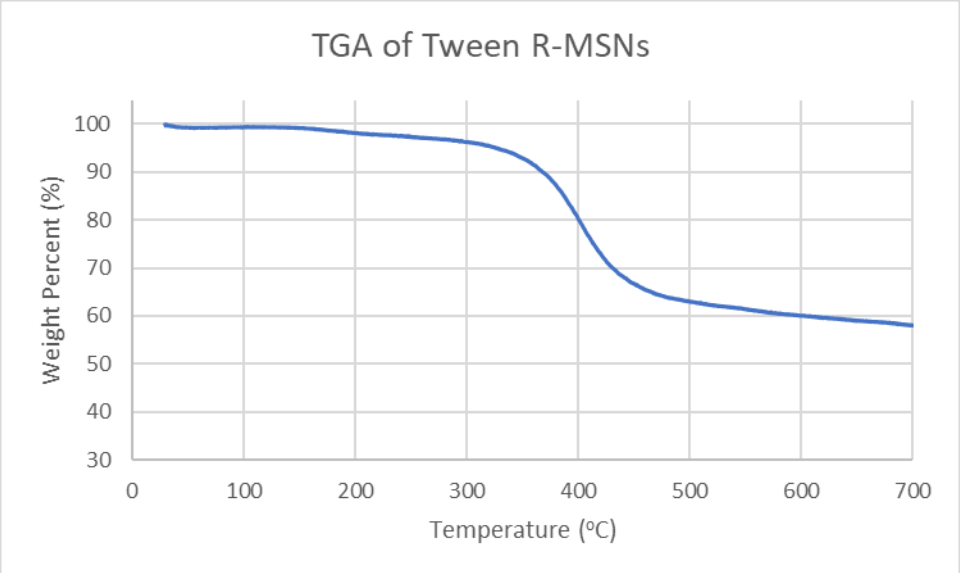

Figure 4.21: TGA of Tween R-MSN.

TEM

P-MSNs

P-MSNs had two different morphologies in their sample. The major structure was meso-mesh made up of multiple small nanoparticles. The less common product was nanostructures shown in Figure 4.16. Both structures are highly porous as show in Figure 4.17. Aggregation was also evident in the TEM images, confirming the assumption made from DLS and Zeta potential.

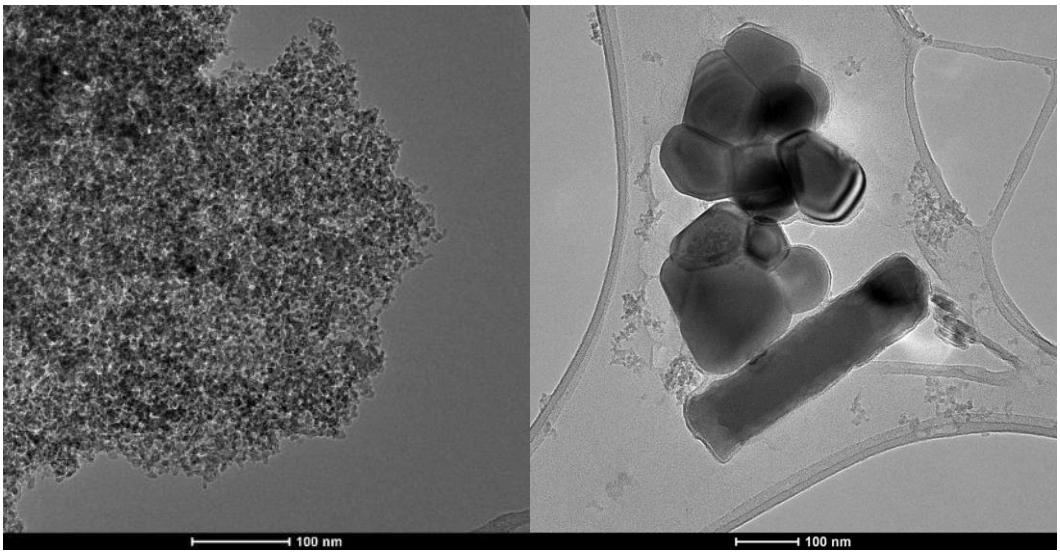

Figure 4.22: TEM of the Two Structures Found in P-MSNs.

Figure 4.23: STEM of P-MSN Showing Porosity.

R-MSNs

Unfortunately, the TEM images were not able to be taken for R-MSNs. It was expected that their structure would be similar to that of the P-MSNs, but due to the differences in earlier characterization this cannot be a definitive. There were also differences observed for the TEMs of Tween MSNs with and without Rhodamine B, making it even more plausible that the structure may be slightly different.

Control Tween MSNs

Control Tween MSNs TEMs did not show a uniform structure. This was surprising, as the expected result was nearly sphere-like structures which were observed when the protocol was used to entrap DOX.[52] The porous, disordered structures can be seen below.

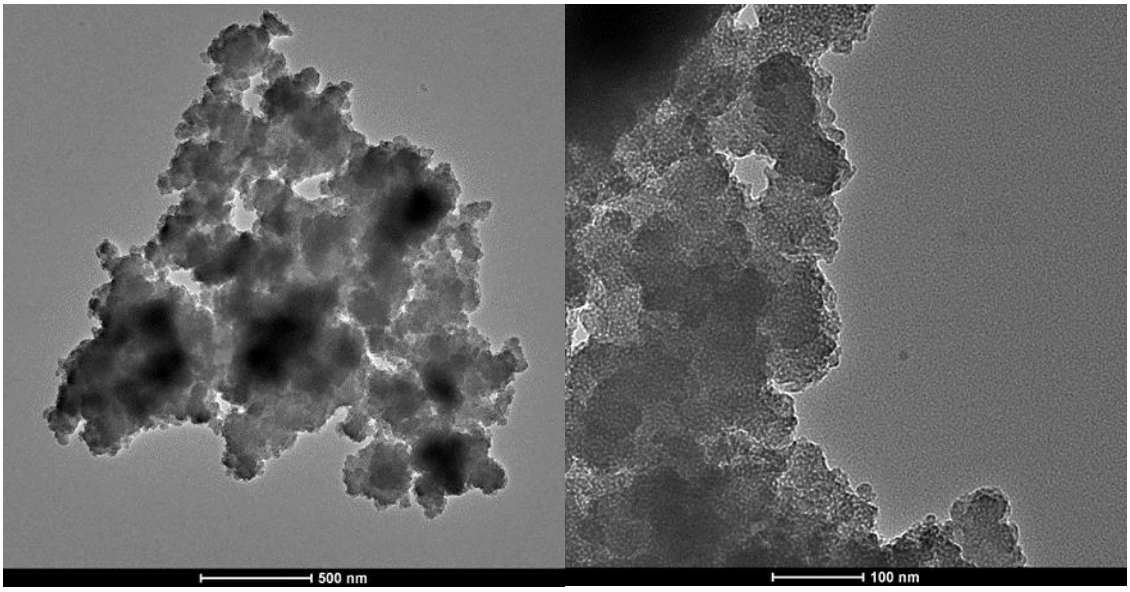

Figure 4.24: TEM of Control Tween MSNs.

Tween P-MSNs

The Tween P-MSNs had a completely different morphology than the P-MSNs and slightly different even from the control Tween MSNs. The images indicate that small nanostructures are clustering together to form larger nanostructures, but there is no longer "meso-mesh". The structures are highly porous. These structures may be easier to envelope in lipid. The average size of the larger nanostructures was just under 900nm.

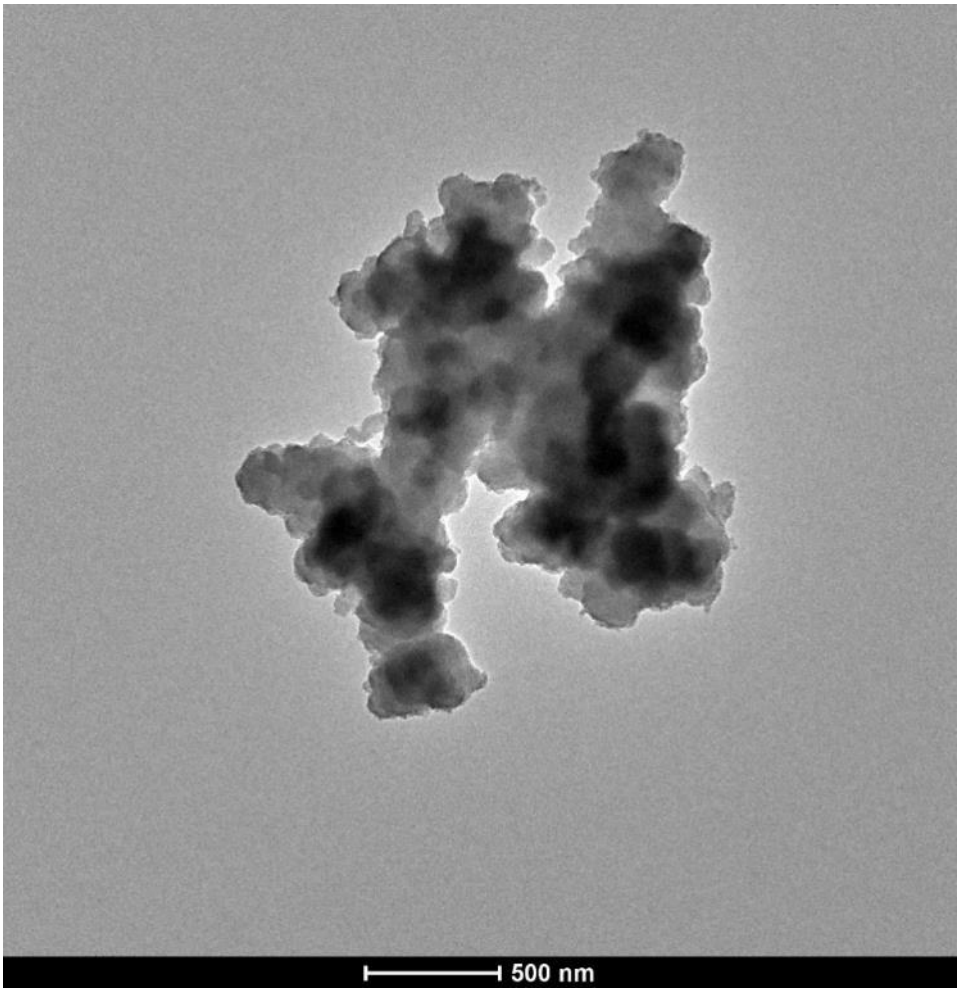

Figure 4.25: TEM of Tween P-MSNs Secondary Structures.

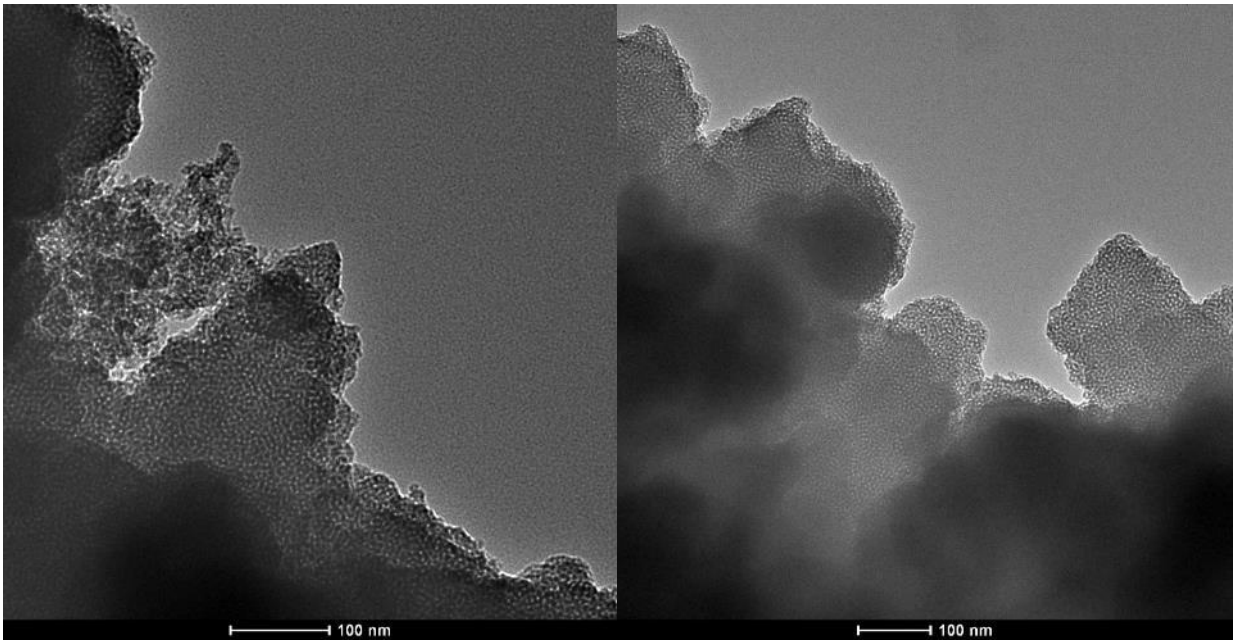

Figure 4.26: Closer View of Tween P-MSN TEM to Show Porosity.

Tween R-MSNs

Tween R-MSNs had an interesting structural change in comparison to Tween P-MSNs. The Tween R-MSNs were spherical in structure and varied greatly in size. The largest spheres were well over 500nm, but the smallest where near 20-30nm. The structures were highly porous which can be observed from the zoomed TEM images. Overall, the Rhodamine B attachment clearly affects the structural outcome of the MSNs. With modification of the procedure it is hoped that the size of the resulting MSNs can be better controlled to provide more uniformity.

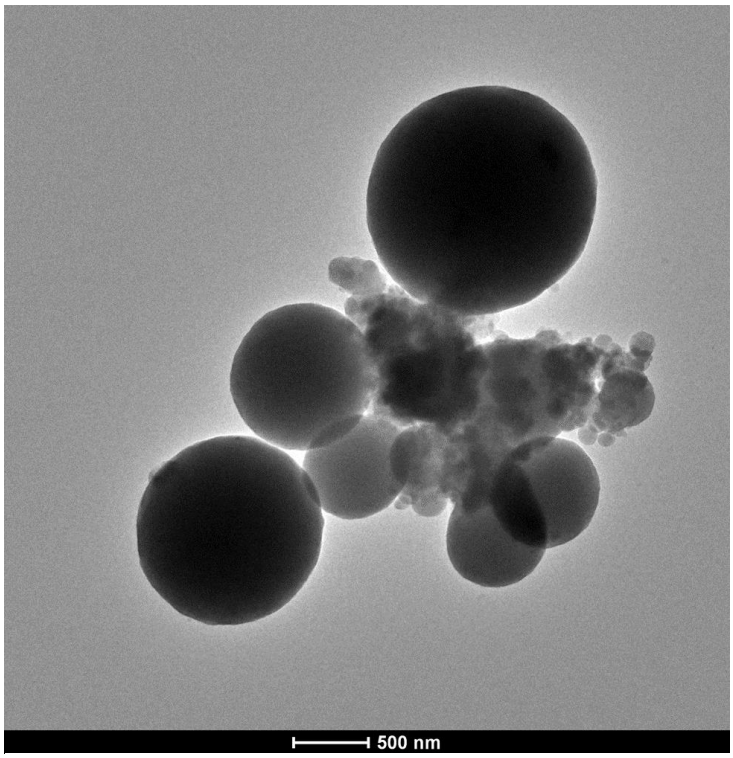

Figure 4.27: TEM of Tween R-MSNs.

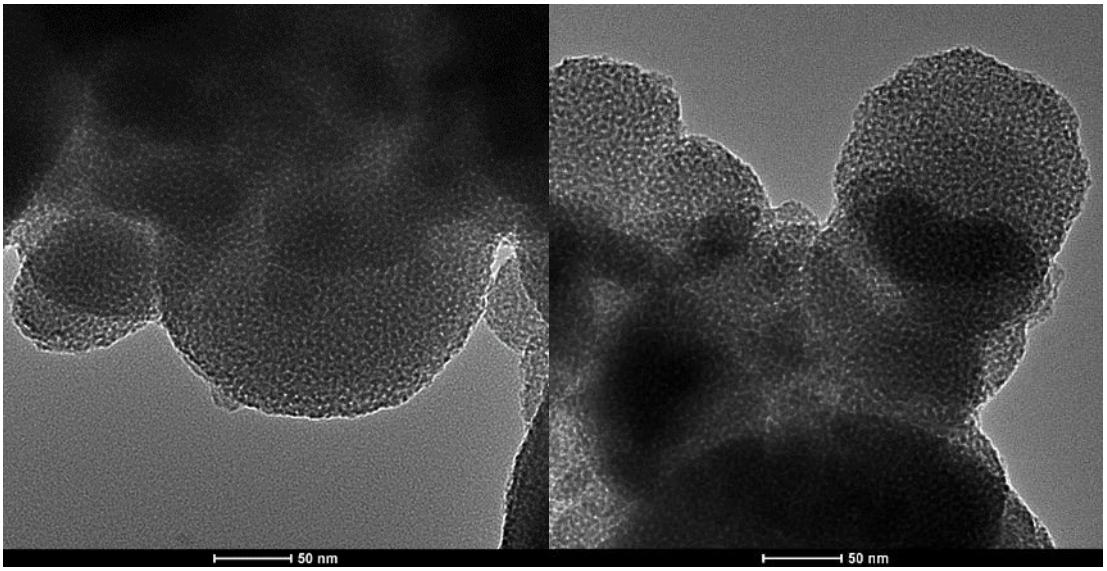

Figure 4.28: TEM of Tween R-MSNs to Show Porosity.

Iron Oxide Nanoparticle Imbedded, Peptide Loaded MSNs

DLS

R-MSNs imbedded with iron oxide nanoparticles (JH-MSNs) were first characterized using DLS. As with the other NaF catalyzed structures, there seemed to be much aggregation. The estimated diameter was 3353nm. The true size of the MSNs would need to be determined by TEM, but clustering was taking place in solution.

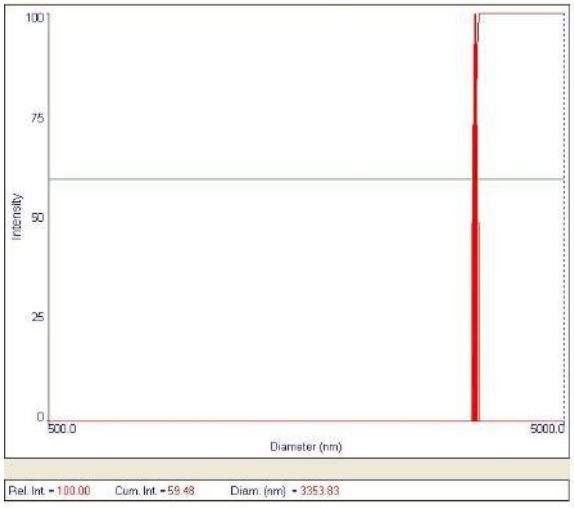

Figure 4.29: DLS of JH-MSNs.

Zeta Potential

The zeta potential of JH-MSNs was closer to zero at only -13mV. The peak was also not uniform suggesting that some populations within the sample may have a slightly higher or lower surface charge. Either way the closeness to neutral explains the aggregation. The zeta potential

also closely resembled that of published work, suggesting the successful incorporation of iron oxide nanoparticles.[55]

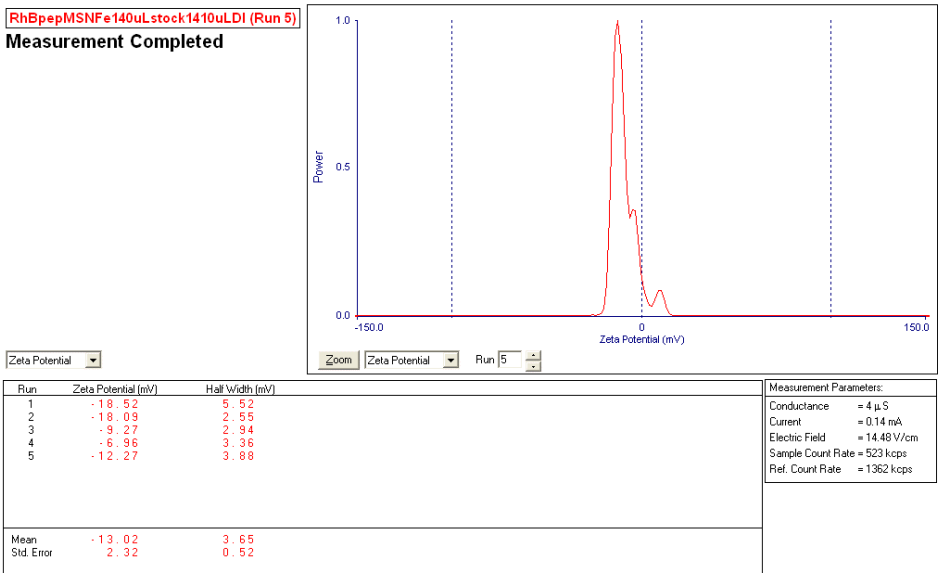

Figure 4.30: Zeta Potential of JH-MSNs.

TGA

The TGA of the JH-MSNs showed a much more rapid release of the encapsulated peptide. This was assumed to be due to the polymer coating. Once it breaks down the peptide is released. The loading efficiency was estimated to high at be 16%, considering R-MSN's was only 3%.

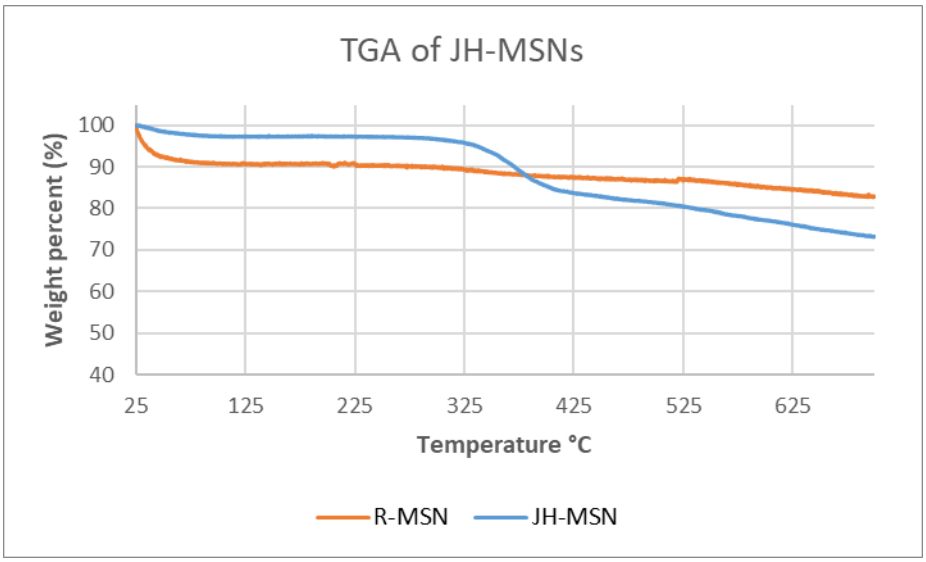

Figure 4.31: TGA of R-MSN vs. JH-MSN.

TEM

Along with TEM, Energy-Dispersive X-ray spectroscopy (EDX) was also used to analyze JH-MSNs. EDX can measure the elemental content of the structures analyzed by TEM. This was used to confirm the presence of iron in the sample. Looking at the images in Figure #, polymer coats the mesoporous structures and iron oxide NPs are imbedded within the polymer. The structures are still porous, which can be observed in Figure #, but have decreased slightly in their porosity. In Figure #, the element content was mapped for carbon, nitrogen, oxygen, silica, and both iron-K and iron-L. The presence of all of the elements proved the nanostructures consisted of the desired reagents.

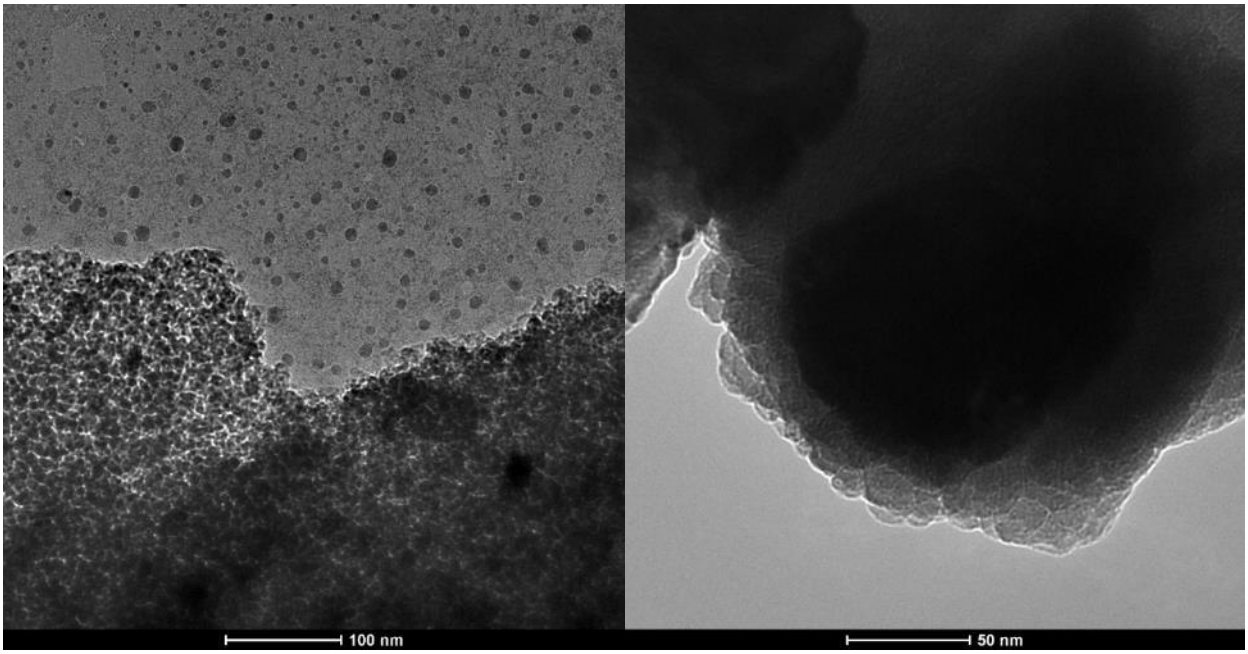

Figure 4.32: TEM of JH-MSNs.

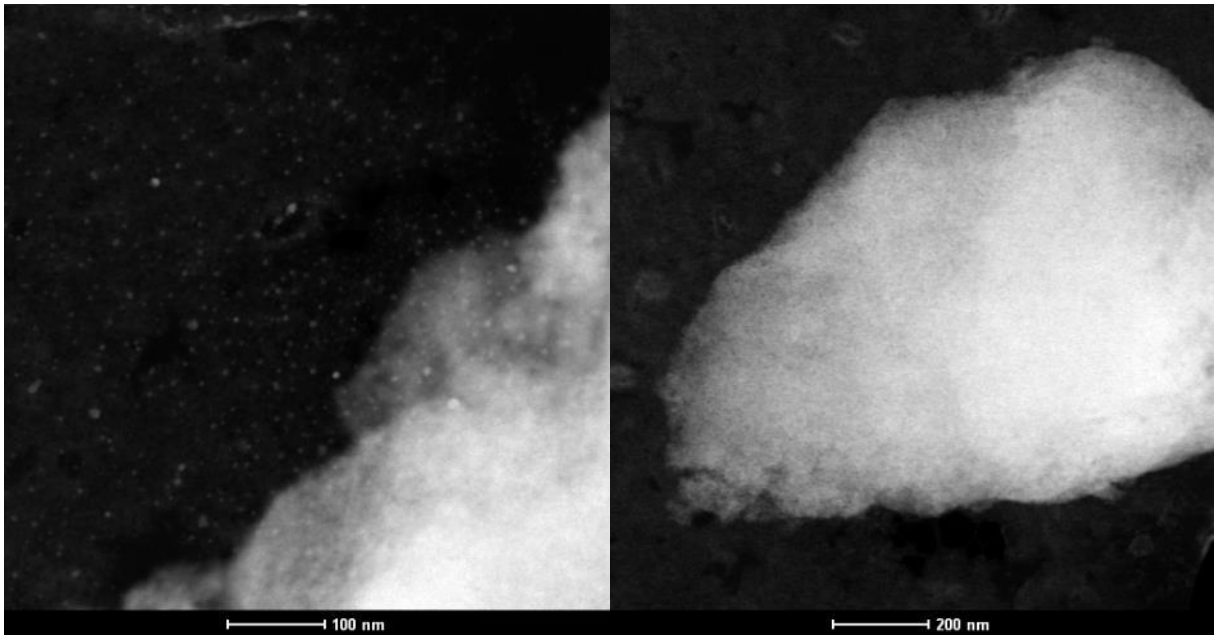

Figure 4.33: STEM of JH-MSN Structures.

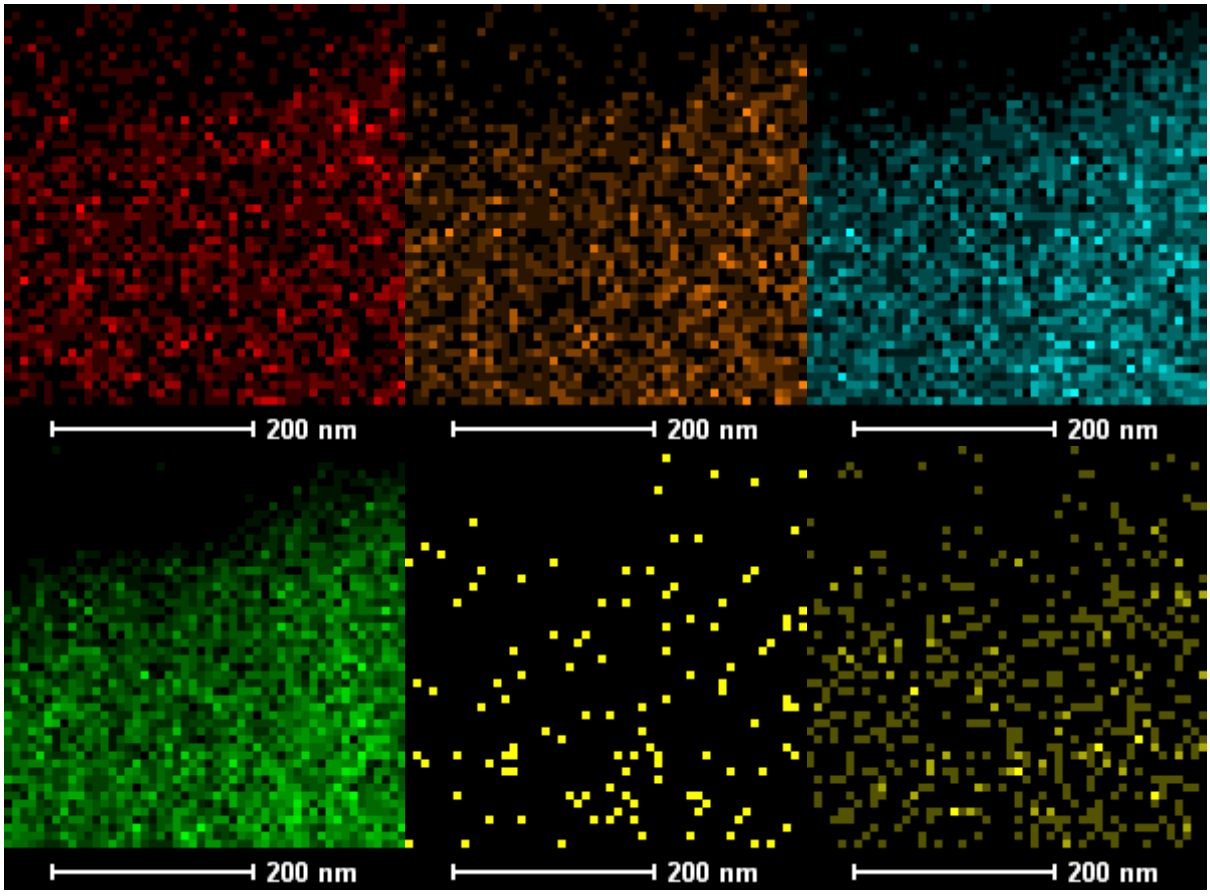

Figure 4.34: EDX Element Mapping of JH-MSNs. Elements Depicted: Carbon (red), Nitrogen (orange), Oxygen (blue), Silica (green), Iron-K and Iron-L Respectively (yellow).

Lipid Enveloped MSNs

From here on the lipid enveloped, iron oxide nanoparticle imbedded, Rhodamine B labeled-peptide loaded MSNs will be referred as JLH-MSNs

DLS

The DLS for the lipid enveloped JH-MSNs was smaller than JH-MSNs alone. It also showed two populations. This was believed to be due to the lipid limiting aggregation slightly. The populations were still far larger than anticipated.

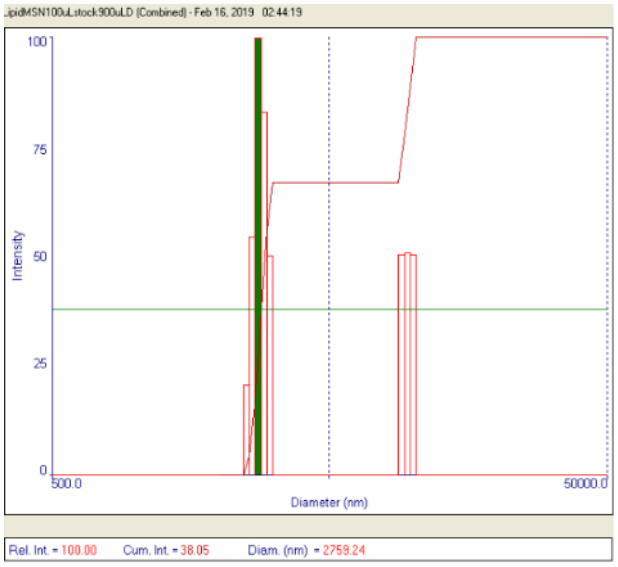

Figure 4.35: DLS of JLH-MSNs.

Zeta Potential

The Zeta potential after lipid enveloping was slightly closer to neutral, but still negative as seen in Figure 4.36. It was expected to increase more due to the positive charge on the lipids.

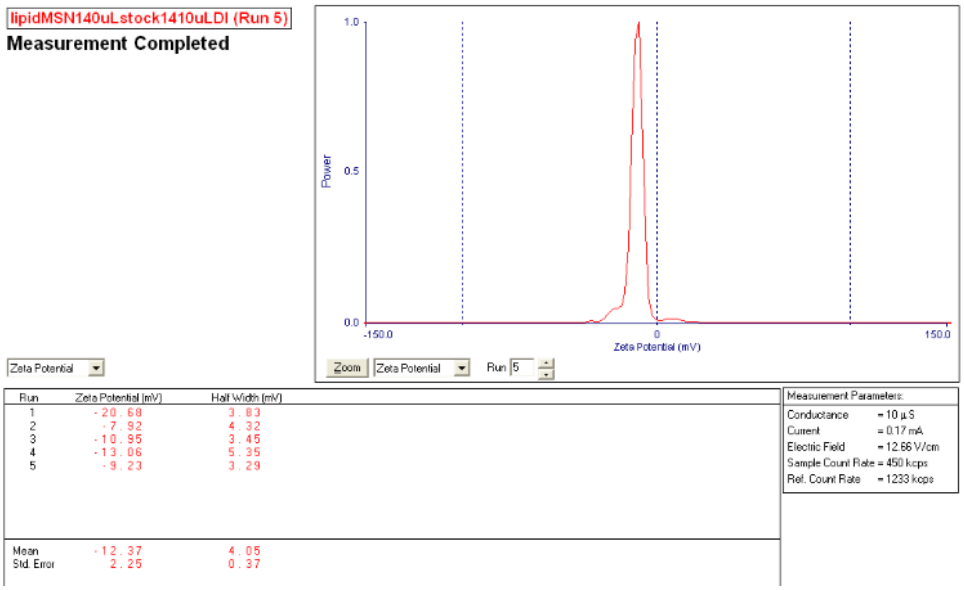

Figure 4.36: Zeta Potential of JHL-MSNs.

TGA

The TGA results gave the most indication of lipid enveloping. The loading efficiency was calculated to be 28% for the appropriate temperature range. This was a 12% increase from JH-MSNs. Considering the MSNs were enveloped directly, all of this weight is attributed to the lipid envelope.

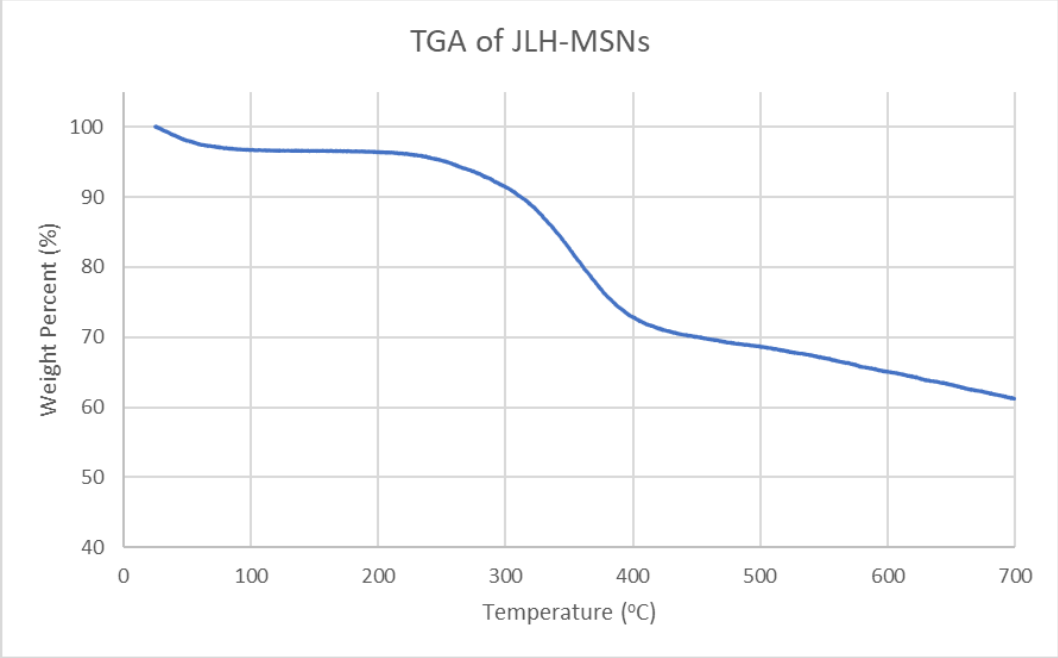

TEM

The TEM images showed that the lipid nicely covered the porous meso-mesh. This was an exciting result and confirmed the findings of the TGA experiments previously performed. It was expected that the coverage would keep the peptide inside the structure and decrease toxicity of the MSNs.

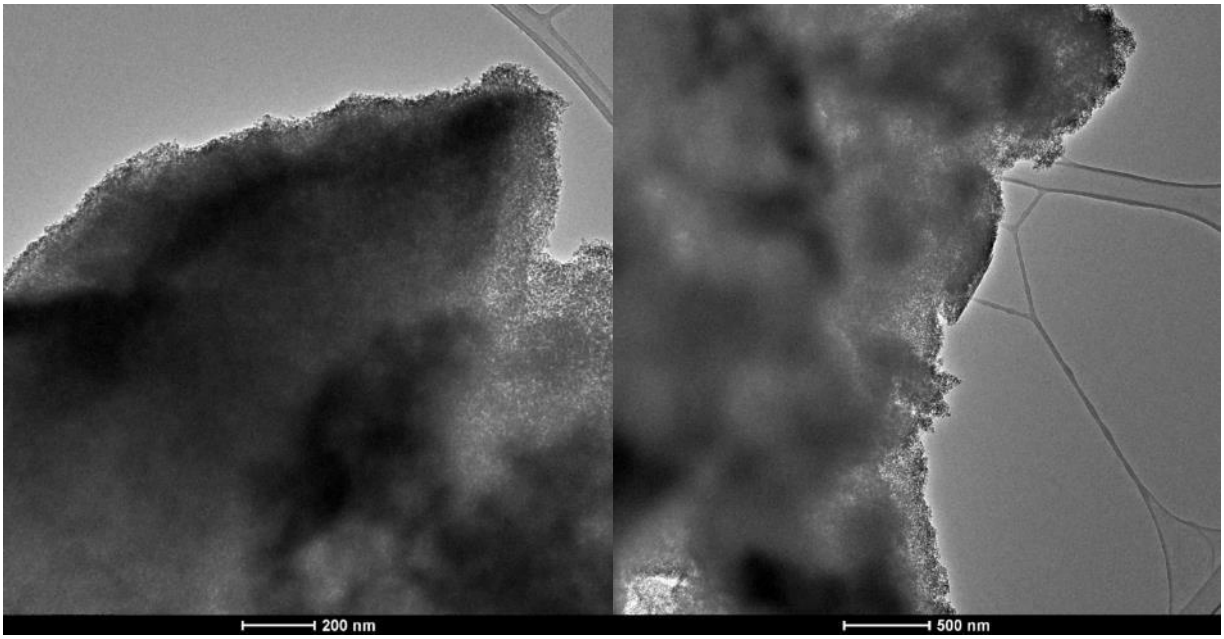

Figure 4.37: TEM of JLH-MSNs.

Cell Viability Assays

Percent cell viabilities were calculated and plotted against concentration of reagent using GraphPad Prism. The data plotted was the mean and error (standard deviation) of 3 side by side replicas. A chart showing the R^2 values for each reagent at 24h and 48h for each cell line can be found in Appendix B.

MSNs Without Gatekeeping System

The first MSNs tested were P-MSNs, R-MSNs, Tween P-MSNs, and Tween R-MSNs. The all MSNs tested exhibited activity toward both cancer cell lines and slightly less activity toward the NSC cell line.

NSC Cell Line

For the NSC cell line it was hoped that there would be less cell death than in other cell lines. Unfortunately, it is known the peptide is not selective and would kill the NSCs if a gatekeeping system is not in place. At 24h, the R-MSNs exhibited the lowest median lethal dose (LC_{50}), then Tween P-MSNs, then P-MSNs third, and finally Tween R-MSNs had the highest LC_{50}

in comparison. This was encouraging because the yields for Tween P-MSNs are significantly higher than that of the P-MSNs and less peptide would be required to make them with the same killing efficiency. This could be beneficial when moving to *in-vivo* and determining dosing. It should also be noted that although Tween R-MSNs had the highest LC_{50}, it killed the most cells at highest concentrations. This is clear when looking at figure 4.8a.

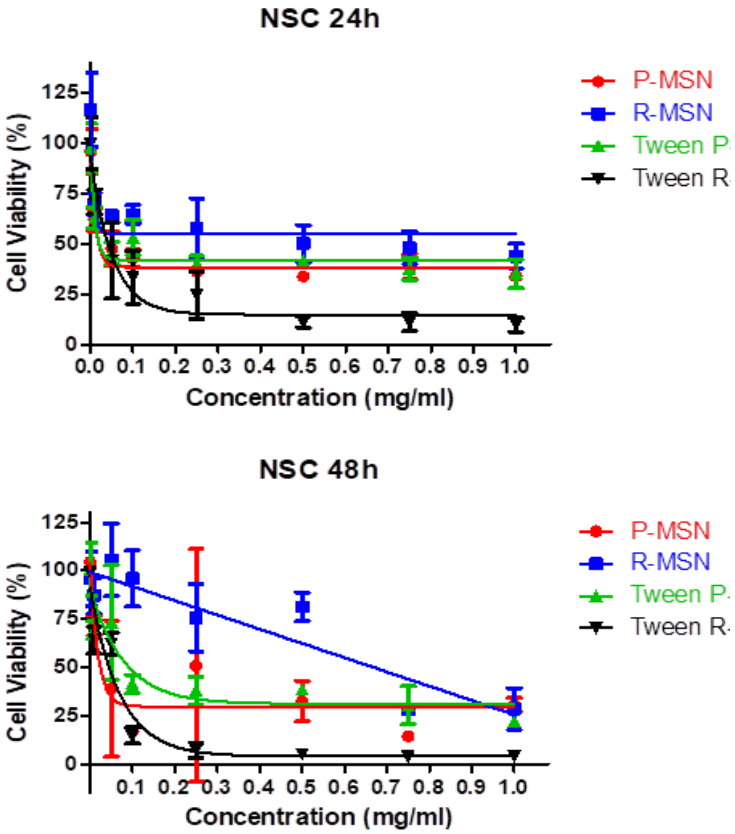

Figure 4.38: Cell Viability Assays of Neural Stem Cells against MSNs Without Gatekeepers at 24h and 48h. P-MSN (red), R-MSN (blue), Tween P-MSN (green), and Tween R-MSN (black).

For the 48h trial, theLC_{50} trend changed slightly with P-MSNs having the lowest LC_{50}, then Tween R-MSNs, then Tween P-MSNs. Unfortunately, for some reason the 48h NSC trials were problematic giving very large 95%CI ranges for both P-MSNs and R-MSNs making the data unreliable. Again, The Tween R-MSNs killed the most cells at high concentrations. Though this did further encourage the use of Tween based MSNs. The LC_{50} values with 95%CI are summarized in Table 4.2.

LC_{50} Values	*P-MSN*	*R-MSN*	*Tween P-MSN*	*Tween R-MSN*
24 hours	0.008419	0.004968	0.007262	0.03562
	0.005788 to 0.01544	0.002929 to 0.01636	0.004768 to 0.01523	0.02442 to 0.06581
48 hours	0.01299	~ 295.1	0.05496	0.04912
	(0.005588 to +infinity)	(Very wide)	0.03173 to 0.2050	0.03614 to 0.07665

Table 4.2: LC_{50} Values in mg/ml and 95% Confidence Intervals for MSNs without Gatekeepers against NSC Cell Line.

B16F10 Cell Line

When tested against the B16F10 cell line all four MSNs showed increased activity in comparison to their activity against NSC. The 24h trial showed excellent LC_{50} values for all four MSNs summarize in TABLE #. Looking at both the 24h and 48h trials it became clear that the MSN with the best overall activity was Tween P-MSNs. The Tween R-MSNs had a statistical outlier at 0.1mg/ml concentration, so it was removed from the plotted and calculated data.

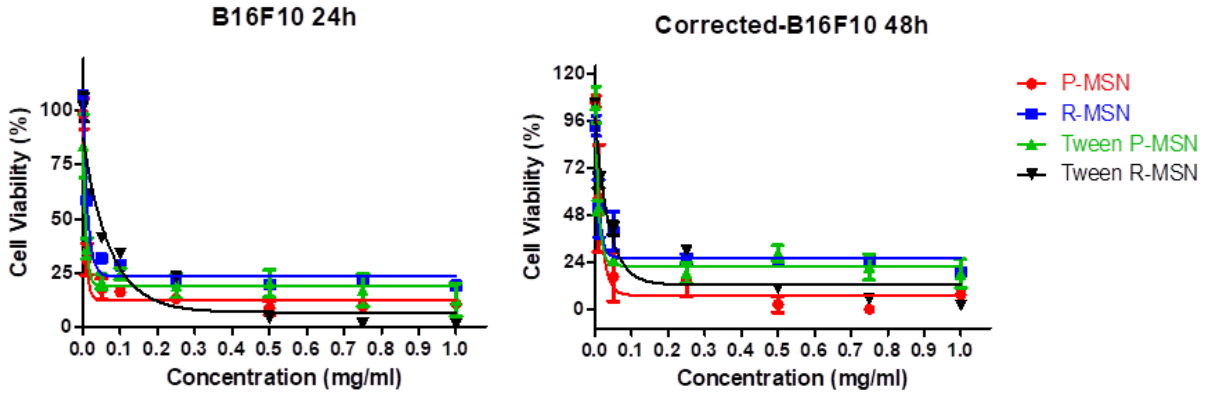

Figure 4.39: Cell Viability Assays of B16F10 against MSNs Without Gatekeepers at 24h and 48h. P-MSN (red), R-MSN (blue), Tween P-MSN (green), and Tween R-MSN (black).

LC_{50} Values	*P-MSN*	*R-MSN*	*Tween P-MSN*	*Tween R-MSN*
24 hours	0.004544	0.008459	0.005283	0.05013
	0.003733 to 0.005806	0.007120 to 0.01042	0.003730 to 0.00905	0.03555 to 0.08499
48 hours	0.01075	0.007586	0.006859	0.02572
	0.007289 to 0.02047	0.005095 to 0.01484	0.005354 to 0.00954	0.01753 to 0.04821

Table 4.3: LC_{50} Values in mg/ml and 95% Confidence Intervals for MSNs without Gatekeepers against B16F10 Cell Line.

GL26 Cell Line

In the past, D-K_6L_9 showed the best activity toward GL26 cell lines, but after running these trials it was clear that the self-assembling peptide's activity toward GL26 cells and B16F10 cells was approximately the same. Again, when the four MSNs were tested all had great activity at both 24h and 48h. when looking at the LC_{50} values summarized in Table#, Tween P-MSNs have the best overall activity because their LC_{50} is not only the lowest, but it is consistent. It is believed that the bulky structure of Rhodamine B may cause the peptide to get slight

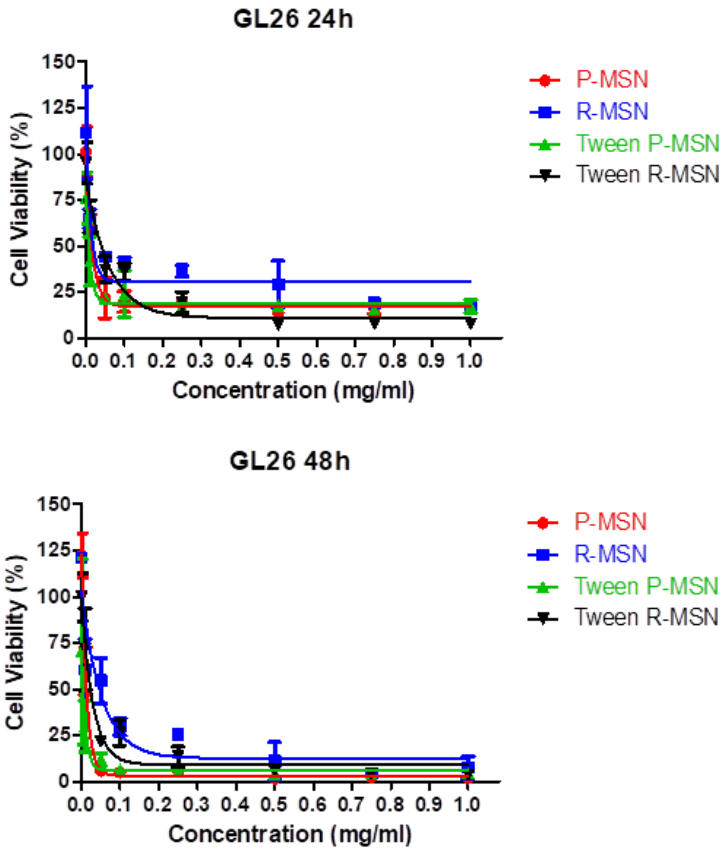

Figure 4.40: Cell Viability Assays of Neural Stem Cells against MSNs Without Gatekeepers at 24h and 48h. P-MSN (red), R-MSN (blue), Tween P-MSN (green), and Tween R-MSN (black).

stuck inside the MSNs and this could be the reason that both R-MSN and Tween R-MSN have slightly worse activity against all three cell lines. These findings reiterate the need for a controlled gatekeeping system.

LC_{50} Values	*P-MSN*	*R-MSN*	*Tween P-MSN*	*Tween R-MSN*
24 hours	0.01132	0.009037	0.007723	0.04219
	0.008745 to 0.01604	0.005652 to 0.02253	0.005177 to 0.01520	0.03064 to 0.06773
48 hours	0.009289	0.03639	0.007200	0.02064
	0.007867 to 0.01134	0.02351 to 0.08056	0.003752 to 0.08853	0.01437 to 0.03659

Table 4.4: LC_{50} Values in mg/ml and 95% Confidence Intervals for MSNs without Gatekeepers against GL26 Cell Line.

JH-MSNs Against NSC Cell Line

Due to a shortage of material the JH-MSNs where only tested against NSC cell lines. The expected outcome of this test was that the MSNs may have slightly lower activity due to the polymer coating containing iron oxide NPs, but it would not be concerning if they still showed activity because this was not the final portion of the gatekeeping system. The cell viability assay showed decreased activity as expected, but even at lowered concentration was toxic enough to encourage the use of a lipid bilayer envelope. The LC_{50} of

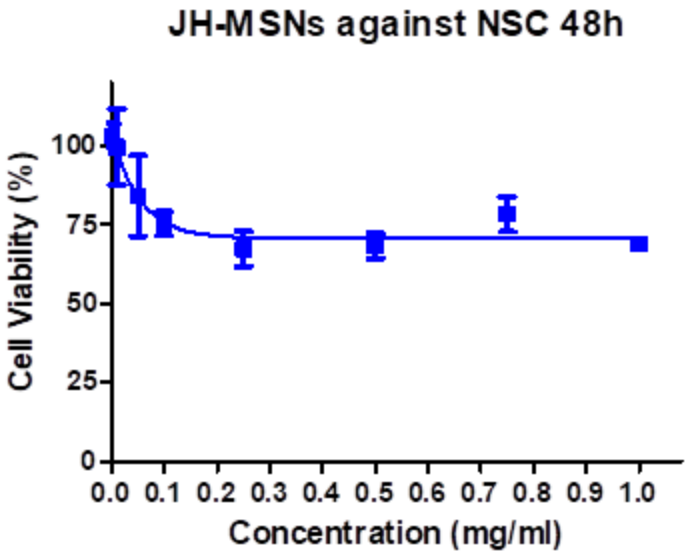

Figure 4.41: Cell Viability Assay of JH-MSNs against NSC Cell Line over a 48h Period.

JH-MSNs against NSC at 48h was 0.03706mg/ml (0.02226 to 0.1106). This is 75 times less than the R-MSNs alone.

JLH-MSNs Against Various Cell Lines

Once the MSNs had a lipid layer added they were tested against all three cell lines. The outcome was not exactly as expected because the MSNs still killed approximately half the population at low concentrations after 48h. The decreased toxicity is a great sign, but the lack of complete gatekeeping is likely due to the lack of uniformity in the MSN structures. This causes the lipid to not cover some portions of the material. To combat this issue, the MSN samples will be separated by size using a unique centrifuge and the experiment will be repeated with more uniformly sized MSNs.

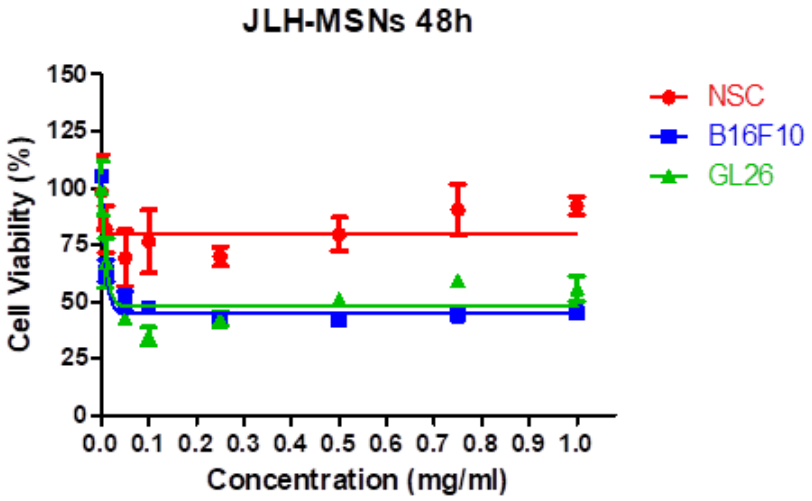

Figure 4.42: Cell Viability Assay of JLH-MSNs Against Several Cell Lines over a 48h Period.

Once the MSNs had a lipid layer added they were tested against all three cell lines. The outcome was not exactly as expected because the MSNs still killed approximately half the population at low concentrations after 48h. The decreased toxicity is a great sign, but the lack of complete gatekeeping is likely due to the lack of uniformity in the MSN structures. This causes the lipid to not cover some portions of the material. To combat this issue, the MSN samples will be separated by size using a unique centrifuge and the experiment will be repeated with more uniformly sized MSNs. Although the calculated LC_{50} is low, it is also notable that significantly

less cell death occurred at all concentrations with the addition of the gatekeeping system. Also, with the exception of the B16F10 cell line the R^2 values of the calculated graphs are very low.

LC_{50} Values	*NSC*	*B16F10*	*GL26*
48 hours	0.003232	0.005903	0.006800
	0.0007237 to +infinity	0.004855 to 0.007529	0.004085 to 0.02029
R^2	0.2106	0.9722	0.7892

Table 4.5: LC_{50} Values is mg/ml and 95% Confidence Intervals of JLH-MSNs against NSC, B16F10, and GL26 Cell Lines.

Discussion

In this chapter the successful incorporation of an anti-cancer, self-assembling peptide into a mesoporous nanostructure was shown. The incorporation was done in a one-pot method either using Tween 80 as a templating agent or without Tween 80 using the peptide alone as the templating agent. All the peptide incorporated MSNs showed great activity against the melanoma and glioma cancer cell lines. Unfortunately, their toxicity was still high against NSC cell lines. The design and application of a novel radio-frequency release gatekeeping system was also discussed. This gatekeeping system limits the toxicity of the MSNs via a triggered release of the encapsulated peptide. The preliminary trials were promising. Iron oxide NPs were successfully imbedded in a polymer coating off the MSN structure and a lipid layer was successfully added to the MSNs. The cell viability assays showed a decrease in cell death with the applied gatekeeping system. Due to the lack of uniformity in the MSNs the lipid results were lackluster, but still opened the door for further improvement of the system.

Future Work

The next steps for this project include finetuning the MSN synthesis protocol to achieve uniform structures or using a centrifuge to separate the MSNs based on size. Once this has been done the gatekeeper will be reapplied and the expectation is that the gatekeeping ability will be improved. The Tween based MSNs will also be investigated further given their LC_{50} values were the all-around best. The R-MSNs where initially used so the peptide could be more easily tracked in either fluorescence studies or confocal imaging. Tween R-MSN will be used in its place for those studies due to the spherical structure and potential ease of enveloping. Once the gatekeeper successfully holds the peptide in, the next rational step will be to perform release studies to determine if temperature increase and radio frequency will release the drug and at what rate. Then cell viability assays will be repeated before moving to *in-vivo* studies.

References

1. Santos, C.S.C.; Gabriel, B.; Blanchy, M.; Menes, O.; García, D,; Blanco, M.; Arconada, N.; Neto, V. *Industrial Applications of Nanoparticles – A Prospective Overview, Materials Today: Proceedings*, **2015**, 2(1), 456-465. ISSN 2214-7853.

2. Anselmo, A.C. and Mitragotri, S. Nanoparticles in the clinic. *Aiche: Bioeng. & Translat. Med*. 2016, 1, 10-29. DOI 10.1002/btm2.10003

3. Bobo, D.; Robinson, K.J.; Islam, J.; Thurecht, K.J.; Corrie, S.R. Nanoparticle-Based Medicines: A Review of FDA-Approved Materials and Clinical Trials to Date. *Pharm Res.* **2016**, 33(10), 2373-2387.

4. Parisi, D.; Vigani, M.; Rodríguez-Cerezo, E. Agricultural Nanotechnologies: What are the current possibilities? *Nano Today*. **2015**, 10, 124-127.

5. Palanikumar, L.; Choi, E.S.; Cheon, J.Y.; Joo, S.H.; Ryu, J-H. Noncovalent Polymer-Gatekeeper in Mesoporous Silica Nanoparticles as a Targeted Drug Delivery Platform. *Adv. Funct. Mater.* **2015**, 25, 957–965.

6. Young, S. K. "Sol-Gel Science for Ceramic Materials" 2006. https://www.sigmaaldrich.com/technical-documents/articles/material-matters/sol-gel-science-for.html (accessed May 9, 2018).

7. Chen, M.; He, X.; Wang, K.; He, D.; Yang, S.; Qiu, P.; Chen, S. A pH-responsive polymer/mesoporous silica nano-container linked through an acid cleavable linker for intracellular controlled release and tumor therapy in vivo J. Mater. Chem. B, 2014, 2, 428

8. Thomas, M.J.K.; Slipper, I.; Walunj, A.; Jain, A.; Favretto, M.E.; Kallinteri, P.; Douroumis, D. Inclusion of poorly soluble drugs in highly ordered mesoporous silica nanoparticles. Int. J. Pharm, 2010, 387(1), 272-277.

9. "CDC: 1 in 3 antibiotic prescriptions unnecessary". *Center for Disease Control.* **2016.** https://www.cdc.gov/media/releases/2016/p0503-unnecessary-prescriptions.html (accessed May 9, 2018).

10. The World Health Organization, Regional Office of Europe. "Pharmacists have decisive role in combating antibiotic resistance, says new WHO European survey". Copenhagen **2014**.

11. "Antibiotic / Antimicrobial Resistance". *Center for Disease Control.* **2018.** https://www.cdc.gov/drugresistance/about.html (accessed May 9, 2018).

12. "Resistance mechanisms – Antibiotic resistance" ReAct. https://www.reactgroup.org/toolbox/understand/antibiotic-resistance/resistance-mechanisms-in-bacteria/ (accessed Jan. 10, 2019).

13. Salager, J-L. "Surfactants - Types and Uses". *Laboratorio FIRP*: **2002**, p. 2-5

14. “Cancer Facts & Figures 2019”. *American Cancer Sociecty.* **2019.** https://www.cancer.org/research/cancer-facts-statistics/all-cancer-facts-figures/cancer-facts-figures-2019.html (accessed Feb. 1, 2019)

15. “Types of Cancer Treatment”. *National Cancer Institute.* **2017.** https://www.cancer.gov/about-cancer/treatment/types (accessed Feb. 1, 2019)

16. “Surgery to Treat Cancer”. *National Cancer Institute.* **2015.** https://www.cancer.gov/about-cancer/treatment/types/surgery (accessed Feb. 1, 2019)

17. “Radiation Therapy to Treat Cancer”. *National Cancer Institute.* **2019.** https://www.cancer.gov/about-cancer/treatment/types/radiation-therapy (accessed Feb. 5, 2019)

18. “Radiation Therapy Side Effects”. *National Cancer Institute.* **2018.** https://www.cancer.gov/about-cancer/treatment/types/radiation-therapy/side-effects (accessed Feb. 28, 2019)

19. “Chemotherapy to Treat Cancer”. *National Cancer Institute.* **2015.** https://www.cancer.gov/about-cancer/treatment/types/chemotherapy (accessed Feb. 18, 2019)

20. “Immunotherapy to Treat Cancer”. *National Cancer Institute.* **2015.** https://www.cancer.gov/about-cancer/treatment/types/immunotherapy (accessed Feb. 18, 2019)

21. “Immunotherapy Fact of the Day #4” *National Cancer Institute.* **2017.** https://www.cancerresearch.org/join-the-cause/cancer-immunotherapy-month/30-facts/04 (accessed Feb. 18, 2019)

22. Tawfik, S.M. “Synthesis, surface, biological activity and mixed micellar phase properties of some biodegradable gemini cationic surfactants containing oxycarbonyl groups in the lipophilic part”. *Ind. Eng. Chem. Res.* 28, **2015**, 71-183, ISSN 1226-086X, https://doi.org/10.1016/j.jiec.2015.02.011.

23. Shaban, S.M.; Fouda, A.S.; Rashwan, S.M.; Ibrahim, H.E.; El-Bhrawy, M.F. Synthesis and characterization of newly cationic surfactants based on 2-(2-(dimethylamino)ethoxy)ethanol: physiochemical, thermodynamic and evaluation as biocide, *J. Mol. Liq*., **2016**, 221, 224-234, ISSN 0167-7322, .https://doi.org/10.1016/j.molliq.2016.05.088

24. Bagher, A.M., Quantum Dots Applications, *Sensors & Transducers*, **2016**, 198(3), 37-43

25. Wen, J.; Yang, K.; Liu, F.; Li, H.; Xu, Y.; Sun, S. Diverse gatekeepers for mesoporous silica nanoparticle based drug delivery systems. *Chem. Soc. Rev.*, **2017**, 46, 6024-6045

26. Engel, S.; Möller, N.; Ravoo, B.J., Stimulus-Responsive Assembly of Nanoparticles using Host–Guest Interactions of Cyclodextrins. *Chem. Eur. J.* **2018,** 24, 4741–4748

27. Chen, X.; Yao, X.; Zhang, Z.; Chen, L. Plug-and-play multifunctional mesoporous silica nanoparticles as potential platforms for cancer therapy. *RSC Adv.*, **2014**, 4, 49137

28. He, D.; Li, X.; He, X.; Wang, K.; Tang, J.; Yang, X.; He, X.; Yang, X.; Zou, Z. Noncovalent assembly of reduced graphene oxide and alkyl-grafted mesoporous silica: an effective drug carrier for near-infrared light-responsive controlled drug release. *J. Mater. Chem. B*, **2015**, 3, 5588-5594

29. He, D.; He, X.; Wang, K.; Cao, J.; Zhao, Y. A Photon-Fueled Gate-Like Delivery System Using i-Motif DNA Functionalized Mesoporous Silica Nanoparticles. *Adv. Funct. Mater*. **2012**, 22, 4704–4710

30. Tan, L.; Wu, H-X.; Yang, M-Y.; Liu, C-J.; Zhou, R-X. The dual-stimulated release of size-selected cargos from cyclodextrin-covered mesoporous silica nanoparticles. *RSC Adv.*, **2015**, 5, 10393-10399

31. Tan, S.; Xu Li, X.; Guo, Y.; Zhang, Z. Lipid-enveloped hybrid nanoparticles for drug delivery. *Nanoscale*, **2013**, 5, 860

32. Liu, C.; Qing, Z.; Zheng, J.; Deng,, L.; Ma, C.; Li, J.; Li, Y.; Yang, S.; Yang, J.; Wang, J.; Tan, W.; Yang, R. DNA-templated in situ growth of silver nanoparticles on mesoporous silica nanospheres for smart intracellular GSH-controlled release. *Chem. Commun.*, **2015**, 51, 6544-6547

33. Zhu, C-L.; Lu, C-H.; Song, X-Y.; Yang, H-H.; Wang, X-R. Bioresponsive Controlled Release Using Mesoporous Silica Nanoparticles Capped with Aptamer-Based Molecular Gate. *J. Am. Chem. Soc.* **2011**, 133, 1278–1281

34. Manicone AM, McGuire JK. Matrix metalloproteinases as modulators of inflammation. *Semin. Cell. Dev. Biol*. **2007,** 19(1), 34-41

35. de la Torre, C.; Mondragón, L.; Coll, C.; Sancenón, F.; Marcos, M. D.; Martínez-Máñez, R.; Amorós, P.; Pérez-Payá, E.; Orzáez, M. Cathepsin-B Induced Controlled Release from Peptide-Capped Mesoporous Silica Nanoparticles. *Chem. Eur. J.*, **2014**, 20, 15309-15314. doi:10.1002/chem.201404382

36. Shaban, S.M.; Aiad, I.; Fetouh, H.A.; Maher, A. "Amidoamine double tailed cationic surfactant based on dimethylaminopropylamine: Synthesis, characterization and evaluation as biocide". *J. Mol. Liq.*, 212, **2015**, 699-707, ISSN 0167-7322, https://doi.org/10.1016/j.molliq.2015.10.024.

37. Zaky, M.F; Aiad, I.A.; Tawfik, S.M. Synthesis, characterization, surface and biocidal effect of some germinate nonionic surfactants, *Ind. Eng. Chem. Res.*, **2015**, 201, 1174-1182, ISSN 1226-086X, https://doi.org/10.1016/j.jiec.2014.05.031.

38. Massi, L.; Guittard, F.; Levy, R.; Géribaldi, S. "Enhanced activity of fluorinated quaternary ammonium surfactants against Pseudomonas aeruginosa". *Eur. J. Med. Chem.*, 2009, 44(4), 1615-1622, ISSN 0223-5234, https://doi.org/10.1016/j.ejmech.2008.07.032.

39. Jelinkova, P.; Splichal, Z.; Jimenez, A.; Haddad, Y.; Mazumdar, A.; Sur, V. P.; Milosavljevic, V.; Kopel, P.; Buchtelova, H.; Guran, R.; Zitka, O.; Richtera, L.; Hegerova, D.; Heger, Z.; Moulick, A.; Adam, V. Novel vancomycin-peptide conjugate as potent antibacterial agent against vancomycin-resistant Staphylococcus aureus. *Infect. Drug Resist.* **2018**, 11, 1807-1817 doi:10.2147/IDR.S160975

40. Arnusch CJ, Pieters RJ, Breukink E. Enhanced membrane pore formation through high-affinity targeted antimicrobial peptides. *PLoS One*. **2012**, 7(6), e39768

41. https://www.ebi.ac.uk/merops/

42. Campbell, M.L.; Marchaim, D.; Pogue, J.M.; Sunkara, B.; Bheemreddy, S.; Bathina, P.; Pulluru, H.; Chugh, N.; Wilson, M.N.; Moshos, J.; Ku, K.; Hayakawa, K.; Martin, E.T.; Lephart, P.R.; Rybak, M.J.; Kaye, K.S. Treatment of Methicillin-Resistant Staphylococcus aureus Infections With a Minimal Inhibitory Concentration of 2 μg/mL to Vancomycin. *Ann Pharmacother*. **2012,** 46(12),1587-1597.

43. Papo, N.; Oren, Z.; Pag, U.; Sahl, H.-G.; Shai, Y., The consequence of sequence alteration of an amphipathic alpha-helical antimicrobial peptide and its diastereomers. *J. Biol. Chem.* **2002**, 277(37), 33913-33921.

43. Braunstein, A.; Papo, N.; Shai, Y., In vitro activity and potency of an intravenously injected antimicrobial peptide and its DL amino acid analog in mice infected with bacteria. *Antimicrobial agents and chemotherapy* **2004**, 48(8), 3127-3129.

44. Birge, R.; Boeltz, S.; Kumar, S.; Carlson, J.; Wanderley, J.; Calianese, D.; Barcinski, M.; Brekken, R.; Huang, X.; Hutchins, J., Phosphatidylserine is a global immunosuppressive signal in efferocytosis, infectious disease, and cancer. *Cell death and differentiation* **2016,** *23* (6), 962.

45. Chen, B.; Le, W.; Wang, Y.; Li, Z.; Wang, D.; Ren, L.; Lin, L.; Cui, S.; Hu, J. J.; Hu, Y., Targeting negative surface charges of cancer cells by multifunctional nanoprobes. *Theranostics,* **2016,** 6(11), 1887.

46. Liberti, M. V.; Locasale, J. W., The Warburg Effect: How Does it Benefit Cancer Cells? *Trends. Biochem. Sci.,* **2016**, 41(3), 211-218.

48. Hanahan, D.; Weinberg, R. A., Hallmarks of cancer: the next generation. *Cell (Cambridge, MA, U. S.)* **2011**, 144(5), 646-674.

49. Chen, Daniel S.; Mellman, I., Oncology Meets Immunology: The Cancer-Immunity Cycle. *Immunity* **2013**, 39(1), 1-10.

50. Gamrekelashvili, J.; Greten, T. F.; Korangy, F., Immunogenicity of necrotic cell death. *Cell. Mol. Life Sci.* **2015**, 72(2), 273-283.

51. Jing Yu, PhD Thesis, Kansas State University, 2018

52. Jiang, S.; Hua, L.; Guo, Z.; Sun, L. One-pot green synthesis of doxorubicin loaded-silica nanoparticles for *in vivo* cancer therapy. *Mater. Sci. Eng. C.*, **2018**, 90, 257-263, ISSN 0928-4931.

53. "Polysorbate 80". *Wikipedia*. **2019.** https://en.wikipedia.org/wiki/Polysorbate_80 (accessed Feb. 21, 2019)

54. Zhang, Q., Chen, X., Shi, H., Dong, G., Zhou, M., Wang, T., & Xin, H. Thermo-responsive mesoporous silica/lipid bilayer hybrid nanoparticles for doxorubicin on-demand delivery and reduced premature release. *Colloids Surf. B*: *Biointerfaces*, **2017**, 160, 527-534.

55. Chandrasekar, N.; Murugu, K.; Kumar, M.; Selvan, K.; Balasubramnian; Varadharajan, R. Facile synthesis of iron oxide, iron-cobalt and zero valent iron nanoparticles and evaluation of their anti-microbial activity, free radicle scavenging activity and antioxidant assay. *Dig. J. Nanomater. Biostruct*. **2103.** 8.

Appendix A - Supplementary Data for MSNs Designed for Antimicrobial Use

Supplemental Material for Synthesized Surfactants

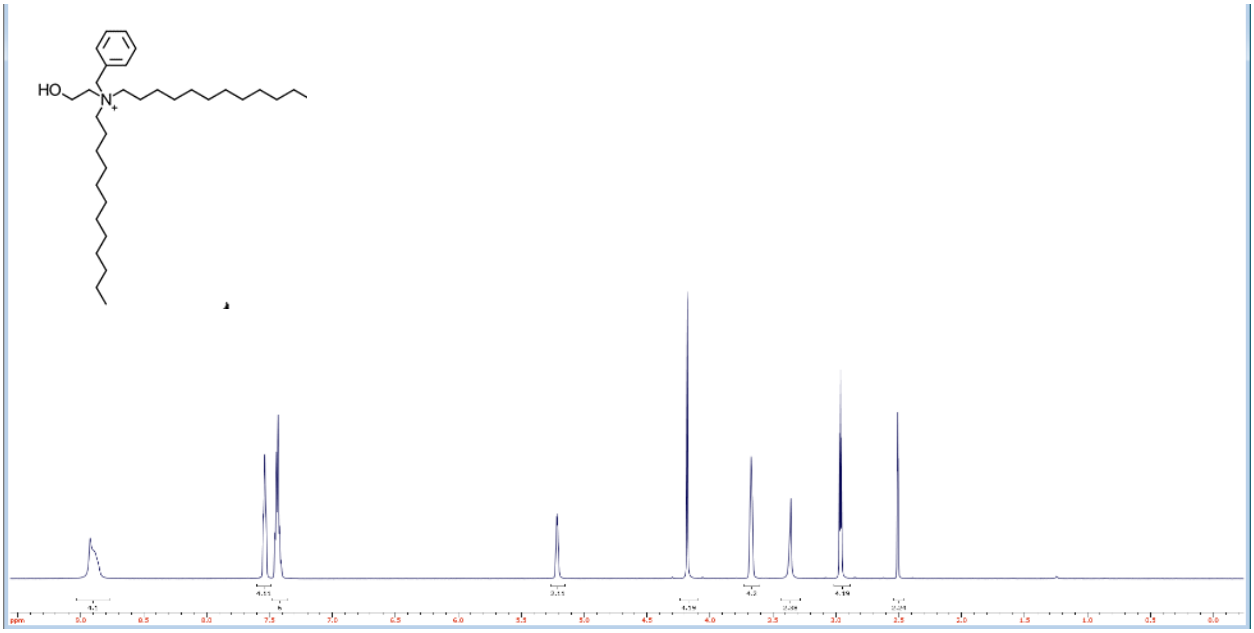

Figure A.1: ^{1}H-NMR of Surfactant A

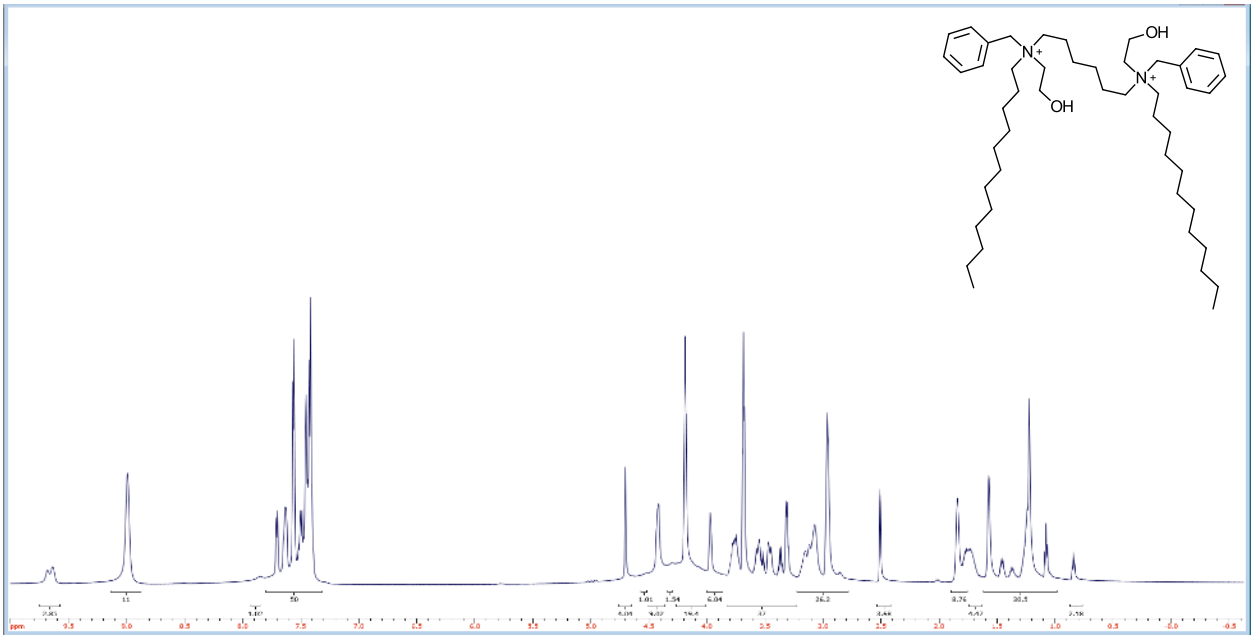

Figure A.243: ^{1}H-NMR of Surfactant B-6

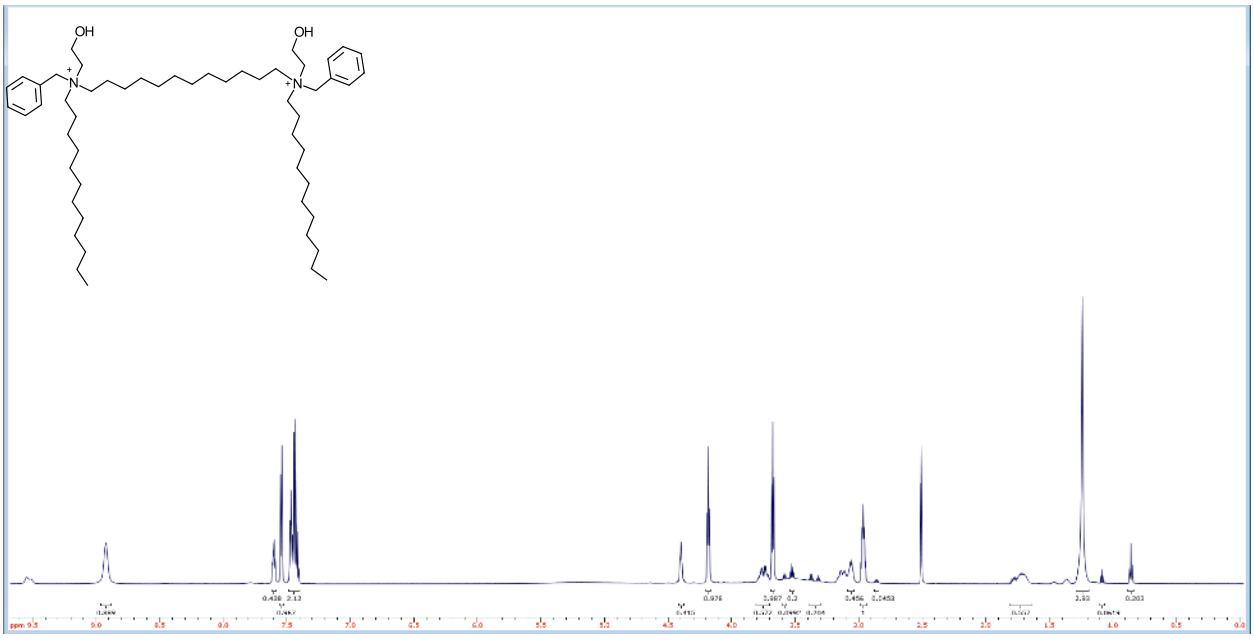

Figure A.3: ^{1}H-NMR of Surfactant B-12

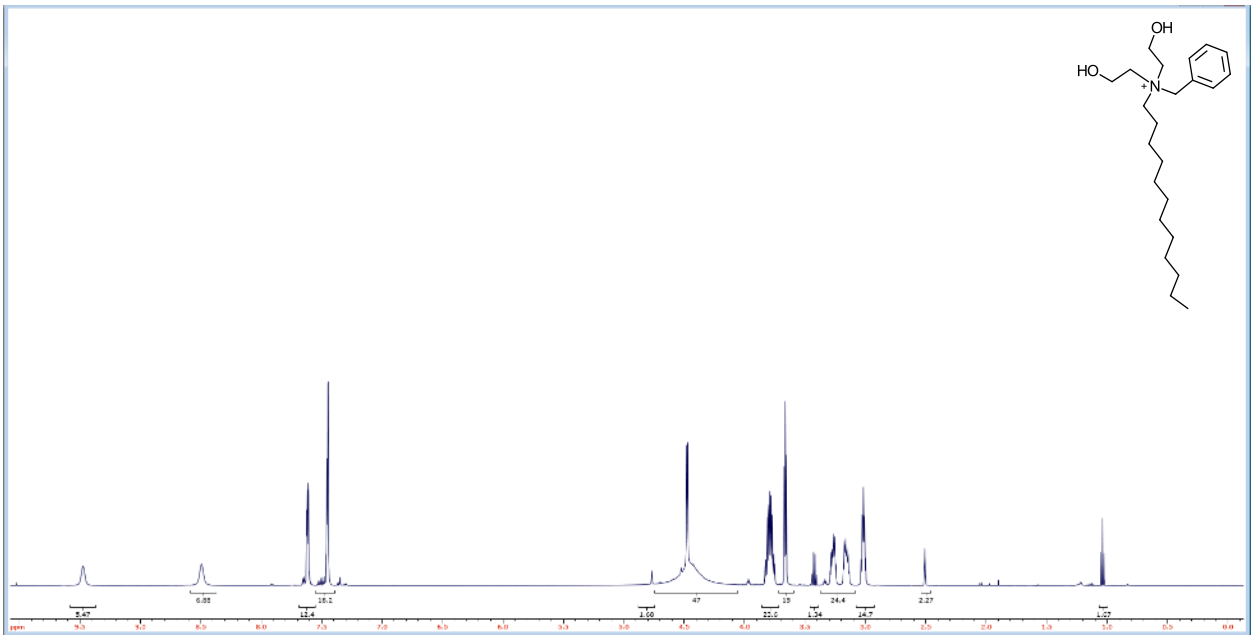

Figure A.4: ^{1}H-NMR of Surfactant C

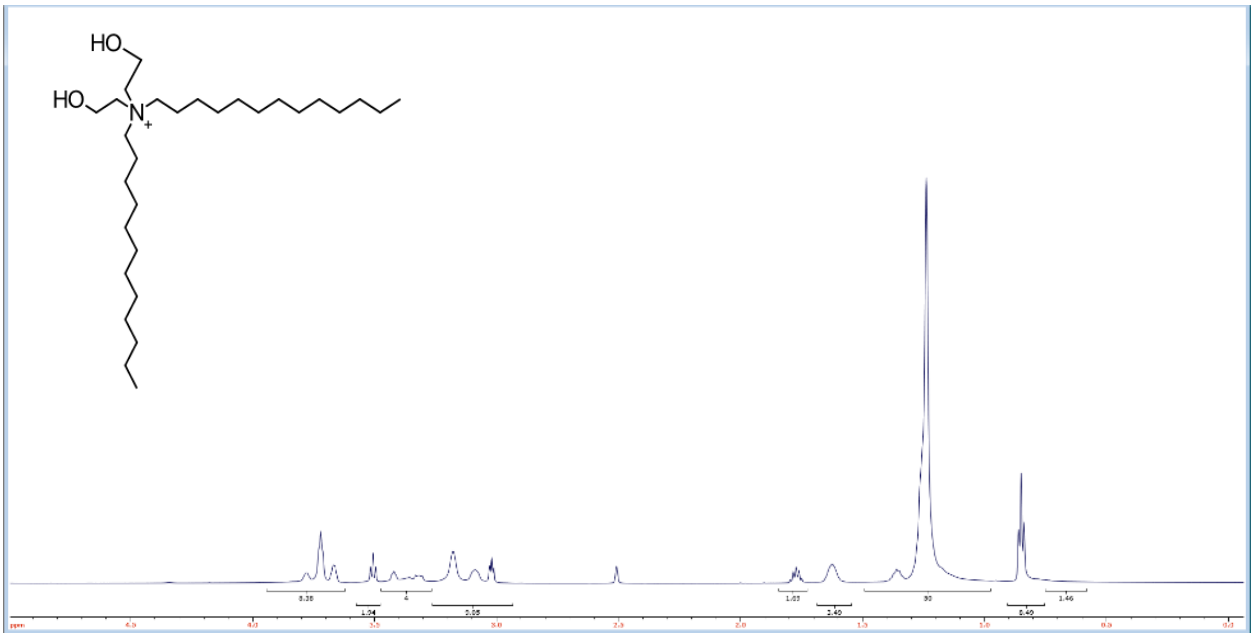

Figure A.5: ^{1}H-NMR of Surfactant V1

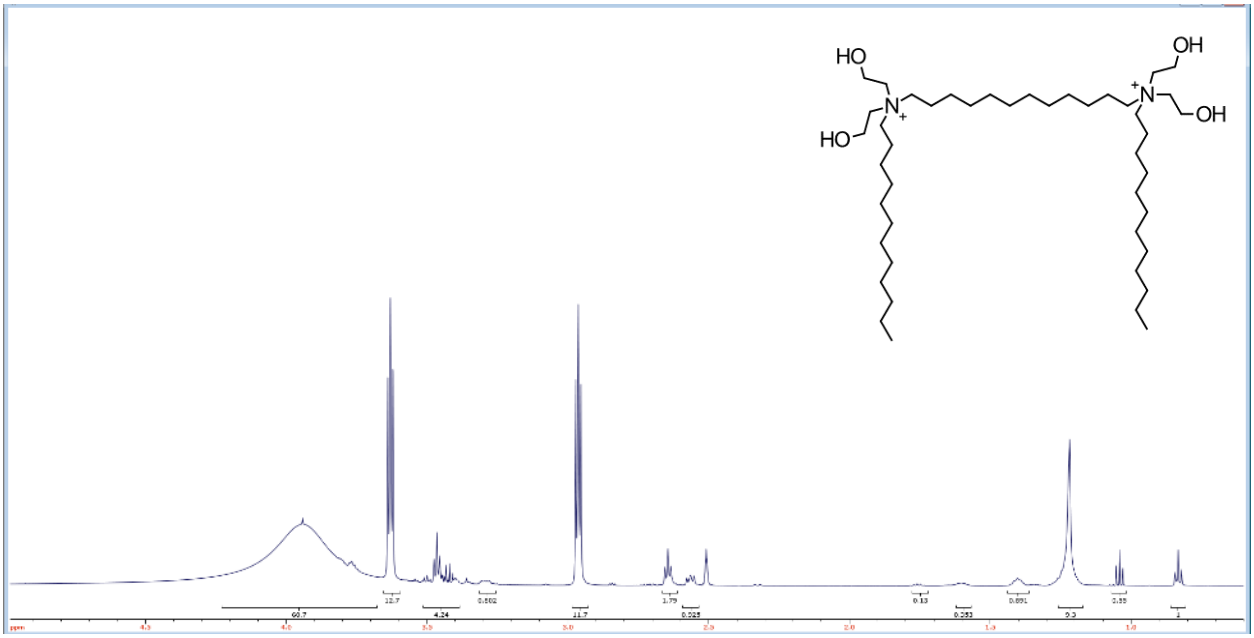

Figure A.6: ^{1}H-NMR of Surfactant V2

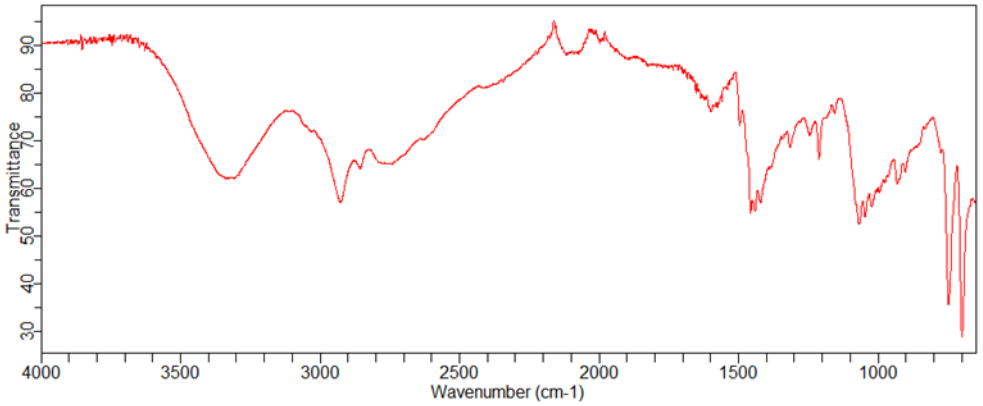

Figure A.7: IR Spectrum of SB6.

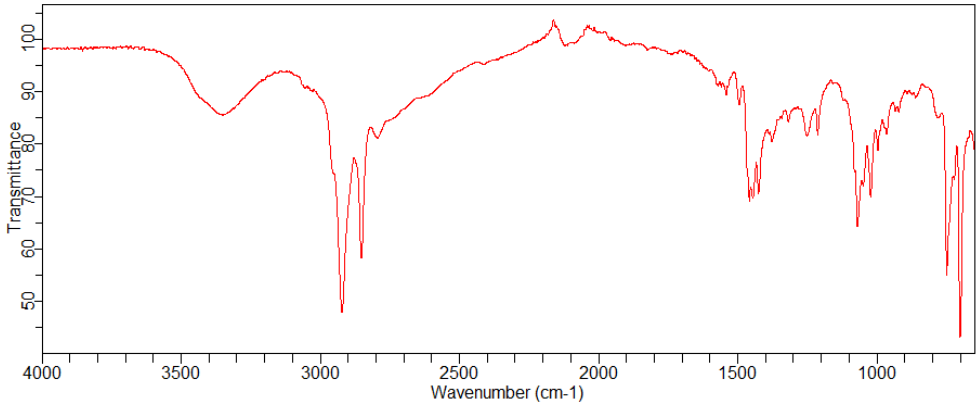

Figure A.8: IR Spectrum of SB12.

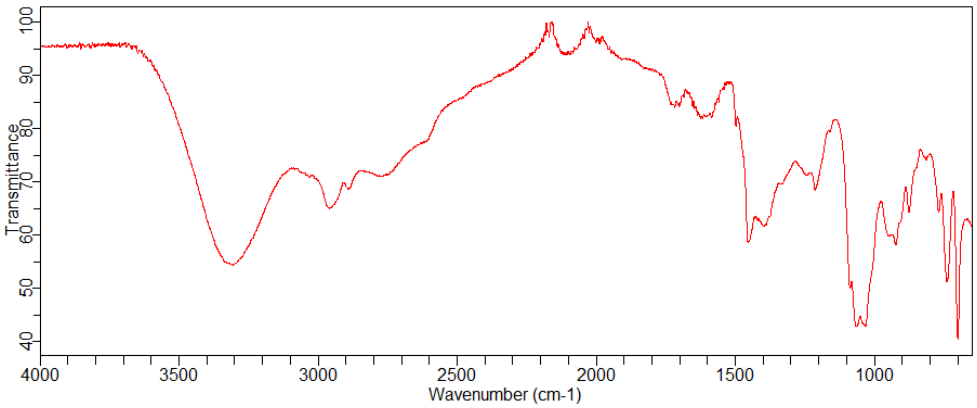

Figure A.9: IR Spectrum of SC.

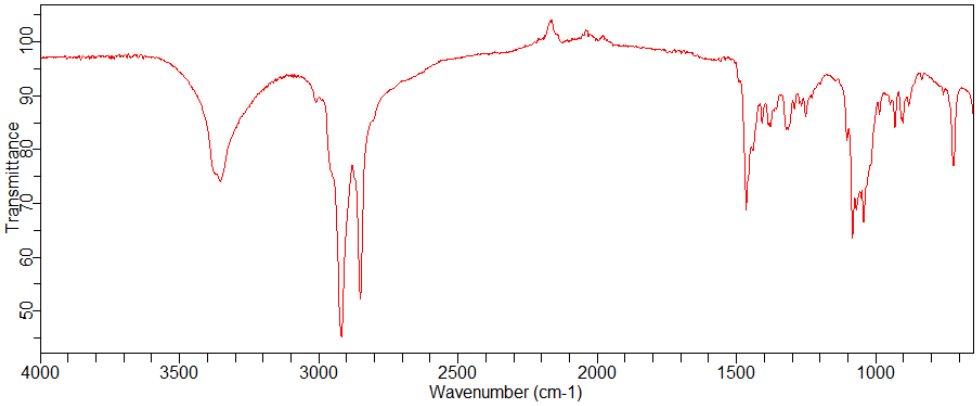

Figure A.10: IR Spectrum of V1.

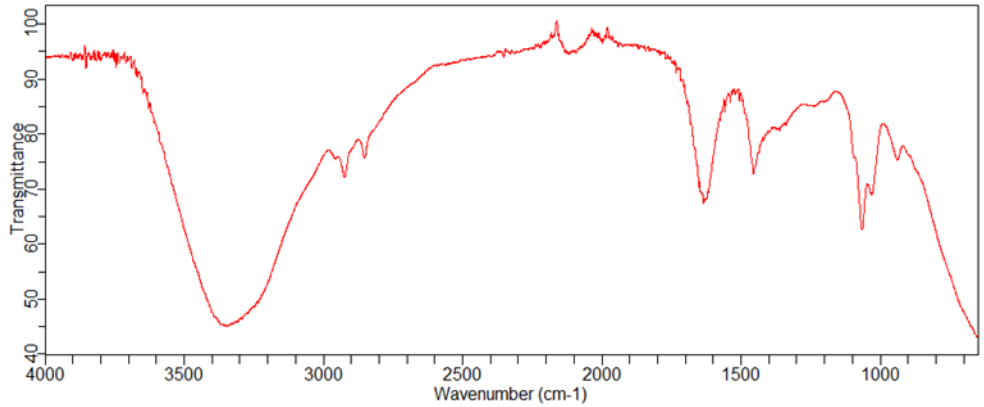

Figure A.11: IR Spectrum of V2.

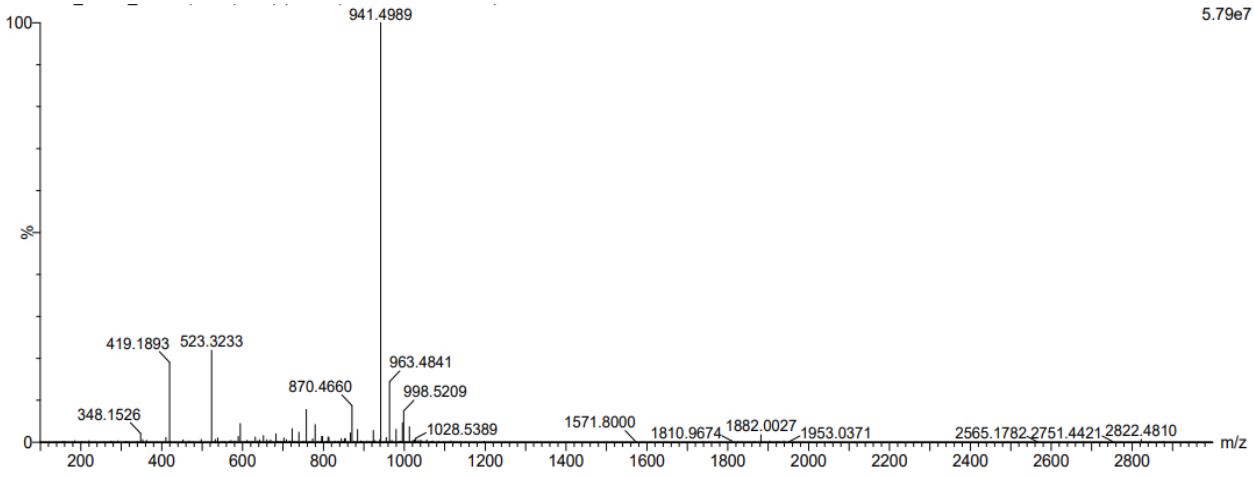

Figure A.12: Mass Spectroscopy Data for Vancomycin Conjugated Peptide, Full Spectra

Appendix B - Supplement Data for MSNs Designed for Cancer Treatment

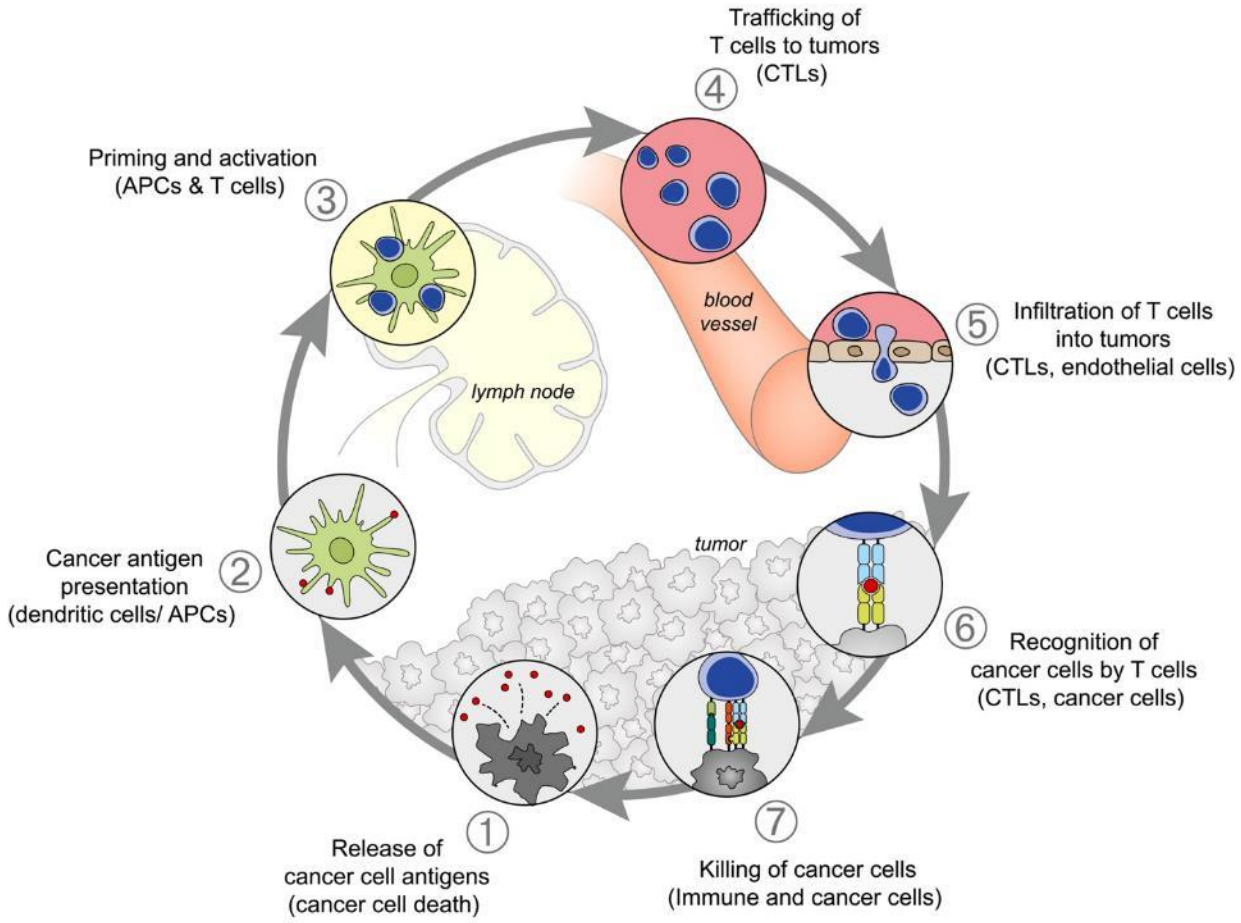

Figure B.1: The Cancer-Immunity Cycle

"The generation of immunity to cancer is a cyclic process that can be self-propagating, leading to an accumulation of immune-stimulatory factors that in principle should amplify and broaden T cell responses. The cycle is also characterized by inhibitory factors that lead to immune regulatory feedback mechanisms, which can halt the development or limit the immunity. This cycle can be divided into seven major steps, starting with the release of antigens from the cancer cell and ending with the killing of cancer cells. Each step is described above, with the primary cell types involved and the anatomic location of the activity listed. Abbreviations are as follows: APCs, antigen presenting cells; CTLs, cytotoxic T lymphocytes."[48] Through necrotic cell death caused

by therapeutic agents, this cycle can be employed. Without a therapeutic agent to initiate the cycle, the body is extremely less likely to begin the cycle on its own.

Sample Cell Viability Calculation

First the difference in absorbance (A_{690}-A_{550} = delta) was determined. Then the average delta of the control wells containing no reagent and only medium was calculated, with the assumption these wells contained 100% living cells. Then the delta of every well was divided by this average and multiply by one hundred to give percent viability as shown below.

$$\frac{abs.\,delta}{control\ average} * 100 = \%\ Cell\ Viability$$

Sample example: A_{690}-A_{550} = 1.100 for well A1. The average delta of control wells was 1.0996. Cell viability for well A1 was found to be 100.04% As shown below.

$$\frac{1.100}{1.09958333333333} * 100 = \ 100.0378931$$